

# 報告書

平成 27 年度（研究補助） 前後輪ステアリング機構を有する電動二輪車の知的  
操作支援制御による安全機能デザイン 補助事業

平成 28 年 3 月

慶應義塾大学 理工学部 システムデザイン工学科

村上俊之

JKA27-130

## はじめに

高齢化社会に向けて、自立生活を支えるための移動支援機器の開発が強く望まれている。特に、小型で取り扱いが容易な機器の開発に多大な関心が寄せられている。現状でもパーソナルモビリティとして様々な移動支援機器が開発されているが、安全機能に関しては未だ十分であるとは言い難く、また小型でかつ低速から中速における安全走行を可能としつつ、操作性の高いものは少ない。そのため、シニアカー や電動自転車での操作ミスが原因での転倒やそれに伴う負傷事例が多く見られる。自立生活のための移動支援機器において、操作ミスや機器の不安定化による事故は本来絶対に防がなければならない事項であり、転倒防止は移動支援機器には必須の機能と考えている。この機能は、虚弱高齢者（特に大きな障害ではなく、体力の低下等で移動が困難となっている高齢者）に対する支援に多大に貢献でき、健康寿命の引き上げにもつながる産業・社会的なインパクトも期待できるものである。

比較的操作が容易なシニアカーの利用者は年々増加の傾向にあり、特に四輪型の機構が多く採用されている。四輪型は安定性の観点からは非常に優れているが、小型化を行うためには限界があるうえ、不注意に速度を出し過ぎてしまう等の原因で、接触事故における対人負傷や段差乗り越え時の転倒等による事故が多発している。一方で、従来から利用されている自転車等の二輪車は若年時からの利用経験から慣れ親しんだ乗り物として注意深い操作が行い易いが、本来不安定な機構を有していることから、低速時の安定性が問題となってしまう。しかしながら、四輪機構に比べて二輪機構の移動機器では小型軽量化が行い易いばかりでなく、路面状態が悪い状況においては安定化し易いケースが多々見られる。こうした点に着目し、開発する電動二輪車では小型軽量化を基本とした機構設計としつつ、転倒防止制御が実現し易い前後輪ステアリング機構を有する二輪車を検討する。前後輪ステアリング機構では、ゼロ速度含めた低速度走行での安定化が行い易いという利点を有するが、利用者の意志を反映した操作（操作性）を実現するためには、走行速度に準じた適切なステアリング制御を組み込む必要がある。そこで、本研究課題では前後輪ステアリング機構を有する電動二輪車（電動バイク）の操作性向上制御アルゴリズムを開発した。

本研究課題は、研究協力員として村上俊之研究室大学院生 Yang Chuan 君、平松 知樹君、鎧 崇雅君、前島 総太朗君、老木 融君より多大なる協力を得ている。本報告書は本研究課題の中心テーマを扱っている大学院修士 2 年生 鎧 崇雅君の研究を中心 にまとめたものであり、同君には研究の総まとめもお願いした。最後に、上記の研究協力員に深く感謝の意を表したい。



# 報告I: 新規実験システムでの検証



報告書I(p2～p43)は、前後輪ステアリングと前後輪駆動システムを有する新規電動2輪システムによる低速走行・旋回動作の安定化制御手法の提案と検証実験を示したものである。

January 11, 2016

JKA130 報告書

T. Murakami 1

## I. 序論



### ■ 背景

#### ● 二輪車の特徴

◆ 小型性・機敏性

◆ 高エネルギー効率

→ 二輪車市場の拡大

#### ● 電動二輪車の開発

◆ 高い経済性

◆ 排出ガスを出さない優れた環境性

→ 新たなパーソナルモビリティとしても期待

世界的にも二輪車への注目が高まっている。

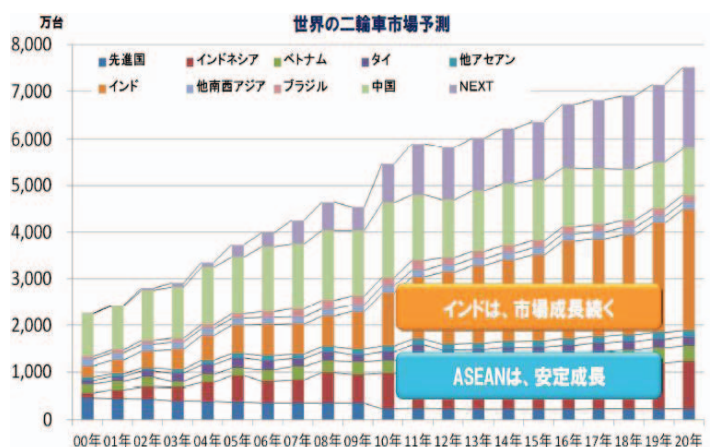


図1:世界の二輪車市場 (参照:新電元工業株式会社)

January 11, 2016

JKA130 報告書

T. Murakami 2

# I. 序論



## ■ 背景

- 不安定な機構
  - ◆ 未経験者や高齢者にとって操作が困難
  - 旋回性と姿勢安定性の重要性

## ■ 従来手法

- 両輪駆動 → ○姿勢安定性 ✕ 旋回性
- 両輪操舵 → ○旋回性 ✕ 姿勢安定性

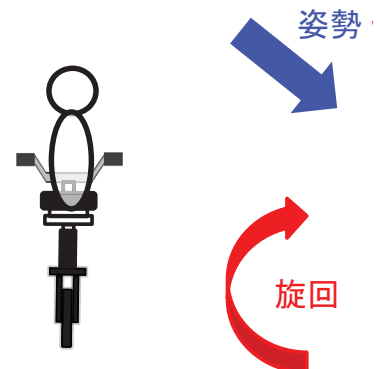


図3: 両輪操舵の旋回走行

## ■ 問題点

- 旋回性と姿勢安定性のトレードオフの関係
  - 低速時における旋回性と姿勢安定性の両立は困難

January 11, 2016

JKA130 報告書

T. Murakami 3

# I. 序論



## ■ 本研究の目的

- 低速時における旋回性と姿勢安定性の向上

## ■ 本研究の提案

- 多自由度電動二輪車の構築
  - ◆ 両輪駆動+両輪操舵システム



図4: 提案システムの概要

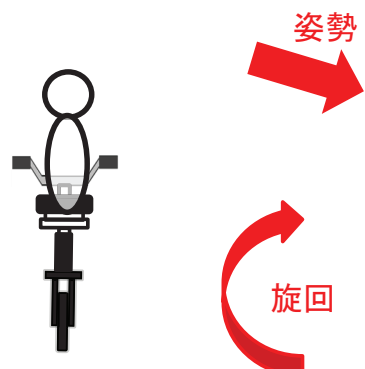


図6: 提案システムの旋回走行

多自由度電動二輪車による高度運動化を実現

January 11, 2016

JKA130 報告書

T. Murakami 4

# I. 序論



## ■ 提案手法: 1段階

### ● 両輪駆動制御

◆ 駆動トルクを前後輪に分配するための駆動比を導入

→ 所望低速度を維持しながら、姿勢安定性の向上

## ■ 提案手法: 2段階

### ● 両輪操舵制御

◆ 両輪駆動を考慮した両輪操舵制御を導入

・前輪操舵: 姿勢安定化制御

・後輪操舵: 軌道追従制御

→ 姿勢安定性を考慮した旋回性の向上

**低速時における高旋回性と高姿勢安定性の両立を実現**

January 11, 2016

JKA130 報告書

T. Murakami 5

# II. モデリング



## ■ 多自由度電動二輪車のモデル

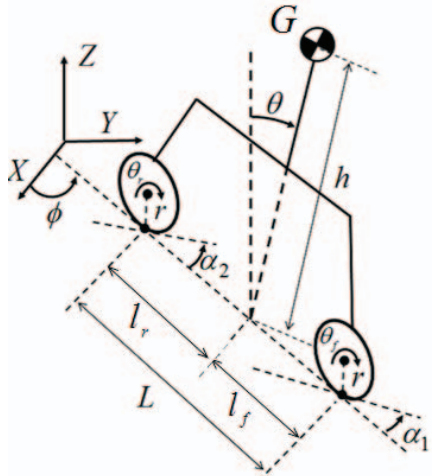


図7: 電動二輪車の俯瞰図

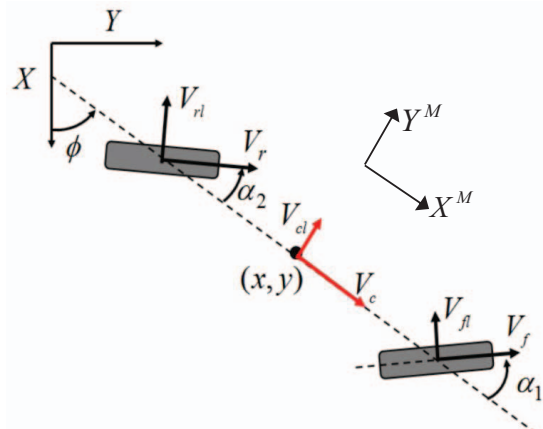


図8: 電動二輪車の上面図

$r$ : 車輪半径	$\theta$ : キャンバ角	$\alpha_1$ : 前輪操舵角
$l_f$ : 前輪接地点からの重心位置	$\theta_f$ : 前輪回転角	$\alpha_2$ : 後輪操舵角
$l_r$ : 後輪接地点からの重心位置	$\theta_r$ : 後輪回転角	$V_f$ : 前輪車輪速
$L$ : ホイールベース	$\phi$ : 旋回角	$V_r$ : 後輪車輪速

January 11, 2016

JKA130 報告書

T. Murakami 6

## II. モデリング



### ■ 運動学

#### ● 位置と速度の関係

$$\begin{bmatrix} \dot{x} \\ \dot{y} \end{bmatrix} = \begin{bmatrix} \frac{l_r \cos(\phi + \alpha_1)}{L} & \frac{l_f \cos(\phi + \alpha_2)}{L} \\ \frac{l_r \sin(\phi + \alpha_1)}{L} & \frac{l_f \sin(\phi + \alpha_2)}{L} \end{bmatrix} \begin{bmatrix} V_f \\ V_r \end{bmatrix}$$

#### ● 旋回角速度

$$\dot{\phi} = \frac{r(\dot{\theta}_f \sin \alpha_1 - \dot{\theta}_r \sin \alpha_2)}{L}$$

#### ● 前輪・後輪接地点の速度

$$V_f = r\dot{\theta}_f$$

$$V_r = r\dot{\theta}_r$$

$$V_{rl} = V_{fl} = 0$$

January 11, 2016

JKA130 報告書

T. Murakami 7

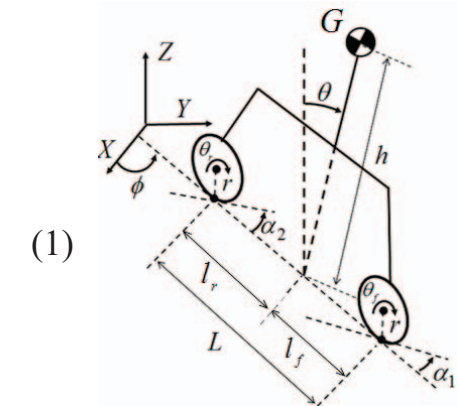
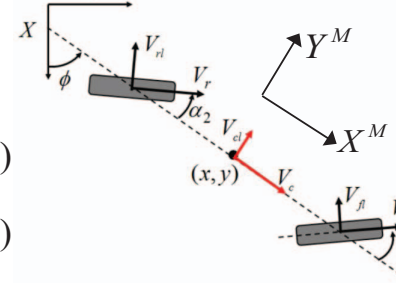


図7: 電動二輪車の俯瞰図

(1)



(2)

(3)

(4)

(5)

図8: 電動二輪車の上面図

## II. モデリング



### ■ 動力学

#### ● 運動方程式

$$M(r)\ddot{r} + K(r, \dot{r}) + G(r) = \tau \quad (6)$$

非ホロノミック拘束を考慮

#### ● キャンバ角に関する運動方程式

$$M_{11}\ddot{\theta} = -M_{12}\ddot{\theta}_f - M_{13}\ddot{\theta}_r - D_1\dot{\alpha}_1 - D_2\dot{\alpha}_2 - K'_1 - G_1 - T_\theta^{dis} \quad (7)$$

キャンバ角に関する外乱

両輪操舵に関する制御入力

両輪駆動に関する制御入力

一般化座標  $r = [\theta \ \theta_f \ \theta_r \ \alpha_1 \ \alpha_2]^T$  入力トルク  $\tau = [0 \ \tau_f \ \tau_r \ \tau_{\alpha 1} \ \tau_{\alpha 2}]^T$   
 慣性行列  $M(r) \in \mathbb{R}^{5 \times 5}$  遠心力, コリオリ力  $K(\dot{r}, r) \in \mathbb{R}^5$  重力  $G(r) \in \mathbb{R}^5$

January 11, 2016

JKA130 報告書

T. Murakami 8

### III. 指令値生成法



#### ■ 旋回角指令値・並進速度指令値

##### ● 直接指令値生成法

$$V_c^{cmd} = V_c^d \quad (8)$$

$$\phi^{cmd} = \phi^d \quad (9)$$

##### ● 金山手法

$$V_c^{cmd} = V_c^d \cos \phi^e + K_x X^e \quad (10)$$

$$\phi^{cmd} = \dot{\phi}^d + V_c^d (K_x Y^e + K_\phi \sin \phi^e) \quad (11)$$

→ 軌道追従性を考慮した指令値生成

#### ■ キャンバ角指令値

$$\theta^{cmd} = \arctan \frac{V_c^{cmd} \dot{\phi}^{cmd}}{g} \quad (12)$$

$V_c^d$ : 並進速度所望値  $V_c^{cmd}$ : 並進速度指令値  $K_\theta$ : 軌道追従制御ゲイン  
 $\phi^d$ : 旋回角所望値  $\phi^{cmd}$ : 旋回角指令値  $\bigcirc^e$ : 位置偏差

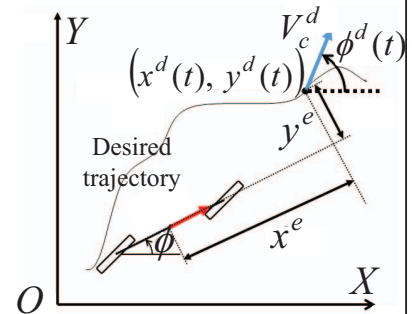


図10: 所望軌道と電動二輪車の位置

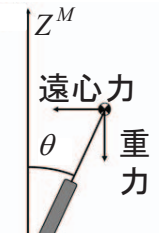


図11: 遠心力と重力

January 11, 2016

JKA130 報告書

T. Murakami 9

### IV. 制御系設計



#### ■ 提案手法: 1段階

##### ● 駆動トルク分配制御

◆ PD制御により全後輪駆動トルク  $\tau_{rt}^{ref}$  を算出

$$\ddot{\theta}_{rt}^{ref} = K_{\theta_{rt}} (\theta_{rt}^{cmd} - \theta_{rt}^{res}) + K_{\dot{\theta}_{rt}} (\dot{\theta}_{rt}^{cmd} - \dot{\theta}_{rt}^{res}) \quad (13)$$

$$\tau_{rt}^{ref} = M_{33n} \ddot{\theta}_{rt}^{ref} + \hat{\tau}_{rt}^{dis} \quad (14)$$

◆ 駆動比  $K_d$  導入により  $\tau_{rt}^{ref}$  を前輪に分配

$$\tau_f^{ref} = K_d \tau_{rt}^{ref} \quad (15)$$

$$\tau_r^{ref} = (1 - K_d) \tau_{rt}^{ref} \quad (16)$$

$$\left. \begin{array}{l} \tau_{rt}^{ref} = \tau_f^{ref} + \tau_r^{ref} \\ \end{array} \right\} \quad (17)$$

→ 所望低速度を維持しながら駆動トルクを分配

January 11, 2016

JKA130 報告書

T. Murakami 10

## IV. 制御系設計



### ■ 提案手法: 2段階

#### ● 両輪操舵制御

- ◆ 前輪操舵角速度指令値: 姿勢安定化制御(リアブノフ安定定理)

$$\dot{\alpha}_1^{cmd} = \frac{1}{D_{1n}} \left\{ K_\theta (\theta^{res} - \theta^{cmd}) - \hat{T}_\theta^{dis} + K_{\dot{\theta}} \dot{\theta} \right\} \quad (18)$$

- ◆ 後輪操舵角速度指令値: 軌道追従制御

$$\dot{\alpha}_2^{cmd} = -W \frac{L}{r \dot{\theta}_r \cos \alpha_2} \left\{ K_\phi (\phi^{res} - \phi^{cmd}) + K_{\dot{\phi}} (\dot{\phi}^{res} - \dot{\phi}^{cmd}) \right\} \quad (19)$$

- ◆ 後輪操舵に関する重み関数(シグモイド関数)

$$W = \frac{2}{1 + \exp(\lambda |\theta^{cmd} - \theta^{res}|)} \quad (20)$$

→ 旋回性と姿勢安定性の両立

## IV. 制御系設計



### ■ 制御系全体のブロック線図

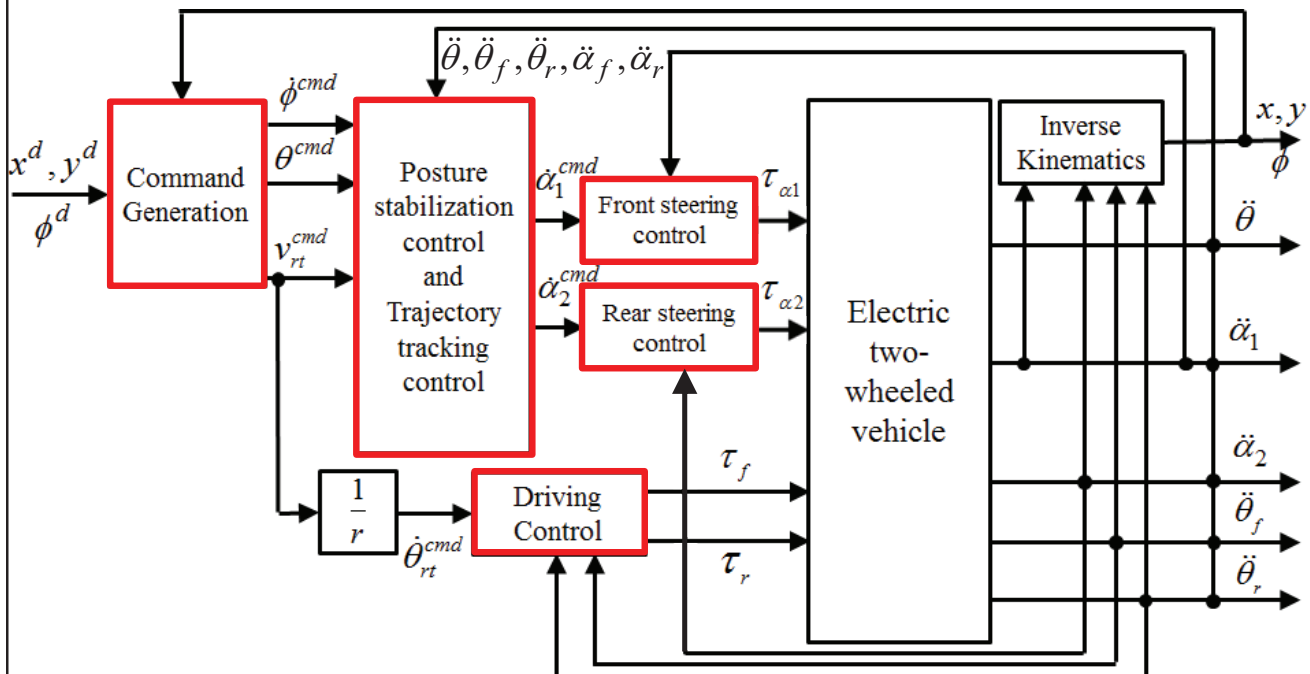


図12: 制御系全体のブロック線図

## V. シミュレーション



### ■ シミュレーション目的

- 多自由度電動二輪車の旋回性と姿勢安定性の確認

### ■ シミュレーション概要

- 低速時における複雑軌道走行

$$\begin{cases} V_c^d = 1.0 \text{ [m/s]} \\ \phi^d = 20.0 \sin\left(\frac{t-4.0}{4.0}\right) \text{ [deg]} \end{cases} \quad \text{if } t \geq 4.0 \text{ [sec]}$$

- 指令値生成:  $V_c^{cmd}$ ,  $\phi^{cmd}$  → 金山手法を使用

- 比較対象

- ◆ 従来手法: 後輪駆動+両輪操舵
- ◆ 提案手法: 両輪駆動+両輪操舵

- 駆動比  $K_d = 0.15$

January 11, 2016

JKA130 報告書

T. Murakami 13

## V. シミュレーション



### ■ シミュレーション結果

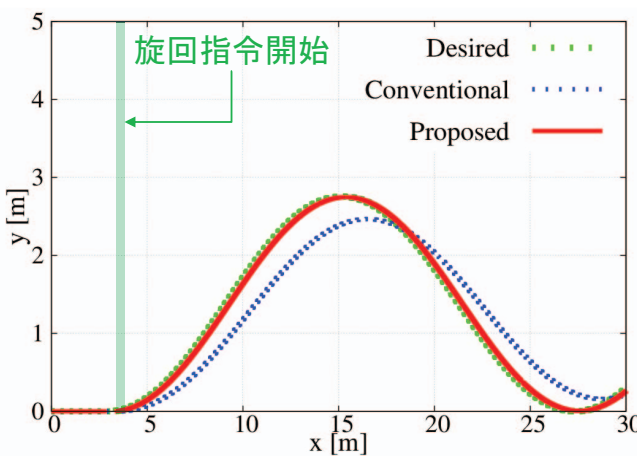


図13: 軌道応答値  
旋回性向上

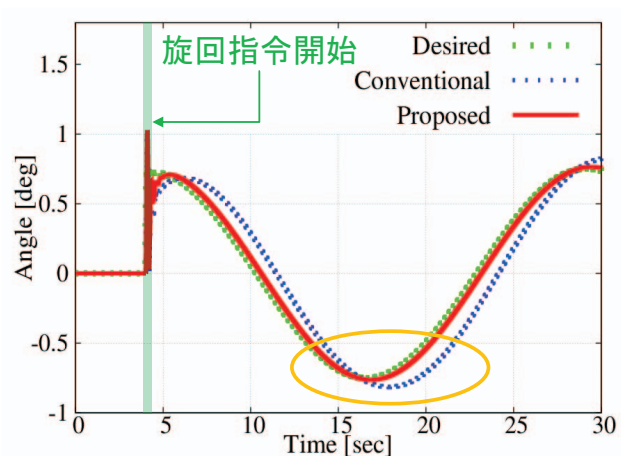


図14: キャンバ角応答値  
姿勢安定性向上

**提案手法の有効性を確認**

January 11, 2016

JKA130 報告書

T. Murakami 14

# VI. 実験



## ■ 実験目的

- 多自由度電動二輪車の旋回性と姿勢安定性の確認

## ■ 実験概要

- 低速時における単純円旋回軌道

$$\begin{cases} V_c^d = 0.8 \text{ [m/s]} & \text{if } t \geq 11.0 \text{ [sec]} \\ \phi^d = 35.0t \text{ [deg]} & \end{cases}$$

- 指令値生成:  $V_c^{cmd}, \phi^{cmd}$  → 直接指令値生成法を使用

- 比較対象

- ◆ 従来手法: 後輪駆動+両輪操舵

- ◆ 提案手法: 両輪駆動+両輪操舵

- 初期走行安定化のため補助輪を使用

- 駆動比  $K_d = 0.5$

January 11, 2016

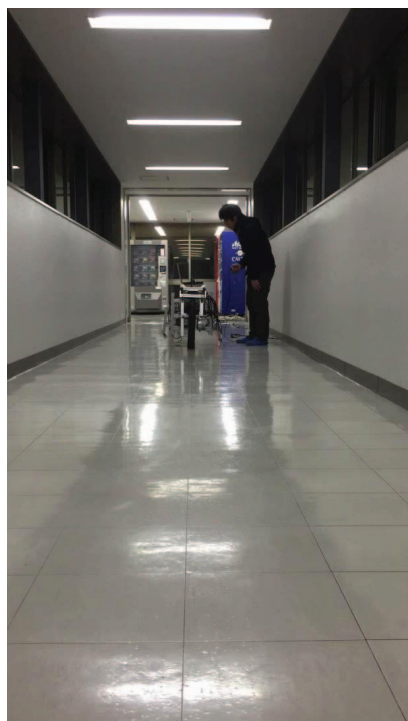
JKA130 報告書

T. Murakami 15

# VI. 実験



## ■ 実験概要の動画



January 11, 2016

JKA130 報告書

T. Murakami 16

# VI. 実験



## 実験結果

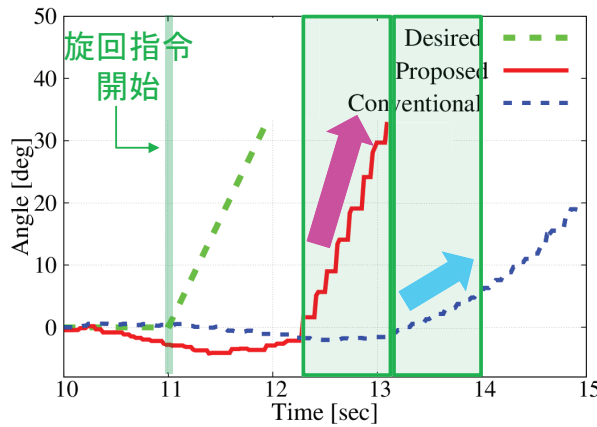


図15: 旋回角応答値

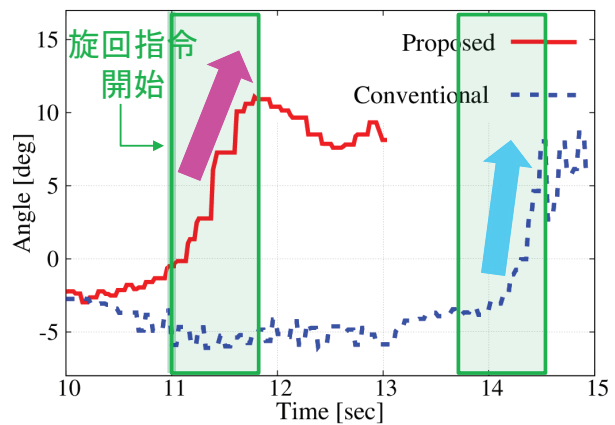


図16: キャンバ角応答値

旋回性向上

提案手法の有効性を確認

January 11, 2016

JKA130 報告書

T. Murakami 17

# VII. 結論



## 研究目的

- 低速時における旋回性と姿勢安定性の向上

## 提案

- 多自由度電動二輪車の構築
- 駆動比導入による両輪駆動制御
- 両輪駆動を考慮した両輪操舵制御

## 結果

- シミュレーションにより低速複雑軌道における有効性を確認
- 実機実験により低速旋回軌道における有効性を確認
- 非ホロノミック拘束を有するシステムへの応用性が期待

January 11, 2016

JKA130 報告書

T. Murakami 18

# VIII. 補足



## ■ 補足

- 実験環境及び実験状況
- 運動方程式パラメータ1
- 運動方程式パラメータ2
- 非ホロノミック拘束
- 動力学導出
- シミュレーションパラメータ
- 実験パラメータ
- シミュレーション結果1-1
- シミュレーション結果1-2
- シミュレーション結果1-3
- シミュレーション結果2-1
- シミュレーション結果2-2
- 低速直線走行実験結果
- 低速旋回走行実験結果

- 駆動比に対する重み関数
- 後輪操舵に対する重み関数
- 独立両輪操舵型CADO
- 全後輪回転角速度指令値
- 金山手法ゲイン設計
- 両輪駆動二輪車
- 両輪操舵二輪車
- パーソナルモビリティ
- 三輪車(トライク)
- 実験機仕様1
- 実験機仕様2
- 並進速度・垂直速度
- 旋回角加速度
- キャンバ角加速度

January 11, 2016

JKA130 報告書

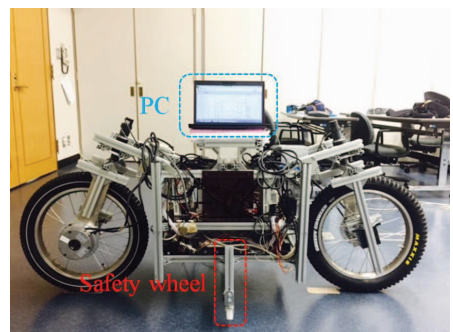
T. Murakami 19

# VIII. 補足



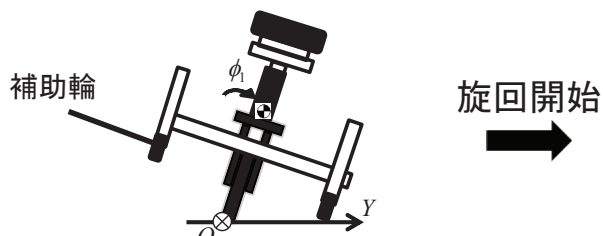
## ■ 実験環境

- 初期走行安定化のため補助輪を使用
- 無人走行を実施

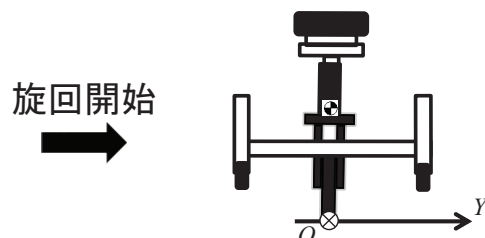


図A：実験機の概要

## ■ 実験状況



図B：初期走行時前面図



図C：旋回走行時前面図

January 11, 2016

JKA130 報告書

T. Murakami 20

# VIII. 補足



## ■ 運動方程式パラメータ1

$$\begin{aligned}
 K_1 &= -hm((-1+g)\sin\theta + \cos\theta(-A^2r(\sin\alpha_1\dot{\theta}_f - \sin\alpha_2\dot{\theta}_r)(l_r\cos\alpha_1 - hr\sin\alpha_1\sin\theta)\dot{\theta}_f \\
 &\quad + (l_f\cos\alpha_2 + hr\sin\alpha_2\sin\theta)\dot{\theta}_r) + h\sin\theta\dot{\theta}^2)) + Ahl_r m(1+r)\cos\alpha_1\cos\theta\dot{\theta}_f \\
 &\quad + Ahm(l_f - Ll_r r)\cos\alpha_2\cos\theta\dot{\theta}_r \\
 K_2 &= Ahm\dot{\theta}(Ar(-l_r\cos\theta\sin 2\alpha_1 + hr\sin^2\alpha_1\sin 2\theta)\dot{\theta}_f - Ar(\cos\theta(l_f\cos\alpha_2\sin\alpha_1 - l_r\cos\alpha_1\sin\alpha_2) \\
 &\quad + hr\sin\alpha_1\sin\alpha_2\sin 2\theta)\dot{\theta}_r - l_r(1+r)\sin\alpha_1\sin\theta\dot{\theta}) \\
 K_3 &= Ahm\dot{\theta}(-Ar(l_f\cos\alpha_2\cos\theta\sin\alpha_1 + \sin\alpha_2(-l_r\cos\alpha_1\cos\theta + hr\sin\alpha_1\sin 2\theta))\dot{\theta}_f \\
 &\quad + Ar(l_f\cos\theta\sin 2\alpha_2 + hr\sin^2\alpha_2\sin 2\theta)\dot{\theta}_r + (-l_f + l_r r)\sin\alpha_2\sin\theta\dot{\theta}) \\
 K_4 &= -Ahm\dot{\theta}(Ar\sin\alpha_1(l_r\cos\alpha_1 + h\sin\alpha_1\sin\theta)\dot{\theta}_f - A(l_f\cos\alpha_2\sin\alpha_1 + \sin\alpha_2((-l_f + l_r r)\cos\alpha_1 \\
 &\quad + hr\sin\alpha_1\sin\theta))\dot{\theta}_r + h\cos\alpha_1\cos\theta\dot{\theta}) \\
 K_5 &= Ahl_r m\dot{\theta}_r(-A(l_r(1+r)\cos\alpha_2\sin\alpha_1 + \sin\alpha_2(-l_r\cos\alpha_1 + hr\sin\alpha_1\sin\theta))\dot{\theta}_f \\
 &\quad + Ar\sin\alpha_2(l_r\cos\alpha_2 + h\sin\alpha_2\sin\theta)\dot{\theta}_r - h\cos\alpha_2\cos\theta\dot{\theta}) \\
 G_1 &= -ghm\sin\theta
 \end{aligned}$$

January 11, 2016

JKA130 報告書

T. Murakami 21

# VIII. 補足



## ■ 運動方程式パラメータ2

$$\begin{aligned}
 M_{11} &= h^2m \\
 M_{12} &= Ahl_r m(1+r)\cos\theta\sin\alpha_1 \\
 M_{13} &= Ahm(l_f - l_r r)\cos\theta\sin\alpha_2 \\
 M_{21} &= Ahl_r m(1+r)\cos\theta\sin\alpha_1 \\
 M_{22} &= A^2m(l_r^2\cos^2\alpha_1 - hl_r r\sin 2\alpha_1\sin\theta + \sin^2\alpha_1(l_r^2(1+r)^2 + h^2r^2\sin^2\theta)) \\
 M_{23} &= A^2m(l_r\cos\alpha_1(l_f\cos\alpha_2 + hr\sin\alpha_2\sin\theta) \\
 &\quad + \sin\alpha_1(-hl_f r\cos\alpha_2\sin\theta + \sin\alpha_2(l_r(1+r)(l_f - l_r r) - h^2r^2\sin^2\theta))) \\
 M_{31} &= Ahm(l_f - l_r r)\cos\theta\sin\alpha_2 \\
 M_{32} &= -A^2l_r mr^2\sin\alpha_1\sin\alpha_2(l_r^2 + h^2\sin^2\theta) \\
 M_{33} &= A^2l_r^2mr^2\sin^2\alpha_2(l_r^2 + h^2\sin^2\theta) \\
 M_{44} &= J_1 \\
 M_{55} &= J_2
 \end{aligned}$$

$$M(r) = \begin{bmatrix} M_{11} & M_{12} & M_{13} & 0 & 0 \\ M_{21} & M_{22} & M_{23} & 0 & 0 \\ M_{31} & M_{32} & M_{33} & 0 & 0 \\ 0 & 0 & 0 & M_{44} & 0 \\ 0 & 0 & 0 & 0 & M_{55} \end{bmatrix} \in R^{5 \times 5}$$

$$K(r, \dot{r}) = [K_1 \ K_2 \ K_3 \ K_4 \ K_5]^T \in R^5$$

$$G(r) = [G_1 \ 0 \ 0 \ 0 \ 0]^T \in R^5$$

January 11, 2016

JKA130 報告書

T. Murakami 22

# VIII. 補足



## ■ 非ホロノミック拘束

$$\dot{s} + A(\mathbf{r}, s) \dot{\mathbf{r}} = 0$$

$$\begin{aligned}\dot{s} &= [\dot{\phi} \quad V_{fl} \quad V_{rl}]^T \\ \dot{\mathbf{r}} &= [\dot{\theta} \quad \dot{\theta}_f \quad \dot{\theta}_r \quad \dot{\alpha}_1 \quad \dot{\alpha}_2]^T \\ A(\mathbf{r}, s) &= \begin{bmatrix} 0 & -\frac{r}{L} \sin \alpha_1 & \frac{r}{L} \sin \alpha_2 & 0 & 0 \\ 0 & 0 & 0 & 0 & 0 \\ 0 & 0 & 0 & 0 & 0 \end{bmatrix}\end{aligned}$$

January 11, 2016

JKA130 報告書

T. Murakami 23

# VIII. 補足



## ■ 動力学導出

$$\begin{aligned}L &= \frac{1}{2} J_1 \dot{\alpha}_1^2 + \frac{1}{2} J_2 \dot{\alpha}_2^2 + \frac{m}{2} \left\{ (V_c - h \sin \theta \dot{\phi})^2 \right. \\ &\quad \left. + (V_{cl} + h \dot{\theta} \cos \theta + l_r \dot{\phi})^2 + (-h \dot{\theta} \sin \theta)^2 \right\} - mgh \cos \theta\end{aligned}$$

$$\begin{aligned}L_c &= \frac{1}{2} J_1 \dot{\alpha}_1^2 + \frac{1}{2} J_2 \dot{\alpha}_2^2 + \frac{m}{2} \left[ V_c + Ah r \sin \theta (-\sin \alpha_1 \dot{\theta}_f + \sin \alpha_2 \dot{\theta}_r) \right]^2 \\ &\quad + \frac{m}{2} h^2 \sin^2 \theta \dot{\theta}^2 + \frac{m}{2} \left[ V_{cl} + Al_r r (\sin \alpha_1 \dot{\theta}_f - \sin \alpha_2 \dot{\theta}_r) + h \cos \theta \dot{\theta} \right]^2 - mgh \cos \theta\end{aligned}$$

### ● 拘束付きラグランジュ方程式

$$\frac{d}{dt} \frac{\partial L_c}{\partial \dot{r}_i} - \frac{\partial L_c}{\partial r_i} + A_{ji} \frac{\partial L_c}{\partial s_i} = - \sum_k^3 \frac{\partial L}{\partial s_k} C_{ij}^k \dot{r}_j + \tau_i \quad (i = 1, 2, \dots, 5, j = 1, 2, 3, k = 1, 2, 3)$$

$$C_{ij}^k = \left( \frac{\partial A_{ki}}{\partial r_j} - \frac{\partial A_{kj}}{\partial r_i} + \sum_l^3 A_{il} \frac{\partial A_{kj}}{\partial s_l} - \sum_l^3 A_{lj} \frac{\partial A_{ki}}{\partial s_l} \right)$$

January 11, 2016

JKA130 報告書

T. Murakami 24

# VIII. 補足



MURA  
KAMI  
LAB.

## ■ シミュレーションパラメータ1

Table 5.1: シミュレーションで用いた物理パラメータ

名称	記号	値
サンプリングタイム	$dt$	0.001 sec
電動二輪車の質量	$m$	70.0 kg
電動二輪車の重心高さ	$h$	0.5 m
ホイールベース	$L$	1.2 m
前輪接地点からの重心位置	$l_f$	0.7 m
後輪接地点からの重心位置	$l_r$	0.5 m
車輪半径	$r$	0.25 m
前輪ステアリングモータの慣性モーメント	$J_1$	1.8 kg·m <sup>2</sup>
後輪ステアリングモータの慣性モーメント	$J_2$	1.8 kg·m <sup>2</sup>

Table 5.2: シミュレーションで用いた制御パラメータ

名称	記号	値
金山手法の時定数	$T_k$	3.0
金山手法の固有角周波数	$\omega_{nk}$	10.0
金山手法の減衰係数	$\zeta_k$	2.0
リアブノフコントローラの固有角周波数	$\omega_n$	2.0
リアブノフコントローラの減衰係数	$\zeta$	1.2
軌道追従制御に関する P ゲイン	$K_\phi$	900.0
軌道追従制御に関する D ゲイン	$K_{\dot{\phi}}$	60.0
前輪駆動モータ制御に関する P ゲイン	$K_{\theta f}$	900.0
前輪駆動モータ制御に関する D ゲイン	$K_{\dot{\theta} f}$	60.0
後輪駆動モータ制御に関する P ゲイン	$K_{\theta r}$	900.0
後輪駆動モータ制御に関する D ゲイン	$K_{\dot{\theta} r}$	60.0
前輪操舵モータ制御に関する P ゲイン	$K_{\alpha l}$	50.0
前輪操舵モータ制御に関する D ゲイン	$K_{\dot{\alpha} l}$	1100.0
後輪操舵モータ制御に関する P ゲイン	$K_{\alpha r}$	50.0
後輪操舵モータ制御に関する D ゲイン	$K_{\dot{\alpha} r}$	1100.0
DOB のカットオフ周波数	$g_d$	100.0
CADO のカットオフ周波数	$g_c$	100.0

January 11, 2016

JKA130 報告書

T. Murakami 25

# VIII. 補足



MURA  
KAMI  
LAB.

## ■ 実験パラメータ

Table 6.1: 実験で用いた物理パラメータ

名称	記号	値
サンプリングタイム	$dt$	0.0002 sec
バイクの質量	$m$	70.0 kg
重心高さ	$h$	0.65 m
ホイールベース	$L$	1.2 m
前輪接地点からの重心位置	$l_f$	0.6 m
後輪接地点からの重心位置	$l_r$	0.6 m
車輪半径	$r$	0.25 m
前輪ステアリングモータの慣性モーメント	$J_1$	0.83 kg·m <sup>2</sup>
後輪ステアリングモータの慣性モーメント	$J_2$	0.83 kg·m <sup>2</sup>

Table 6.2: 実験で用いた制御パラメータ

名称	記号	値
リアブノフコントローラの固有角周波数	$\omega_n$	4.0
リアブノフコントローラの減衰係数	$\zeta$	0.7
軌道追従制御に関する P ゲイン	$K_\phi$	9.0
軌道追従制御に関する D ゲイン	$K_{\dot{\phi}}$	6.0
前輪駆動モータ制御に関する P ゲイン	$K_{\theta f}$	100.0
前輪駆動モータ制御に関する D ゲイン	$K_{\dot{\theta} f}$	20.0
後輪駆動モータ制御に関する P ゲイン	$K_{\theta r}$	100.0
後輪駆動モータ制御に関する D ゲイン	$K_{\dot{\theta} r}$	20.0
前輪操舵モータ制御に関する P ゲイン	$K_{\alpha l}$	9.0
前輪操舵モータ制御に関する D ゲイン	$K_{\dot{\alpha} l}$	6.0
後輪操舵モータ制御に関する P ゲイン	$K_{\alpha r}$	9.0
後輪操舵モータ制御に関する D ゲイン	$K_{\dot{\alpha} r}$	6.0
DOB のカットオフ周波数	$g_d$	50.0
CADO のカットオフ周波数	$g_c$	5.0

January 11, 2016

JKA130 報告書

T. Murakami 26

## VIII. 補足



### ■ シミュレーション結果1-1(単純円旋回走行)

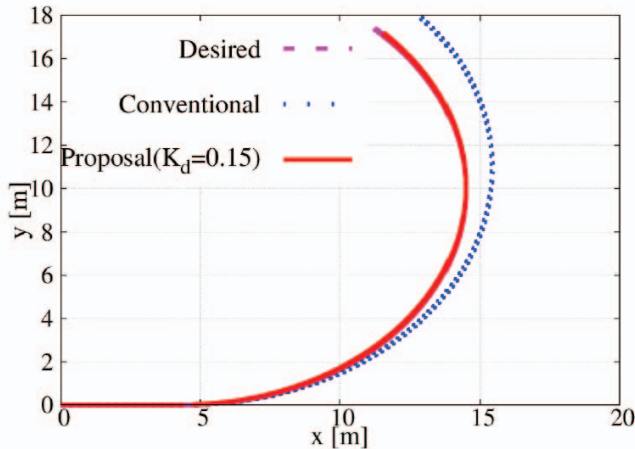


Fig. 5-1: 電動二輪車の軌道応答値(シミュレーション1)

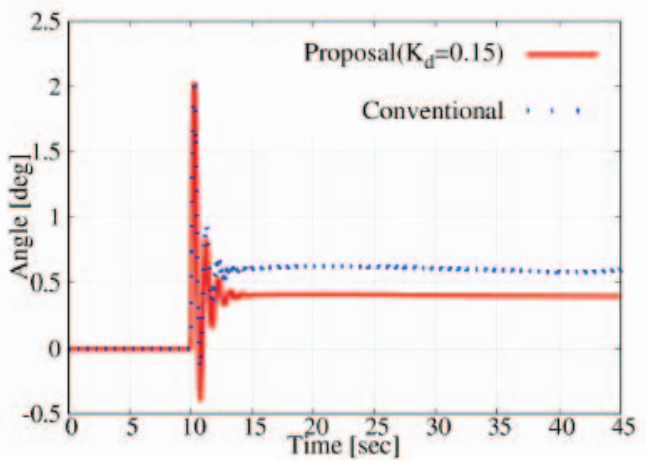


Fig. 5-2: キャンバ角応答値(シミュレーション1)

January 11, 2016

JKA130 報告書

*T. Murakami* 27

## VIII. 補足



### ■ シミュレーション結果1-2(単純円旋回走行)

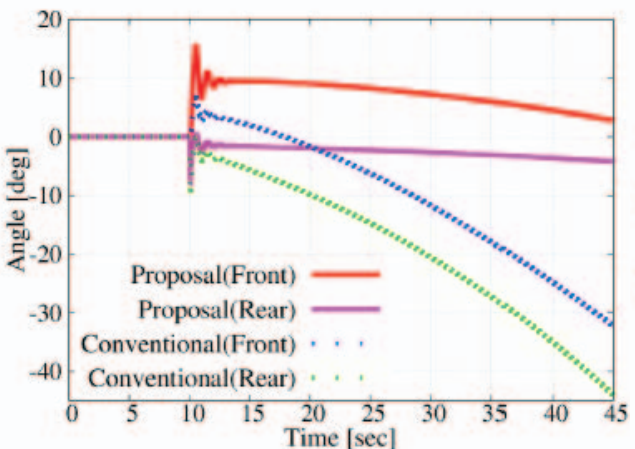


Fig. 5-3: 操舵角応答値(シミュレーション1)

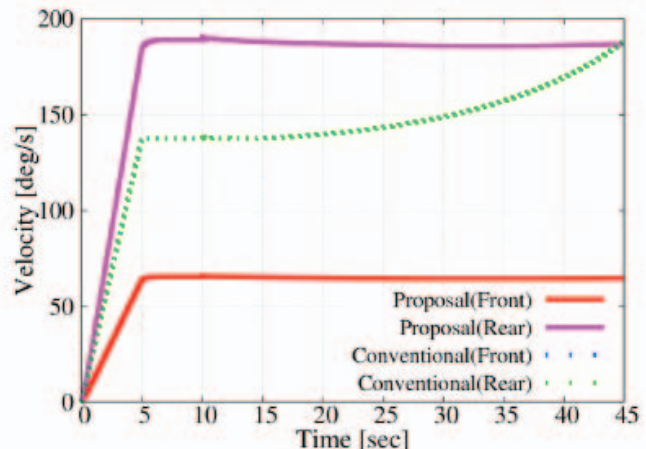


Fig. 5-4: 車輪速度応答値(シミュレーション1)

January 11, 2016

JKA130 報告書

*T. Murakami* 28

## VIII. 補足



### ■ シミュレーション結果1-3(単純円旋回走行)

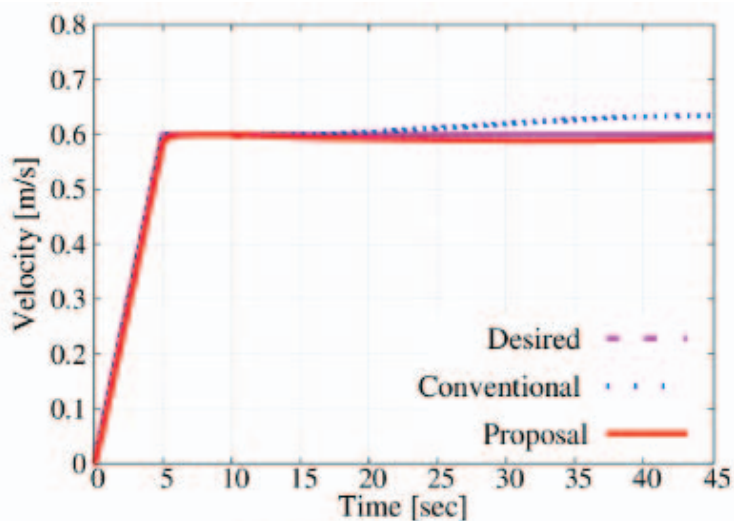


Fig. 5-5: 車体速度応答値(シミュレーション1)

January 11, 2016

JKA130 報告書

T. Murakami 29

## VIII. 補足



### ■ シミュレーション結果2-1(複雑軌道走行)

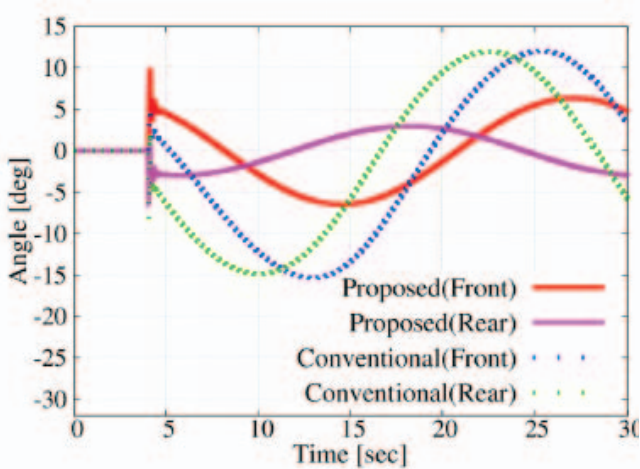


Fig. 5-8: 操舵角応答値(シミュレーション2)

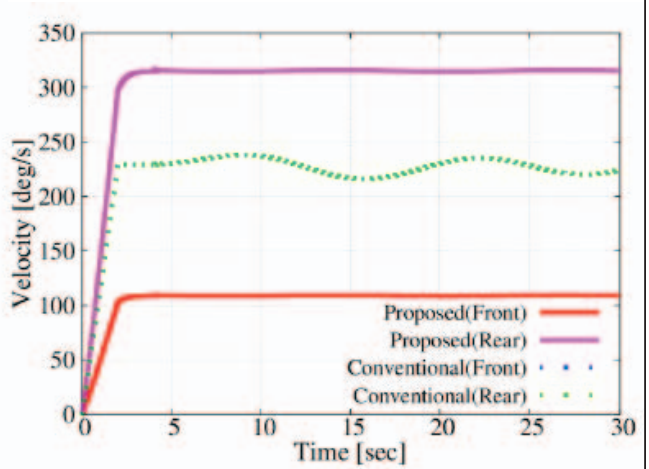


Fig. 5-9: 車輪速度応答値(シミュレーション2)

January 11, 2016

JKA130 報告書

T. Murakami 30

## VIII. 補足



### ■ シミュレーション結果2-2(複雑軌道走行)

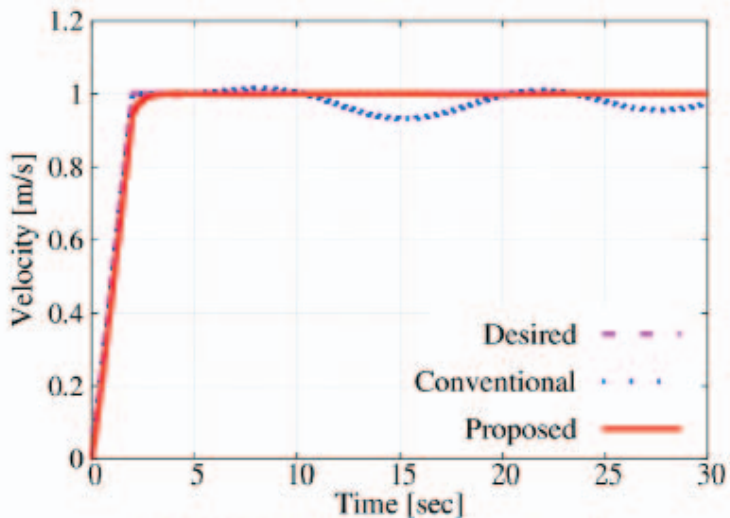


Fig. 5-10: 車体速度応答値(シミュレーション2)

January 11, 2016

JKA130 報告書

T. Murakami 31

## VIII. 補足



### ■ 低速直線走行実験結果

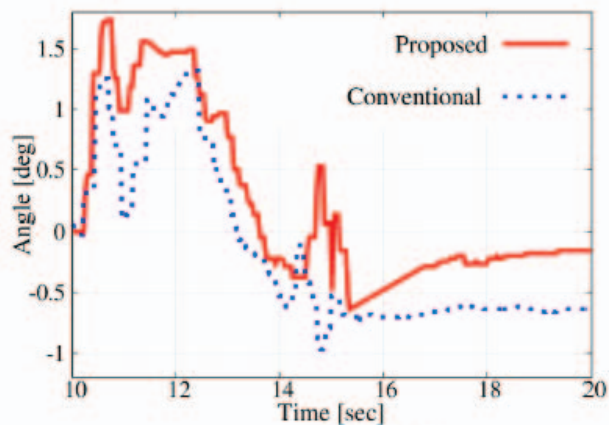


Fig. 6-3: キャンバ角応答値(実験1)

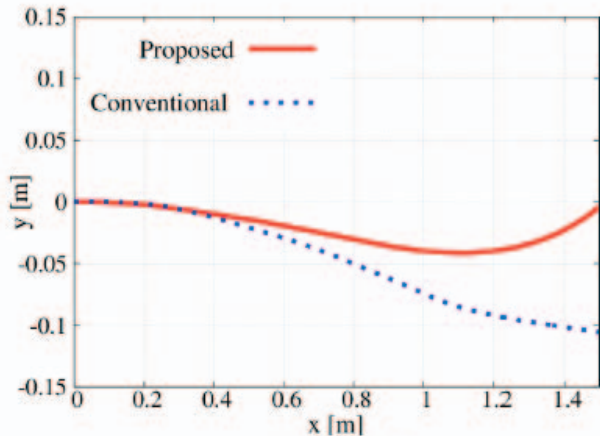


Fig. 6-4: 軌道応答値(実験1)

January 11, 2016

JKA130 報告書

T. Murakami 32

## VIII. 補足



### ■ 低速旋回走行実験結果

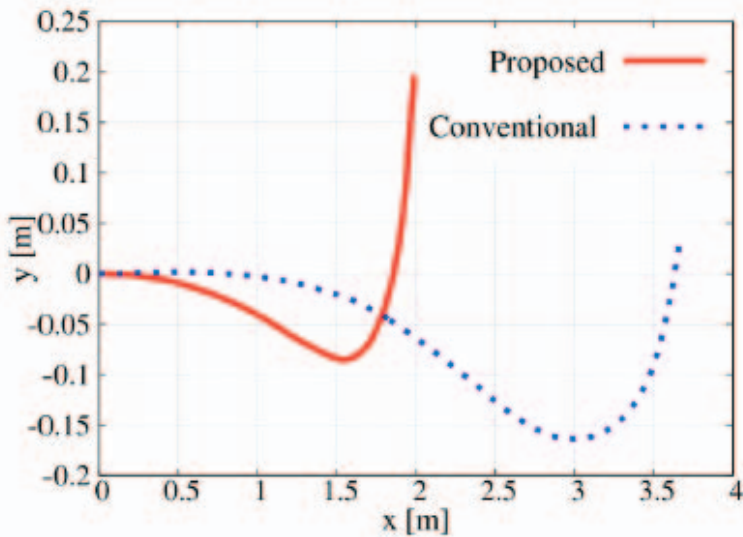


Fig. 6-5: 軌道応答値 (実験 2)

January 11, 2016

JKA130 報告書

T. Murakami 33

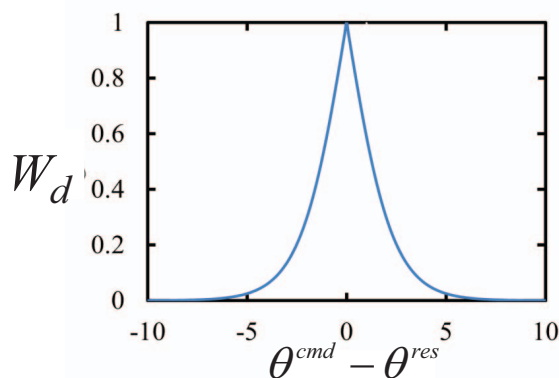
## VIII. 補足



### ■ 駆動比に関する重み関数

#### ● シグモイド関数

$$W_d = \frac{2K_d}{1 + \exp(\lambda|\theta^{cmd} - \theta^{res}|)}$$



図D. 重み関数

January 11, 2016

JKA130 報告書

T. Murakami 34

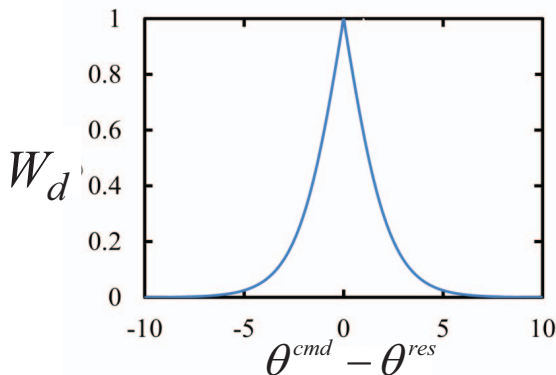
## VIII. 補足



### ■ 後輪操舵に関する重み関数

#### ● シグモイド関数

$$W = \frac{2}{1 + \exp(\lambda|\theta^{cmd} - \theta^{res}|)}$$



図E. 重み関数

January 11, 2016

JKA130 報告書

T. Murakami 35

## VIII. 補足



### ■ 独立両輪操舵型CADO

$$M_{11n}\ddot{\theta} = -D_{1n}\dot{\alpha}_1 - D_{2n}\dot{\alpha}_2 - \hat{T}_{\theta}^{dis}$$

$$\hat{T}_{\theta}^{dis} = \frac{g_c}{s + g_c} (M_{11n}g_c\dot{\theta} - D_{1n}\dot{\alpha}_1 - D_{2n}\dot{\alpha}_2) - M_{11n}g_c\dot{\theta}$$

$$V_{\theta prop2} = \frac{1}{2}M_{11n}\dot{\theta}^2 + \frac{1}{2}K_{\theta}(\theta - \theta^{cmd})$$

$$\dot{\alpha}_1^{cmd} = \frac{1}{D_m} \{-\hat{T}_{\theta}^{dis} + K_{\theta}(\theta - \theta^{cmd}) + K_{\theta}\dot{\theta}\}$$

$$\dot{V}_{\theta prop2} = -K_{\theta}\dot{\theta}^2 - D_{2n}\dot{\alpha}_2$$

$$\dot{V}_{\theta prop2} = -K_{\theta}\dot{\theta}^2 \leq 0$$

$$\begin{aligned} \omega_n &= \sqrt{\frac{K_{\theta}}{M_{11n}}} \\ \zeta &= \frac{K_{\theta}}{2\omega_n M_{11n}} \\ K_{\theta} &= M_{11n}\omega_n^2 \\ K_{\theta} &= 2\zeta\omega_n M_{11n} \end{aligned}$$

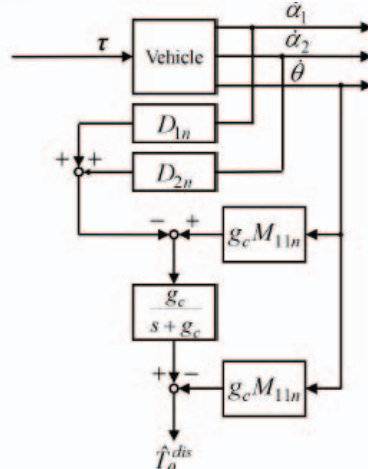


Fig. 4-4: 提案手法 2 用キャンバ角外乱推定オプザーバ (CADO)

January 11, 2016

JKA130 報告書

T. Murakami 36

## VIII. 補足



### ■ 全後輪回転角速度指令値

$$\begin{aligned} V_{rt}^{cmd} &= \frac{V_c^{cmd}}{\cos \alpha_2} \\ \dot{\theta}_{rt}^{cmd} &= \frac{V_{rt}^{cmd}}{r} \\ \theta_{rt}^{cmd} &= \int \dot{\theta}_{rt}^{cmd} dt \end{aligned}$$

January 11, 2016

JKA130 報告書

T. Murakami 37

## VIII. 補足



### ■ 金山手法ゲイン設計

$$\dot{P}^e = \begin{bmatrix} \dot{x}^e \\ \dot{y}^e \\ \dot{\phi}^e \end{bmatrix} = \begin{bmatrix} y^e \dot{\phi} - V_c + V_c^d \cos \phi^e \\ -x^e \dot{\phi} + V_c^d \sin \phi^e \\ \dot{\phi}^d - \dot{\phi} \end{bmatrix}$$

$$\begin{aligned} K_x &= \frac{1}{T} \\ K_y &= \frac{\omega_{nk}^2}{V_c^d} \\ K_\phi &= \frac{2\zeta_k \omega_{nk}}{V_c^d} \end{aligned}$$

January 11, 2016

JKA130 報告書

T. Murakami 38

# VIII. 補足



MURA  
KAMI  
LAB.

## ■ 実験機仕様1

Table A.1: 車輪の AC サーボモータの仕様

種類	AC サーボモータ
製造メーカー	株式会社ハーモニック・ドライブ・システムズ
型式	FHA-25C-50-E250-AC
定格電圧	100V
瞬時最大トルク	150Nm
瞬時最大電流	7.3A
トルク定数	22Nm/A
減速比	50

Table A.2: ステアリングの DC サーボモータの仕様

種類	DC サーボモータ
製造メーカー	株式会社ハーモニック・ドライブ・システムズ
型式	RH-14D-3002-E100AL
定格電圧	24V
瞬時最大トルク	20Nm
定格トルク	5.9Nm
瞬時最大電流	4.1A
定格電流	1.8A
トルク定数	5.76Nm/A
減速比	100

Table A.3: AC サーボモータドライバ仕様

種類	AC サーボモータドライバ
製造メーカー	株式会社ハーモニック・ドライブ・システムズ
型式	HA-800A-6C-100
定格出力電流	A
最大出力電流	6.0
A	19.0

Table A.4: DC サーボモータドライバ仕様

種類	DC サーボモータドライバ
製造メーカー	サーボテクノ株式会社
型式	PMA6
定格出力電圧	±88V
定格出力電流	±6.0A
最大出力電圧	±88V
最大出力電流	±15.0A
入力電源	AC16V~110V 又は DC20V~DC150V
指令入力	DC 0~±10.0V (+2.5V で出力電流ゼロ)

January 11, 2016

JKA130 報告書

T. Murakami 39

# VIII. 補足



MURA  
KAMI  
LAB.

## ■ 実験機仕様2

Table A.6: ジャイロセンサの詳細

製造元	株式会社 データ・テック		
型番	GU-3024		
センサ構成	振動ジャイロ (x3), 加速度計 (x 3)		
検出角速度	ロール角	±5°/s ~ 100°/s	
	ピッチ角	±5°/s ~ 100°/s	
	ヨー角	±5°/s ~ 100°/s	
検出角度	ロール角	±60°	
	ピッチ角	±60°	
	ヨー角	±180°	
精度	ロール角	±0.5°	
	ピッチ角	±0.5°	
	ヨー角	±1.0°	
出力周期		60Hz(16ms)	

January 11, 2016

JKA130 報告書

T. Murakami 40

## VIII. 補足



### ■ 並進速度・垂直速度

$$V_c = \frac{l_r V_f \cos \alpha_1 + l_f V_r \cos \alpha_2}{L}$$

$$V_{cl} = \frac{l_r V_f \sin \alpha_1 + l_f V_r \sin \alpha_2}{L}$$

January 11, 2016

JKA130 報告書

*T. Murakami* 41

## VIII. 補足



### ■ 兩輪駆動における旋回角加速度

#### ● 等速走行時

$$\ddot{\phi} = \frac{r}{L} (\dot{\theta}_f \dot{\alpha}_1 \cos \alpha_1 - \dot{\theta}_r \dot{\alpha}_2 \cos \alpha_2)$$

### ■ 後輪駆動における旋回角加速度

#### ● 等速走行時

$$\ddot{\phi} = \frac{r}{L} (\dot{\theta}_r \dot{\alpha}_1 \cos \alpha_1 - \dot{\theta}_r \dot{\alpha}_2 \cos \alpha_2)$$

January 11, 2016

JKA130 報告書

*T. Murakami* 42

## VIII. 補足



### ■ 両輪駆動におけるキャンバ角加速度

$$M_{11}\ddot{\theta} = -M_{12}\ddot{\theta}_f - M_{13}\ddot{\theta}_r - K_1 - G_1 - T_\theta^{dis}$$

### ■ 後輪駆動におけるキャンバ角加速度

$$M_{11}\ddot{\theta} = -M_{13}\ddot{\theta}_r - D_1\dot{\alpha}_1 - K'_1 - G_1 - T_\theta^{dis}$$

### ■ キャンバ角に関する外乱推定

$$M_{11n}\ddot{\theta} = -D_{1n}\dot{\alpha}_1 - D_{2n}\dot{\alpha}_2 - \tilde{T}_\theta^{dis}$$

$$\hat{T}_\theta^{dis} = \frac{g_c}{s + g_c} (M_{11n}g_c\dot{\theta} - D_{1n}\dot{\alpha}_1 - D_{2n}\dot{\alpha}_2) - M_{11n}g_c\dot{\theta}$$

January 11, 2016

JKA130 報告書

T. Murakami 43

## 報告II：小型2輪車での初期段階実験



報告書I(p45～p60)は、前後輪ステアリングと後輪駆動システムを有する小型2輪システムによる静止・走行動作の安定化制御手法の提案と検証実験を示したものである。特に、動作モードによる制御系の構成法を提案している。

January 11, 2016

JKA130 報告書

T. Murakami 44

# Introduction of Two-wheel System



## Aim of Study

1. Self-balancing by two-wheel steering controlling at low speed.
2. Find out a suitable posture controller.

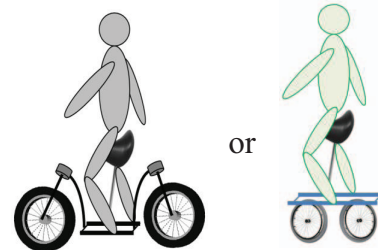


Fig.II-1 Conceptual sketch of the handleless motorcycle.

## Key Problems

Steering work motion and posture controller design.

### \*Advantages:

1. Feel more safety for moving forward.
2. Sport utility EV.
3. Only one driver for moving.

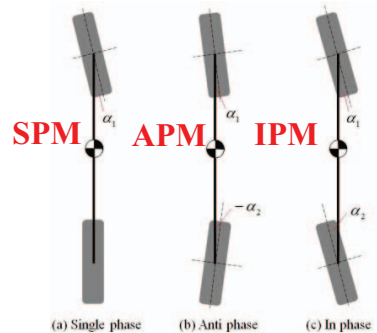


Fig.II-2 Three kinds of steering modes.

January 11, 2016

JKA130 報告書

T. Murakami 45

# Modeling of Two-wheel System



In Fig.4 the geometry of motorcycle are:

$$R_2 \tan(\varphi_1) = \frac{L}{2} \quad (\text{II.1})$$

$$R_2 \tan(\alpha_1) = L \quad (\text{II.2})$$

$$R \sin(\varphi_1) = \frac{L}{2} \quad (\text{II.3})$$

where  $\varphi_1$  or  $\varphi_2$  is the angle of motorcycle motion at CoM,  $\alpha_1, \alpha_2$  are steering angles of front and rear respectively.

If  $\alpha_1$  and  $\varphi_1$  are small, denote  $\varphi$  is the direction angle of CoM, thus for the SPM:

$$\varphi = \varphi_1 \approx \frac{\alpha_1}{2} \quad (\text{II.4})$$

$$R \approx \frac{L}{\alpha_1} \quad (\text{II.5})$$

For the IPM:

$$\varphi \approx \alpha_1 = -\alpha_2 \quad (\text{II.6})$$

$$R \approx \frac{L}{2\alpha_1} \quad (\text{II.7})$$

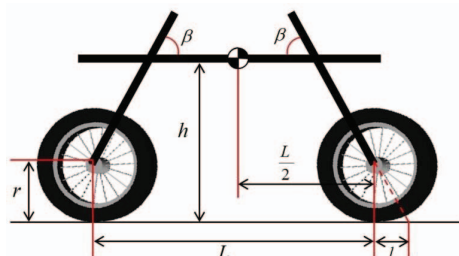


Fig.II-3 Motorcycle modeling.

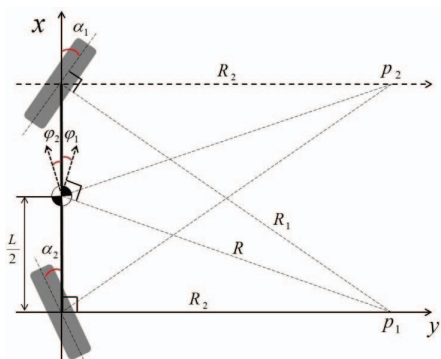


Fig.II-4 Top view in the world coordinates.

January 11, 2016

JKA130 報告書

T. Murakami 46

# Modeling of Two-wheel System



In Fig.II-5,  $\theta$  is the camber angle,  $F$  is composite force of centrifugal force  $F_o$  and steering rotation force  $F_r$ , for the SPM,

$$F = F_o + F_r \quad (\text{II.8})$$

$$F_r = \frac{mv^2}{R} \approx \frac{mv^2\alpha_1}{L} \quad (\text{II.9})$$

where  $v$  is motorcycle moving velocity,  $m$  is mass.

If the steering axis angle  $\beta$  is 90 degree,

$$F_r = m\left(\frac{v}{2} \frac{d\alpha_1}{dt}\right) \quad (\text{II.11})$$

By using the Newton's second,

$$mgh\sin\theta - Fh\cos\theta = J\ddot{\theta} \quad (\text{II.13})$$

Assume the camber angle is small, then,

$$mgh\theta - Fh = J\ddot{\theta} \quad (\text{II.14})$$

The dynamics for the SPM is,

$$J\ddot{\theta} - mgh\theta = -\frac{mhv^2\alpha_1}{L} - \frac{mhv\dot{\alpha}_1}{2} \quad (\text{II.15})$$

The dynamics for the APM and IPM are,

$$J\ddot{\theta} - mgh\theta = -\frac{2mhv^2\alpha_1}{L} - mhv\dot{\alpha}_1 \quad (\text{II.16}) \quad J\ddot{\theta} = mgh\theta \quad (\text{II.17})$$

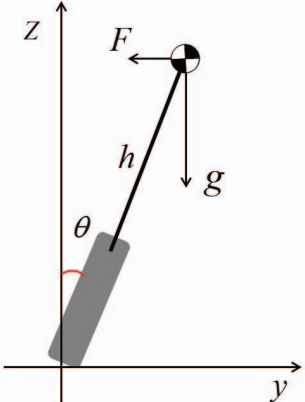


Fig.II-5 Rear view of a naive motorcycle  
(both front and rear steering angles are zero).

# Modeling of Two-wheel System



But the steering axis angle  $\beta$  is not 90 degree in the real applications, thus the design of the front fork or rear fork has a major impact on motorcycle dynamics. For the SPM, the steering angle influences the camber angle.

$$\theta_f = \theta - \alpha_1 \cos \beta \quad (\text{II.18})$$

Then effective front fork angle is,

$$\alpha_{1f} = \alpha_1 \sin \beta \quad (\text{II.19})$$

A new torque is generated by shifting the CoM while the steering is rotating,

$$\tau_f = \frac{-mg l \sin \beta}{2} \alpha_1 \quad (\text{II.20})$$

The final dynamics are:

$$\text{SPM: } J\ddot{\theta} - mgh\theta = -\frac{m(hv^2 - \frac{L}{2}gl)\sin \beta}{L} \alpha_1 - \frac{mhv\sin \beta}{2} \dot{\alpha}_1 \quad (\text{II.21})$$

$$\text{APM: } J\ddot{\theta} - mgh\theta = \frac{m(Lgl - 2hv^2)\sin \beta}{L} \alpha_1 - (mhv\sin \beta) \dot{\alpha}_1 \quad (\text{II.23})$$

For the IPM, the two steering generate the new torque in the opposite direction, thus torque is equal to zero.

# Modeling of Two-wheel System



To make the motorcycle self-balancing even it stops, the IPM (like Segway) is applied. In Fig.6,

$$\dot{x} \sin \phi - \dot{y} \cos \phi = 0 \quad (\text{II.24})$$

$$\dot{x} \cos \phi + \dot{y} \sin \phi + \frac{L \sin \alpha_1}{2} \dot{\phi} = r \dot{\theta}_f \quad (\text{II.25})$$

$$\dot{x} \cos \phi + \dot{y} \sin \phi - \frac{L \sin \alpha_1}{2} \dot{\phi} = r \dot{\theta}_r \quad (\text{II.26})$$

where  $\phi$  is the motorcycle orientation.  $\theta_f, \theta_r$  are the rotate angles of front and rear wheel respectively.

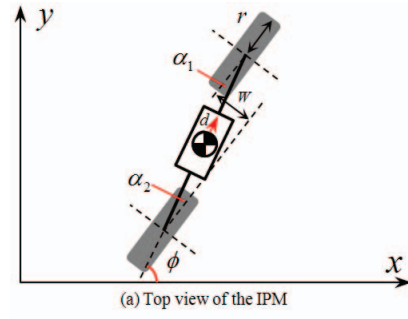
Its moving velocity  $\dot{d}$  and angular velocity  $\dot{\phi}$  are,

$$\dot{d} = \frac{r}{2}(\dot{\theta}_f + \dot{\theta}_r) \quad (\text{II.27})$$

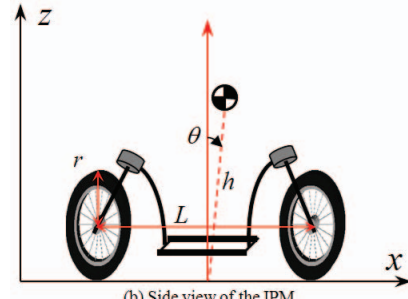
$$\dot{\phi} = \frac{2}{L \sin \alpha_1}(\dot{\theta}_f - \dot{\theta}_r) \quad (\text{II.28})$$

**Kinematics of the IPM:**

$$\begin{bmatrix} \dot{\theta} \\ \dot{d} \\ \dot{\phi} \end{bmatrix} = \begin{bmatrix} 1 & 0 & 0 \\ 0 & r/2 & r/2 \\ 0 & r/L \sin \alpha_1 & -r/L \sin \alpha_1 \end{bmatrix} \begin{bmatrix} \dot{\theta}_f \\ \dot{\theta}_r \\ \dot{\phi} \end{bmatrix} = J\ddot{q} \quad (\text{II.29})$$



(a) Top view of the IPM



(b) Side view of the IPM

Fig.II-6 IPM modeling.

# Modeling of Two-wheel System



By solving Lagrange equation,

$$\tau = \frac{d}{dt} \frac{\partial L}{\partial \dot{q}} - \frac{\partial L}{\partial q} \quad (\text{II.31})$$

where  $q = [\theta \ \theta_f \ \theta_r]^T$  and  $\tau = [\tau_\theta \ \tau_{\theta_f} \ \tau_{\theta_r}]^T$ .

**Dynamics of the IPM:**

$$\tau = M(q)\ddot{q} + H(q, \dot{q}) + G(q) \quad (\text{II.32})$$

where,

$$M = \begin{bmatrix} M_{uu} & M_{ua} & M_{ua} \\ M_{ua} & M_{ff} & M_{fr} \\ M_{ua} & M_{fr} & M_{rr} \end{bmatrix}$$

$$H = \begin{bmatrix} H_u \\ H_f \\ H_r \end{bmatrix}, \quad G = \begin{bmatrix} G_u \\ G_f \\ G_r \end{bmatrix}$$

In this study, only straight motion of the IPM is considered, therefore,

$$\tau_w = \tau_f + \tau_r$$

$$\theta_w = \theta_f = \theta_r$$

**New dynamics of the IPM:**

$$M = \begin{bmatrix} M_{uu} & M_{ua} \\ M_{ua} & M_{aa} \end{bmatrix} \quad (\text{II.35})$$

$$H = \begin{bmatrix} H_u \\ H_a \end{bmatrix}, \quad G = \begin{bmatrix} G_u \\ G_a \end{bmatrix} \quad (\text{II.36})$$

For linearization, the nominal inertia matrix,

$$M_n = \begin{bmatrix} M_{nuu} & M_{nua} \\ M_{nua} & M_{naa} \end{bmatrix} \quad (\text{II.37})$$

# Modeling of Two-wheel System



## The IPM Synthesized Camber Angle Disturbance Observer (SCOB)

$T_c^{dis}$  is the camber angle disturbance and  $T_w^{dis}$  is the wheel angle disturbance.

$$M_{uu}\ddot{\theta}^{res} + M_{ua}\ddot{\theta}_w^{res} + G_u + H_u + T_c^{dis} = 0 \quad (\text{II.38})$$

$$M_{ua}\ddot{\theta}^{res} + M_{aa}\ddot{\theta}_w^{res} + H_a + T_w^{dis} = T_w^{ref} \quad (\text{II.39})$$

In Fig.II-7, the synthesized camber angle disturbance is,

$$M_{nuu}\ddot{\theta}^{res} + \frac{M_{nua}}{M_{naa}}T_w^{ref} = -\hat{T}_s^{dis} \quad (\text{II.44})$$

The estimated synthesized camber angle disturbance is,

$$\tilde{T}_s^{dis} = -\frac{g_s}{s+g_s}(\frac{M_{nua}}{M_{naa}}T_w^{ref} - M_{nuu}g_s\dot{\theta}^{res}) - M_{nuu}g_s\dot{\theta}^{res} \quad (\text{II.45})$$

where  $g_s$  is cut off frequency for pseudo differentiator.  $\tilde{T}_s^{dis}$  contains camber angle disturbance and wheel angle disturbance.

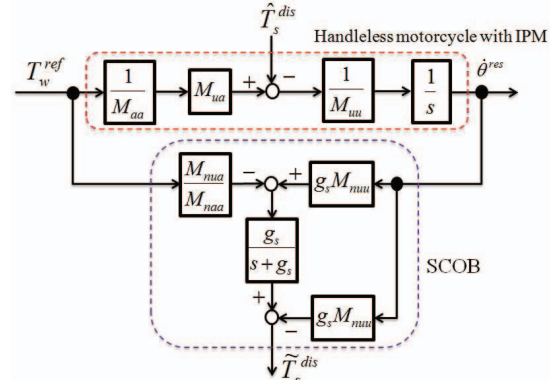


Fig.II-7 Synthesized camber angle disturbance observer.

January 11, 2016

JKA130 報告書

T. Murakami 51

## Controller Design for Two-wheel System

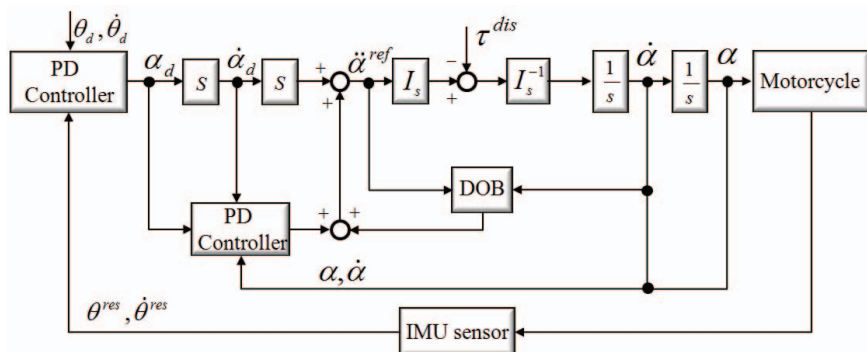


Fig.II-8 Posture control for the SPM and APM.

$$\text{Desired steering angle: } \alpha_d = K_m(\theta_d - \theta) + K_d(0 - \dot{\theta}) \quad (\text{II.46})$$

where,  $K_m$  and  $K_d$  are the PD gains.

$$\text{Acceleration reference: } \ddot{\alpha}^{ref} = \ddot{\alpha}_d + K_n(\dot{\alpha}_d - \dot{\alpha}) + K_a(\alpha_d - \alpha) \quad (\text{II.47})$$

where,  $K_n$  and  $K_a$  are the steering rotate velocity and rotate angle gains respectively.

January 11, 2016

JKA130 報告書

T. Murakami 52

# Controller Design for Two-wheel System



The transfer function for the SPM from its final dynamics eq.(21),

$$G_s = \frac{\theta(s)}{\alpha_1(s)} = -\frac{\frac{mhv\sin\beta}{2}s + \frac{m(hv^2 - Lgl/2)\sin\beta}{L}}{Js^2 - mgh} \quad (\text{II.48})$$

It is an unstable system.

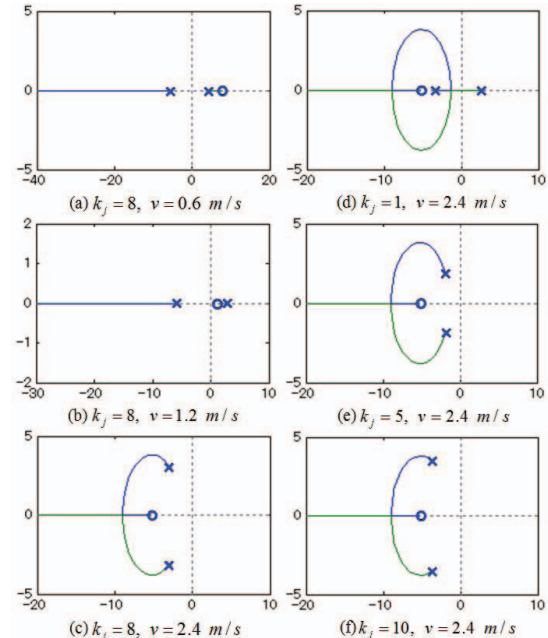
To get a stable system, active control is introduced, define the external force is  $\tau_e$  and the steering command is,

$$\alpha_1 = -k_i \tau_e + k_j \dot{\theta} \quad (\text{II.49})$$

A new closed-loop system,

$$\begin{aligned} J\ddot{\theta} + k_j m h v \sin \beta \dot{\theta} + [k_j \frac{m(2hv^2 - Lgl)\sin\beta}{L} - mgh]\theta \\ = k_i m h v \sin \beta \dot{\tau}_e + k_i \frac{m(2hv^2 - Lgl)\sin\beta}{L} \tau_e \end{aligned} \quad (\text{II.50})$$

The system is stable if  $k_j > 0$  and  $v > \sqrt{(\frac{1}{2k_j \sin \beta} + \frac{l}{2h})gL}$ . Fig.II-9 Root locus by variable speed and  $k_j$ .



January 11, 2016

JKA130 報告書

T. Murakami 53

# Controller Design for Two-wheel System

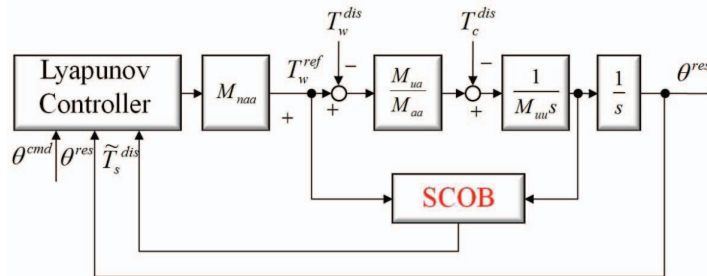


Fig.II-10 Lyapunov control for the IPM.

Lyapunov-Based Control for the IPM.

$$\text{Lyapunov candidate function: } V = \frac{1}{2} K_1 (\theta^{cmd} - \theta^{res})^2 + \frac{1}{2} K_2 (\dot{\theta}^{cmd} - \dot{\theta}^{res})^2 \quad (\text{II.54})$$

$$\text{From the SCOB and do once derivation: } V = (\dot{\theta}^{cmd} - \dot{\theta}^{res}) [K_1 (\theta^{cmd} - \theta^{res}) + \ddot{\theta}^{cmd} - \frac{K_2}{M_{nuu}} (M_{nua} \ddot{\theta}_w^{ref} + \tilde{T}_s^{dis})] \quad (\text{II.56})$$

$$\text{The acceleration of translational distance: } \ddot{\theta}_w^{ref} = \frac{M_{nuu}}{M_{nua}} [K_p (\theta^{cmd} - \theta^{res}) + K_v (\dot{\theta}^{cmd} - \dot{\theta}^{res})] - \frac{1}{M_{nua}} \tilde{T}_s^{dis} \quad (\text{II.57})$$

$$\Rightarrow \dot{V} = -K_3 (\dot{\theta}^{cmd} - \dot{\theta}^{res})^2 \leq 0 \quad (\text{II.58})$$

January 11, 2016

JKA130 報告書

T. Murakami 54

# Controller Design for Two-wheel System



Lyapunov controller gains,  $K_1, K_2, K_3$  are redesigned by,

$$K_p = \frac{K_1}{K_2}$$

$$K_v = \frac{K_3}{K_2}$$

Then the transfer function for the IPM system with SCOB is,

$$G_s = \frac{\theta^{res}}{\theta^{cmd}} = \frac{s^3 + B}{As^3 + B} \quad (\text{II.59})$$

where,

$$A = \frac{M_{uu}M_{aa}M_{nua}}{M_{nuu}M_{naa}M_{ua}}$$

$$B = (K_v + g_s)s^2 + (K_p + K_v g_s)s + K_p g_s$$

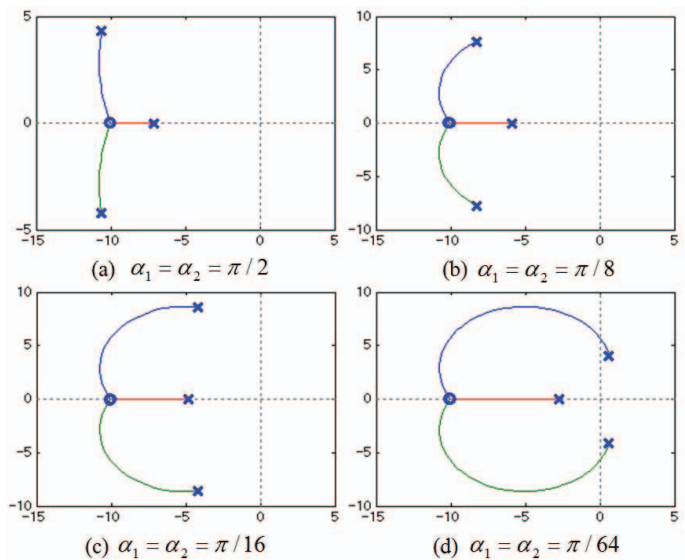


Fig.II-11 Root locus by variable steering angle.

January 11, 2016

JKA130 報告書

T. Murakami 55

# Experiments for Two-wheel System

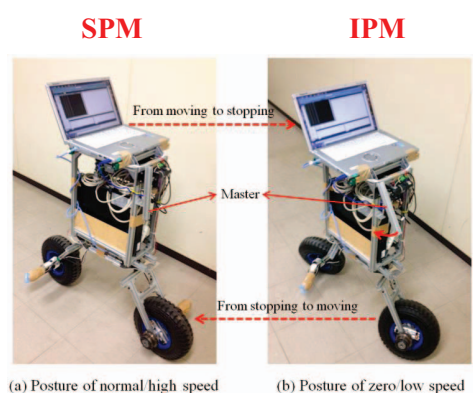
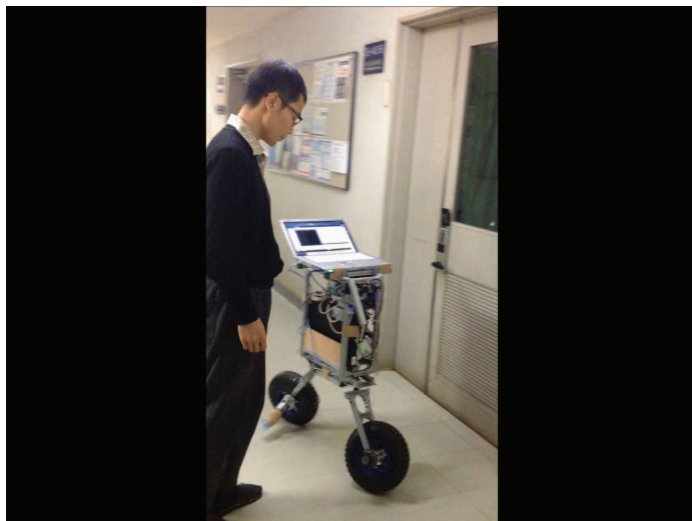


Fig.II-18 A photograph of the final handleless motorcycle.

Wheel radius: 13 cm

Wheel rotate speed: 60 rpm

Moving speed: 0.82 m/s

January 11, 2016

JKA130 報告書

T. Murakami 56

# Experiments for Two-wheel System

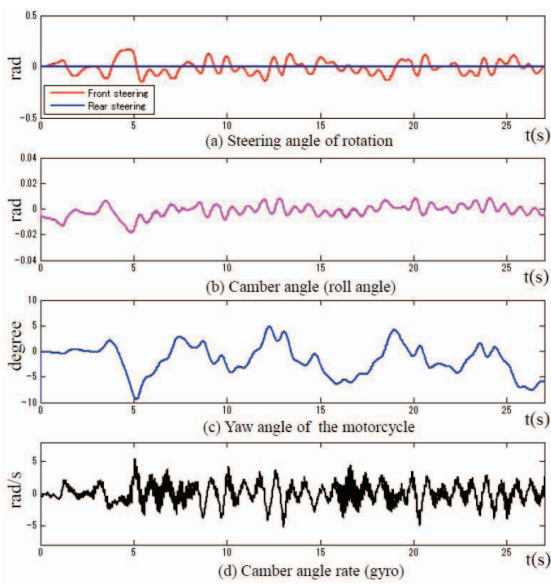


Fig.II-13 The SPM performance on a straight way.



Good self-balancing performance.



Fig.II-12 Experiment photograph on a straight way.

\*Fig.13(a) :plays a major role in keeping self-balancing.

\*Fig.13(b) :the direct expression of self-balancing.

\*Fig.13(c) :a parameter to measure the orientation when the motorcycle running on the straight way.

\*Fig.13(d) :angle rate command for the steering.

January 11, 2016

JKA130 報告書

T. Murakami 57

# Experiments for Two-wheel System

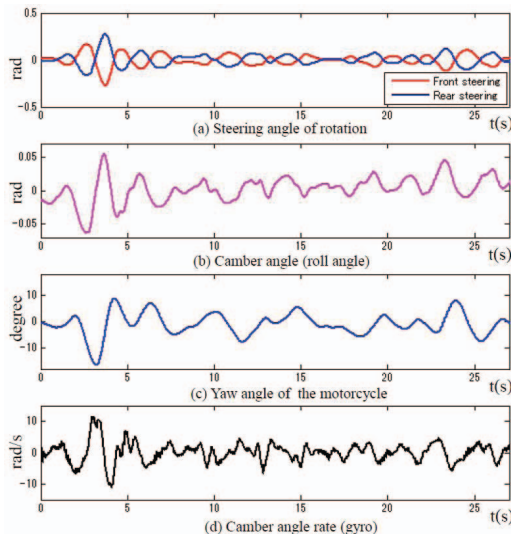


Fig.II-14 The APM performance on a straight way.



Performance is not good.

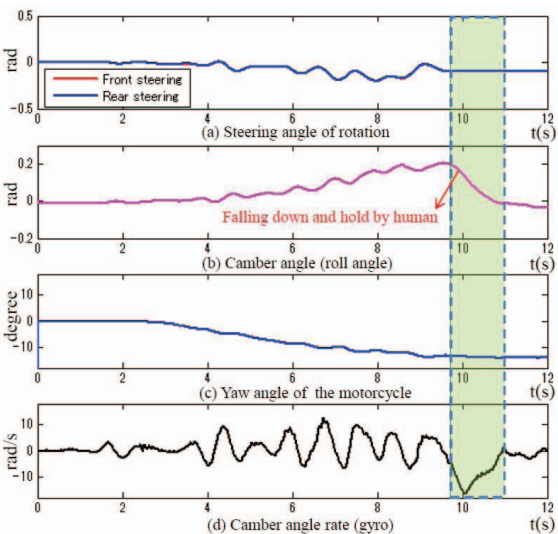


Fig.II-15 The IPM performance without speed control on a straight way.



Failure for the balanced straight moving.

January 11, 2016

JKA130 報告書

T. Murakami 58

# Experiments for Two-wheel System



MURA  
KAMI  
LAB.

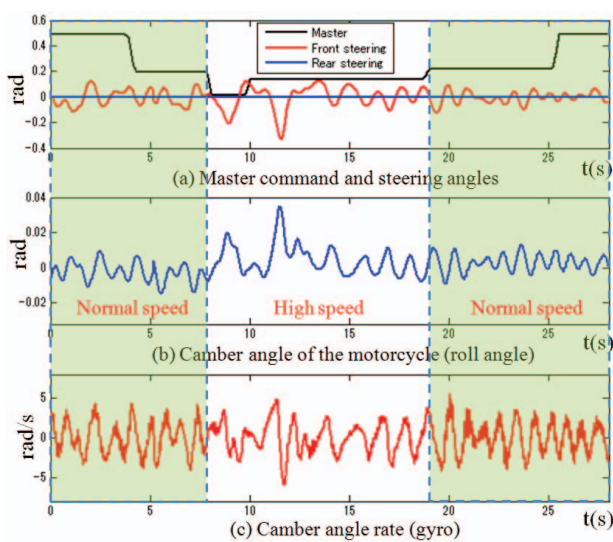


Fig.II-16 The SPM runs by variable speed on a straight way.

SPM for straight moving.

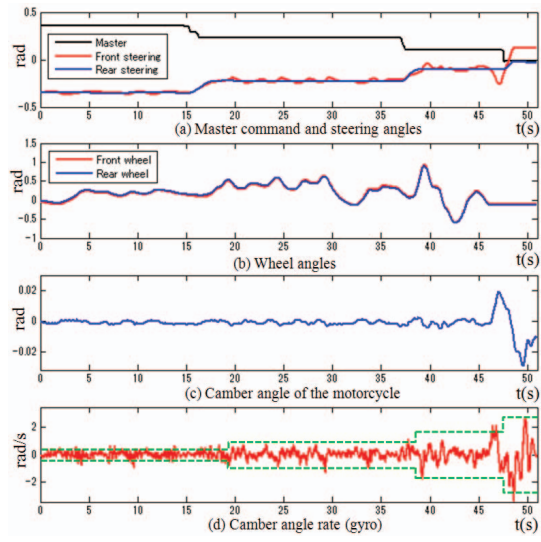


Fig.II-17 The IPM with Lyapunov control stands by variable steering angle.

IPM for stopping.

January 11, 2016

JKA130 報告書

T. Murakami 59

# Experiments for Two-wheel System



MURA  
KAMI  
LAB.

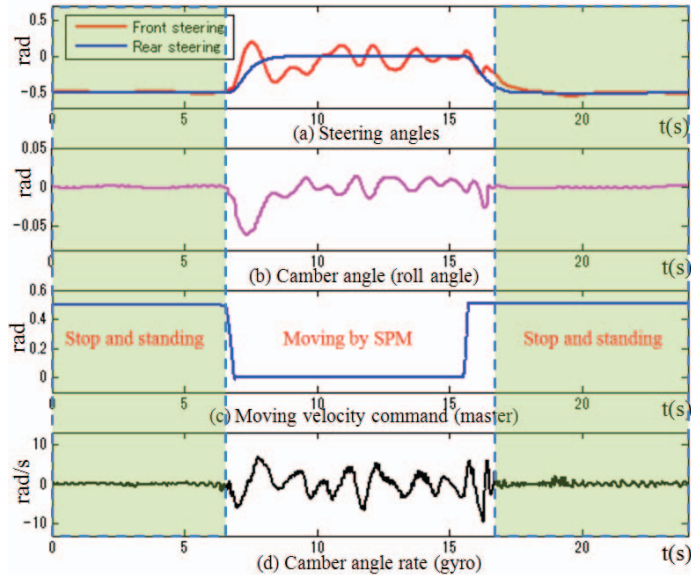


Fig.II-19 Final and total results of the proposal.

\*0 – 7 s, the motorcycle keeps standing by the IPM with Lyapunov control.

\*8 – 16 s, the motorcycle moves at a normal speed by the SPM with posture control.

\*After 17 s, the motorcycle stops and stands again.

\*The motorcycle can keep relatively self-balancing in full speed range.

January 11, 2016

JKA130 報告書

T. Murakami 60

学会等への発表

1. Chuan Yang, Seonghye KIM, Takahiro Nozaki, Toshiyuki Murakami, "A Self-Balancing Performance Comparison of Three Modes of Handleless Electric Motorcycles", INDIN 2015 IEEE International Conference on Industrial Informatics, pp352-357, Cambridge, UK, 2015
2. Toru Oiki and Toshiyuki Murakami, "Inspection of Interference in a Decentralized Control of Redundant Master-Slave System", The Fifth Asia International Symposium on Mechatronics, pp199-203, 2015 (JKA謝辞未記入)
3. Takamasa Abumi and Toshiyuki Murakami, "Posture Stabilization Control of Two-Wheel Drive Electric Motorcycle with Assistant Pendulum for Rider Motion", The Fifth Asia International Symposium on Mechatronics, pp201-209, 2015 (JKA謝辞未記入)
4. Sotaro Maejima and Toshiyuki Murakami, " Posture Stabilization Control of Two-Wheel Drive Electric Motorcycle with Assistant Pendulum for Rider Motion", IECON2015-Yokohama, pp1658-1661, 2015

# A Self-Balancing Performance Comparison of Three Modes of Handleless Electric Motorcycles

Chuan YANG, Seonghye KIM

School of Integrated Design Engineering,  
Keio University,  
Yokohama, Japan.  
Email: yang@sum.sd.keio.ac.jp

Takahiro NOZAKI, Toshiyuki MURAKAMI

Department of System Design Engineering,  
Keio University,  
Yokohama, Japan.  
Email: mura@sd.keio.ac.jp

**Abstract**—Since the two-wheel electric motorcycle has good portability and flexibility, it is popular in many countries nowadays. However, keeping the motorcycles balanced, which is a valuable research in an accelerating ageing society, has not been thoroughly researched. In this paper, a novel self-balancing electric motorcycle without the handlebar is put forward to cover this deficiency. By controlling the steering, the balance of the motorcycle can be kept with its wheels swaying. And the motorcycle direction can be operated by human body. Also, three different steering phases of handleless motorcycles were discussed. The difference of these three modes were showed by preliminary experimental results.

**Keywords**—self-balancing; handleless; steering control; three different phases

## I. INTRODUCTION

Considering the background of the ageing society in many countries, researchers need to focus on the people who merely have limited walking ability so that robots can provide these people with walking or transportation support. As a successful application of new automotive driving technology, Google's new driverless car [1] only contains two buttons (start and stop). With no steering, no gas pedal, and no driver, this revolutionary transportation technology makes possible the children and elders could operate a car very easily. With the development of new technology, two-wheel electric bicycles and motorcycles with good flexibility were invented and utilized as means of transportation too. A.V.Beznos *et al.* [2] described a bicycle with a gyroscopic stabilisation capable of autonomous motion along a straight line as well as along a curve. As a self-balancing electric motorcycle, Lit Motors C-1 [3] with two gyroscopic stabilizers can also keep its balance. However, the two gyroscopic stabilizers are so weighed that the electric power it cost is largely increased, and the cruising distance is accordingly reduced. T.Kimura who works in Yamaha company *et al.* [4] developed a new mechanical two-wheel steering system for motorcycles. But the dynamics of this system was not included. In order to analyze the dynamics, Y.Zhang *et al.* [5][6] proposed the dynamics with an accurate steering mechanism model and nonlinear balance control for the one wheel steering systems. They also got some good experimental results.

For a simpler linearized dynamic model of the bicycle, K.J.Astrom *et al.* [7] proposed a stability and control method. Also, P.A.J.Ruijs *et al.* [8] and Y.Tanaka *et al.* [9] proposed a lateral dynamics of bicycle. But all of them only considered



Fig. 1: Conceptual sketch of the handleless motorcycle.

about the one steering electric bicycle or motorcycle system. Based on the linearized model and mechanical two-wheel steering system, in this paper, another dynamics method to keep the balance by steering control with a disturbance observer (DOB) [10] is studied. Fig.1 shows a conceptual sketch of the proposed handleless electric motorcycle. There are two steering wheels in the proposal. Both front and rear wheel can be effectively controlled to swaying to keep the balance. Although this proposal is somewhat similar with Segway [11], the difference between the two proposals is quite obvious. The balance of segway is kept by rotating its wheels forward and back, but the balance of the electric motorcycle in the proposal is kept by swaying its wheeling leftward and rightward. This is not the first time the two-wheel steering electric bicycle or motorcycle has been proposed. C.Nakagawa *et al.* [12] proposed a personal mobility vehicle with two-wheel steering and two-wheel driving. However, it was also based on the theory of Segway, although a two-wheel steering was added. And, it was not a self-balancing system which is a handy tool for the young and old drivers. In order to precisely measure the posture of the electric motorcycle, an inertial measurement unit (IMU) sensor is utilized in this research. The IMU sensor contains a 3-D accelerometer, a 3-D angular rate sensor and 3-D magnetometer. It can measure a good posture information for the robot [13] [14]. By studying the modeling of posture controller design for the proposed electric motorcycle, the self-balancing was achieved. Moreover, it is also a handy tool for the children and elders who want to ride a motorcycle.

The authors summarize the primary contributions of the paper as follows: 1) the dynamics modeling are introduced

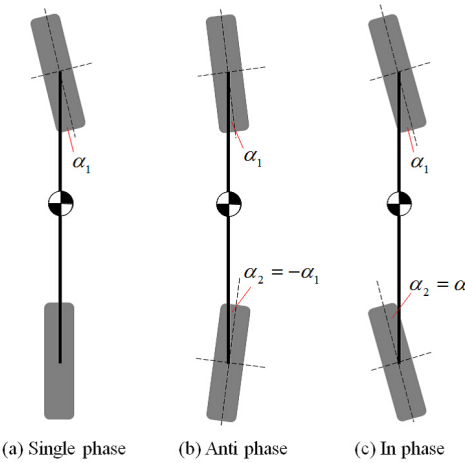


Fig. 2: Three kinds of steering working modes.

for the proposed electric motorcycle; 2) the performance of the three kinds of steering working modes are compared; 3) a control strategy is introduced for the two-wheel steering electric motorcycles without the handlebar at low speed. This paper is organized as follows. Section II explains the vehicle modeling of the proposed electric motorcycle. Three kinds of steering working mode are described. Also, their dynamics are studied. In Section III, the posture controller is designed. In Section IV, the preliminary experiments are done to determine stable systems. Finally, this paper is concluded and the future works are described in Section V.

## II. MOTORCYCLE DYNAMICS

In order to get a self-balancing electric motorcycle, the motorcycle dynamics modeling is described firstly. Fig.2 shows three kinds of steering working modes. Fig.2(a) is single phase mode (SPM) which means only the front steering rotating; Fig.2(b) is anti phase mode (APM), the front and rear steers rotate in the opposite direction; Fig.2(c) is in phase mode (IPM), the front and rear steers rotate in the same direction.  $\alpha_1$  and  $\alpha_2$  are the steering angles of front and rear wheel respectively. Fig.3 shows the geometry parameters of the electric motorcycle.  $r$  is the radius of wheel and  $L$  is wheelbase.  $\beta$  is the angle of the steering axis. Assuming the center of mass (CoM) of the motorcycle is the middle of wheelbase, thus the distance from the CoM to the wheel in vertical line is  $L/2$ .  $h$  is the height of CoM,  $l$  is the distance between the ground contact point of wheels and the cross point of the steering axis extension line with ground.

If the motorcycle run with constant steering angles and constant speed, the trajectory is a circular orbit. Fig.4 shows the top view of the motorcycle in the world coordinates.  $R$  is the radius of curvature around center of  $P_1$  or  $P_2$ .  $\varphi_1$  or  $\varphi_2$  is the angle of motorcycle motion at the CoM. The geometry of motorcycle can be calculated by the following equations,

$$R_2 \tan(\varphi_1) = \frac{L}{2} \quad (1)$$

$$R_2 \tan(\alpha_1) = L \quad (2)$$

$$R \sin(\varphi_1) = \frac{L}{2} \quad (3)$$

If the steering angle  $\alpha_1$  and the CoM motion angle  $\varphi_1$  are

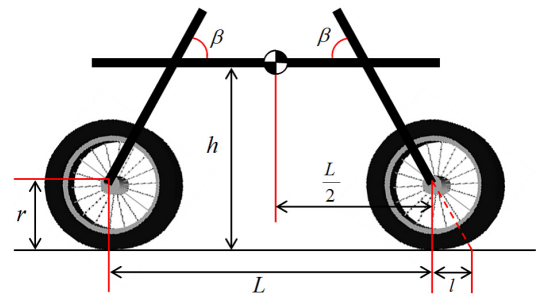


Fig. 3: Motorcycle modeling.

small, it can be linearized as  $\tan(\varphi_1) \approx \varphi_1$ ,  $\tan(\alpha_1) \approx \alpha_1$  and  $\sin(\varphi_1) \approx \varphi_1$ . In the SPM,  $\alpha_2$  is equal to zero. Denote  $\varphi$  is the direction angle of the CoM, then  $\varphi = \varphi_1 + \varphi_2$ . Therefore, the relationship between  $\alpha_1$  and  $\varphi$  is [7],

$$\varphi = \varphi_1 \approx \frac{\alpha_1}{2} \quad (4)$$

$$R \approx \frac{L}{\alpha_1} \quad (5)$$

In the APM,  $\alpha_2$  is equal to minus  $\alpha_1$ . The relationship between  $\alpha_1$  and  $\varphi$  is,

$$\varphi \approx \alpha_1 = -\alpha_2 \quad (6)$$

$$R \approx \frac{L}{2\alpha_1} \quad (7)$$

In the IPM,  $\alpha_2$  is equal to  $\alpha_1$ . This case looks like the Segway. The direction angle of the CoM is not depend on  $\alpha_1$  or  $\alpha_2$  anymore. But  $\varphi$  is depend on the different speed of the front and rear wheels. Fig.5 shows the rear view of the motorcycle with zero steering angles.  $\theta$  is the camber angle which means the inclination angle of the motorcycle.  $F$  is composite force of centrifugal force  $F_o$  and steering rotation force  $F_r$ .

$$F = F_o + F_r \quad (8)$$

Denote the motorcycle moving velocity is  $v$  and the mass is  $m$ . For the SPM,

$$F_o = \frac{mv^2}{R} \approx \frac{mv^2\alpha_1}{L} \quad (9)$$

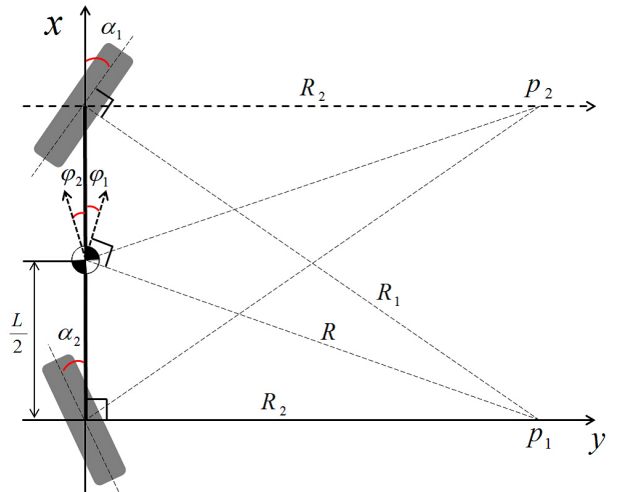


Fig. 4: Top view in the world coordinates.

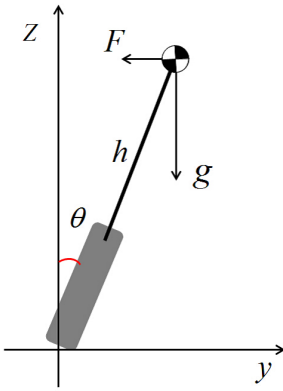


Fig. 5: Rear view of a naive motorcycle (both front and rear steering angles are zero).

And for the APM,

$$F_o \approx \frac{2mv^2\alpha_1}{L} \quad (10)$$

For the IPM, in this paper, both of the front and rear wheels are designed as the same speed. Thus its centrifugal force is equal to zero. If the steering axis angle  $\beta$  is equal to  $90^\circ$ ,  $F_r$  of the SPM can be found as [7],

$$F_r = m\left(\frac{1}{2}\frac{vda_1}{dt}\right) \quad (11)$$

For the APM, because the two steerings effect to the same direction,

$$F_r = m\frac{vda_1}{dt} \quad (12)$$

For the IPM, two steerings effect to the opposite direction, then  $F$  is equal to zero. From the Fig.5, dynamics of the motorcycle can be found by using the Newton's second.

$$mgh\sin\theta - Fh\cos\theta = J\ddot{\theta} \quad (13)$$

Assume the camber angle  $\theta$  is small, then  $\sin\theta \approx \theta$  and  $\cos\theta \approx 1$ , then the dynamics equation can be linearized as,

$$mgh\theta - Fh = J\ddot{\theta} \quad (14)$$

where  $J$  denotes the moment of inertia of the motorcycle body with respect to the  $x$  axis. Substitute the force  $F$ , then for the SPM,

$$J\ddot{\theta} - mgh\theta = -\frac{mhv^2\alpha_1}{L} - \frac{mhv\dot{\alpha}_1}{2} \quad (15)$$

For the APM,

$$J\ddot{\theta} - mgh\theta = -\frac{2mhv^2\alpha_1}{L} - mhv\dot{\alpha}_1 \quad (16)$$

For the IPM,

$$J\ddot{\theta} = mgh\theta \quad (17)$$

However, the steering axis angle  $\beta$  is not equal to  $90^\circ$ . Thus the design of the front fork or rear fork has a major impact on motorcycle dynamics. For the SPM, the steering angle influences the camber angle.

$$\theta_f = \theta - \alpha_1 \cos\beta \quad (18)$$

and the effective front fork angle is,

$$\alpha_{1f} = \alpha_1 \sin\beta \quad (19)$$

A new torque is generated by shifting the CoM while the steering is rotating [7].

$$\tau_f = \frac{-mglsin\beta}{2}\alpha_1 \quad (20)$$

Then the final dynamics for the SPM is,

$$J\ddot{\theta} - mgh\theta = -\frac{m(hv^2 - \frac{L}{2}gl)\sin\beta}{L}\alpha_1 - \frac{mhv\sin\beta}{2}\dot{\alpha}_1 \quad (21)$$

For the APM, the two steerings generate the new torque in the same direction, thus,

$$\tau_f = -mgla_1\sin\beta \quad (22)$$

$$J\ddot{\theta} - mgh\theta = -\frac{m(2hv^2 - Lgl)\sin\beta}{L}\alpha_1 - (mhv\sin\beta)\dot{\alpha}_1 \quad (23)$$

For the IPM, the two steers generate the new torque in the opposite direction, thus  $\tau_f$  is equal to zero.

### III. POSTURE CONTROLLER DESIGN

Consider about the transfer function for the SPM from its final dynamics in eq.(21),

$$G_s = \frac{\theta(s)}{\alpha_1(s)} = -\frac{\frac{mhv\sin\beta}{2}s + \frac{m(hv^2 - Lgl/2)\sin\beta}{L}}{Js^2 - mgh} \quad (24)$$

If  $v < \sqrt{Lgl/h}$ , this transfer function has one pole and one zero in the right-half plane. Such a system is not easy to control robustly when the pole and zero are too close [15]. But the problem with right-zeros can be eliminated by introducing extra sensors and actuators [7]. Thus in the space form, the state variables can be defined  $x = [\theta \quad \dot{\theta} - k\alpha_1]^T$ , where  $k = -\frac{mhv\sin\beta}{2J}$ . And the input  $u = \alpha_1$ , then,

$$\begin{bmatrix} \dot{x}_1 \\ \dot{x}_2 \end{bmatrix} = \begin{bmatrix} 0 & 1 \\ \frac{mgh}{J} & 0 \end{bmatrix} \begin{bmatrix} x_1 \\ x_2 \end{bmatrix} + \begin{bmatrix} -\frac{mhv\sin\beta}{2J} \\ -\frac{m(hv^2 - Lgl/2)\sin\beta}{JL} \end{bmatrix} u \quad (25)$$

By the same principle, for the APM, the transfer function is,

$$G_s = \frac{\theta(s)}{\alpha_1(s)} = -\frac{(mhv\sin\beta)s + \frac{m(2hv^2 - Lgl)\sin\beta}{L}}{Js^2 - mgh} \quad (26)$$

Redefine the  $k = -\frac{mhv\sin\beta}{J}$ , the state-space function is,

$$\begin{bmatrix} \dot{x}_1 \\ \dot{x}_2 \end{bmatrix} = \begin{bmatrix} 0 & 1 \\ \frac{mgh}{J} & 0 \end{bmatrix} \begin{bmatrix} x_1 \\ x_2 \end{bmatrix} + \begin{bmatrix} -\frac{mhv\sin\beta}{2J} \\ -\frac{m(2hv^2 - Lgl)\sin\beta}{JL} \end{bmatrix} u \quad (27)$$

$$y = [1 \quad 0] \begin{bmatrix} x_1 \\ x_2 \end{bmatrix} \quad (27)$$

This method make the two state convert to zero. It means that the self-balancing with straight heading is possible. The motorcycle orientation is controlled by human body. It means that if the CoM is changed by human body, the orientation is forced to change. But after the human body recovers to the vertical state, self-balancing with straight heading works again. For the IPM, because the self-balancing method is similar to

the Segway, only the preliminary experiments for comparison will be introduced in the following sections. As a future work, its self-balancing method will be studied. In this section, the proposed control strategy for the self-balancing is described. And in this paper, for the APM and IPM, the two-steering motion are considered. It means that there are two different relationships of  $\alpha_1$  and  $\alpha_2$ ,

$$\alpha_1 = -\alpha_2 \quad (28)$$

$$\alpha_1 = \alpha_2 \quad (29)$$

when  $\alpha_1$  equates to  $\alpha_2$ , the front and rear steerings are rotating in the same motion. On the opposite, if  $\alpha_1$  equates to minus  $\alpha_2$ , the front and rear steerings are rotating in the reverse motion.

If the motorcycle moving speed is not very high and the steering angle is small, it is assumed that this linearized model is enough. From the equation (23), the camber angle  $\theta$  is depending on the steering angle  $\alpha_1$  or  $\alpha_2$ . Denoting  $\alpha = |\alpha_1| = |\alpha_2|$ , the desired steering angle  $\alpha_d$  can be given by,

$$\alpha_d = K_p(\theta_d - \theta) + K_d(0 - \dot{\theta}). \quad (30)$$

where,  $K_p$  and  $K_d$  are the PD gains respectively. Then the steering acceleration reference  $\ddot{\alpha}_2^{ref}$  is determined by,

$$\ddot{\alpha}^{ref} = \ddot{\alpha}_d + K_v(\dot{\alpha}_d - \dot{\alpha}) + K_a(\alpha_d - \alpha). \quad (31)$$

where,  $K_v$  and  $K_a$  are the rotate angle velocity and rotate angle gains respectively. Fig.6 shows posture controller block diagram for the self-balancing electric motorcycle.

#### IV. EXPERIMENTS

In this section, experiment procedures and results are explained. In order to compare with the performance of the three kinds of steering working modes, all of the three types (SPM, APM and IPM) are confirmed by experiments. Fig.7 shows a photograph of the real handleless electric motorcycle. An iBIS system that is a PC based DSP was used as a processor in this vehicle. A 24V battery was used to supply power for the whole system. An IMU sensor is fixed on the top of the motorcycle to measure the gyro (roll angular rate), roll angle and yaw angle. Table 1 shows physical parameters of the motorcycle and actuators.

##### A. Experiment Procedures

The experiments were implemented on a straight way firstly. All of the three types (SPM, APM and IPM) are

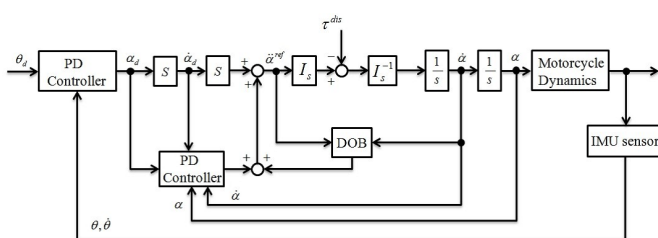


Fig. 6: Block diagram of the motorcycle posture controller.



Fig. 7: A photograph of the proposed vehicle.

tested to achieve self-balancing respectively. For the SPM, the steering command is,

$$\begin{aligned} \alpha_1 &= K_1(\theta - \theta_{int}) + K_2\dot{\theta} \\ \alpha_2 &= 0 \end{aligned} \quad (32)$$

where,  $\theta_{int}$  is the initial camber angle for the motorcycle body balance,  $K_1$  and  $K_2$  are gains between camber angle and camber angle rate. For the APM, the steering command is,

$$\begin{aligned} \alpha_1 &= K_3(\theta - \theta_{int}) + K_4\dot{\theta} \\ \alpha_2 &= -K_3(\theta - \theta_{int}) - K_4\dot{\theta} \end{aligned} \quad (33)$$

the front and rear steering angle command is set as a smaller gain than the SPM. For the IPM, the steering command is,

$$\begin{aligned} \alpha_1 &= K_5(\theta - \theta_{int}) + K_6\dot{\theta} \\ \alpha_2 &= K_5(\theta - \theta_{int}) + K_6\dot{\theta} \end{aligned} \quad (34)$$

the steering angle gains are smaller than the SPM as well. Then experiments were implemented on a right angle way. Because the IPM is similar to Segway, the control method is different. Therefore, only the SPM and APM are tested in these experiments respectively.

##### B. Experiment Results

When the electric motorcycle runs in a high speed, it is more easy to keep self-balancing. However, if the electric motorcycles can keep self-balancing at a low speed, the performance comparison is more meaningful. Therefore, in this

TABLE I: Physical parameters of the motorcycle.

Name	Value
Wheel radius $r$ [m]	0.13
Structure wheelbase $L$ [m]	0.63
Distance $l$ [m]	0.48
Steering axis angle $\beta$ [ $^\circ$ ]	30
CoM vertical position $h$ [m]	0.8
Mass of motorcycle body $m$ [kg]	25.1
Speed of driving wheel $\omega$ [rpm]	30
Motorcycle normal moving speed $v$ [m/s]	0.82
Rotary encoder resolution $R_e$ [PPR]	400000
Gear reduction of motors $G_r$	100

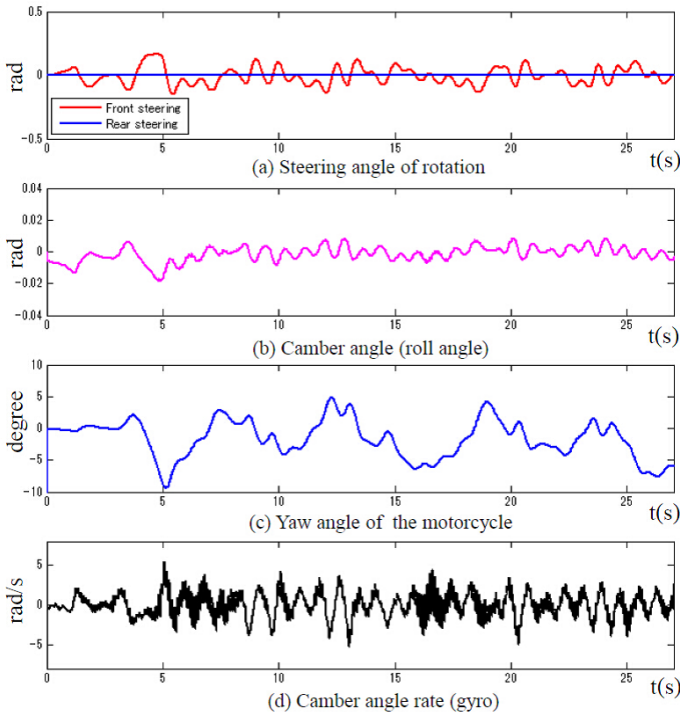


Fig. 8: The SPM performance on a straight way.

paper, the handleless electric motorcycle driving motors runned as a low speed (30 rpm). Fig.8 shows the SPM performance on a straight way. Fig.8(a) indicates the angle of the front and rear steering rotation. They play a major role in keeping self-balancing. Fig.8(b) shows the camber angle of the electric motorcycle body. It is the direct expression of self-balancing. Fig.8(c) indicates the yaw angle of the motorcycle body. This is a parameter to measure the orientation when the motorcycle running on the straight way. Fig.8(d) shows the camber angle rate. It is the angle rate command for the steering. Fig.9 shows the IPM performance on the straight way. Fig.9(a) and (b) indicate the steering rotation range is bigger than the SPM, but the motorcycle body sway frequency is smaller than the SPM. Fig.9(c) and (d) indicate the APM has a bigger yaw angle and camber angle rate than the SPM.

Since the IPM is similar to Segway, if the experiment is only implemented by steering control, it is not easy to keep self-balancing. The results are showed in Fig.10. It indicates that the IPM could not keep self-balancing after 10 second. And Fig.10(c) shows the motorcycle orientation could not be changed during the moving. That is why the SPM cannot keep self-balancing for a longer time. In order to achieve the self-balancing, the SPADO [16] is applied. Then the new results are showed in Fig.11. It combines the advantages of the SPM and Segway. But the speed must be changing during the moving because of the speed control. Therefore, it is worth to do a further study in the future works.

Because this paper proposed a handleless electric motorcycle, the turning performance which is controlled by human body should be studied as well. As the IPM has not been studied well, only the performance comparison of SPM and APM on the right angle way is showed in Fig.12. Fig.12(a) indicates the camber angle difference of the SPM and APM. For stability, the SPM has a better performance. But Fig.12(b) shows that the APM has a better turning performance than

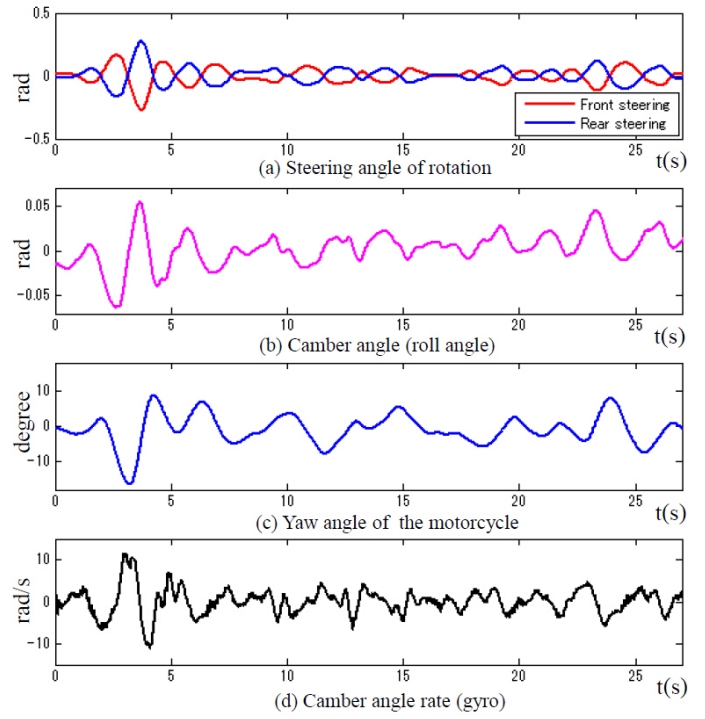


Fig. 9: The APM performance on a straight way.

the SPM. It means that the APM has a more faster and more convenient turning performance. The advantages and disadvantages of each mode should be considered when a novel motorcycle system is designed. In this paper, only the self-balancing performance of three modes of handleless electric motorcycles was compared. In short, the IPM has a good low speed stability and the SPM has a high speed stability, a novel motorcycle system with both of these two advantages will be studied in the future works.

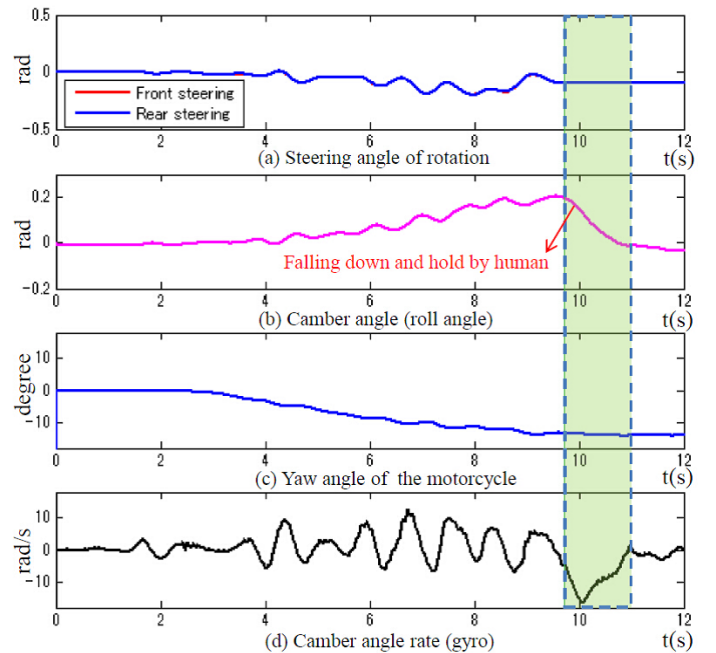


Fig. 10: The IPM performance without speed control on a straight way.

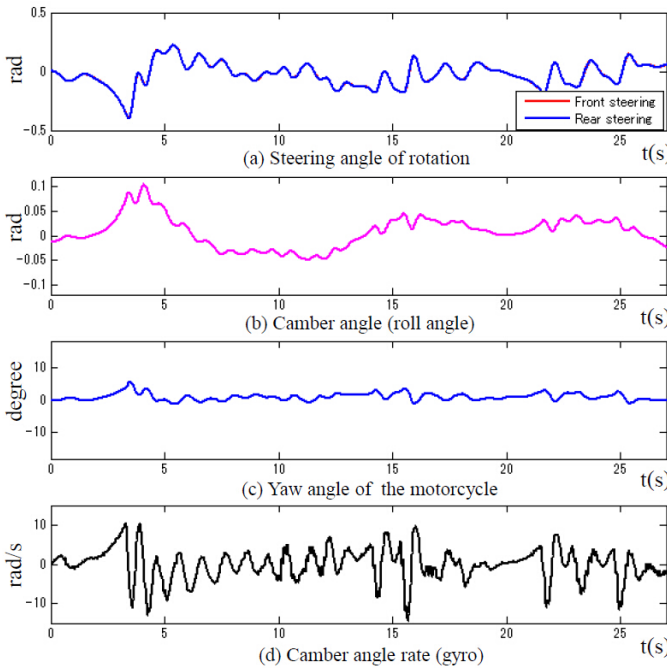


Fig. 11: The IPM performance with speed control on a straight way.

## V. CONCLUSION AND FUTURE WORKS

In the paper, three kinds of steering working modes (SPM, APM and IPM) of the handleless electric motorcycle were introduced. The preliminary experiment results showed the performance comparison of them. The SPM has the best self-balancing stability. Its speed can be controlled by rider's feet in the practical application. The APM only has the fastest turning performance. The IPM possesses both of stability and flexibility, but its speed is not easy to be controlled. In addition, because the orientation of motorcycle was controlled by human body, it is possible to get a stable electric motorcycle robot system without the handlebar. In the future works, the IPM should be done in a further study. A seat can be fixed on the motorcycle as well, then it can be ridden by human. Also, a better self-balancing controller should be studied.

## ACKNOWLEDGMENT

This report was subsidized in part by JKA(27-130) through its promotion funds from KEIRIN RACE.

## REFERENCES

- [1] Google's new driverless car website, <http://googleblog.blogspot.jp> (accessed: Jan. 10th, 2015)
- [2] A. V. Beznos, A.M. Formal'sky, E. V. Gurfinkel, D. N. Jicharev, A. V. Lensky, K. V.Savitsky, and L.S. Tchesalin, "Control of autonomous motion of two-wheel bicycle with gyroscopic stabilisation", in *Proceedings of the IEEE International Conference on Robotics and Automation*, vol.3, pp.2670-2675, 1998.
- [3] Self-balancing Lit Motors website, <https://litmotors.com/reserve/> (accessed: Jan. 10th, 2015)
- [4] T.Kimura, Y.Ando, and E.Tsuji, "Development of new concept two-wheel steering system for motorcycles", *SAE Technical Paper*, no. 2013-32-9106, 2013.
- [5] Y.Zhang, J.Li, J.Yi, and D.Song, "Balance control and analysis of stationary riderless motorcycles", in *Proceedings of the IEEE International Conference on Robotics and Automation*, pp. 3018-3023, 2011.
- [6] Y.Zhang, P.Wang, J.Yi, D.Song, and T.Liu, "Stationary balance control of a bikebot", in *Proceedings of the IEEE International Conference on Robotics and Automation*, pp. 6706-6711, 2014.
- [7] K.J.Astrom, R.E.Klein, and A.Lennartsson, "Bicycle dynamics and control", *IEEE Control Systems Magazine*, vol.25, no.4, pp.26-47, 2005.
- [8] P.A.J.Ruijs and H.B.Pacwka, "Research in lateral dynamics of motorcycles", *Vehicle System Dynamics*, vol.14, issue 1-3, pp.149-152, 1985.
- [9] Y.Tanaka and T.Murakami, "A study on straight-line tracking and posture control in electric bicycle", *IEEE Transactions on Industrial Electronics*, vol.56, no.1, 2009.
- [10] K.Ohnishi, M. Shibata, and T. Murakami, "Motion control for advanced mechatronics", *IEEE/ASME Transactions on Mechatronics*, vol.1, issue 1, pp.56-67, 1996.
- [11] H.G. Nguyen, J. Morrell, K. Mullens, A. Burmeister, S. Miles, N. Farrington, K.Thomas, and D.W. Gage, "Segway robotic mobility platform", in *Proceedings of the International Society for Optics and Photonics*, pp.207-220, 2004.
- [12] C.Nakagawa, Y.Suda, K.Nakano, and S.Takehara, "Stabilization of a bicycle with two-wheel steering and two-wheel driving by driving forces at low speed", *Journal of Mechanical Science and Technology*, vol.23, no.4, pp.980-986, 2009.
- [13] C.Yang and T.Murakami, "Novel walking assist device based on mobile manipulator and inertial measurement unit", *IEEJ Journal of Industry Applications*, vol.3, no.5, pp.381-387, 2014.
- [14] C.Yang and T.Murakami, "Walking-assist principle analysis for a multi-legged system", *IEEJ Journal of Industry Applications*, vol.4, no.3, pp.294-300, 2015.
- [15] S.Skogestad and I.Postlethwaite, "Multivariable feedback control: analysis and design", *New York: Wiley*, vol.2, 2007.
- [16] K.Hirata and T.Murakami, "A realization of step passage motion in two-wheel wheelchair systems utilizing variable repulsive compliance control", in *Proceedings of the IEEE International Symposium on Industrial Electronics*, pp.1-6, 2013.

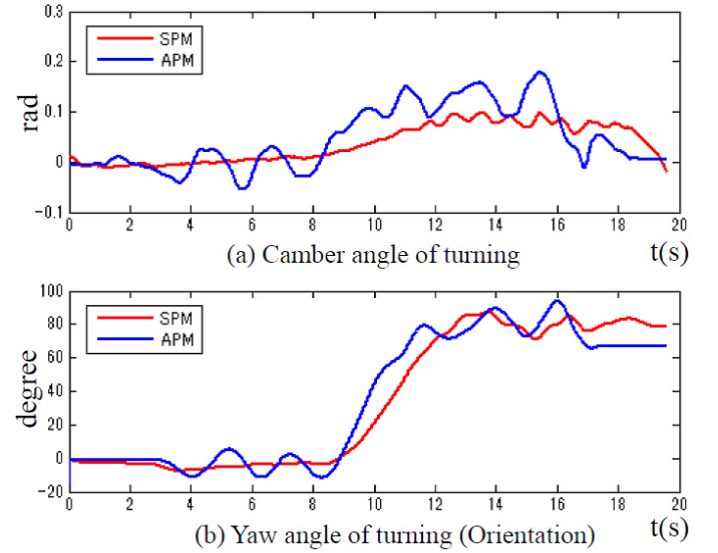


Fig. 12: The performance comparison of SPM and APM on the right angle way.

- 357

# Inspection of Interference in a Decentralized Control of Redundant Master-Slave System

**T. Oiki<sup>1</sup>, T. Murakami<sup>2</sup>**

<sup>1</sup>*Department of System Design Engineering, Keio University, Yokohama, Japan  
(Tel : +81-45-566-1741; E-mail: oiki@sum.sd.keio.ac.jp)*

<sup>2</sup>*Department of System Design Engineering, Keio University, Yokohama, Japan.  
(Tel : +81-45-566-1741; E-mail: mura@sd.keio.ac.jp)*

**Keywords:** bilateral control, autonomous control, disturbance observer(DOB), decentralized control, redundant manipulator

## Abstract

In this research, a unified control of autonomous control and bilateral control in redundant master-slave system is proposed. 2 DOF planar manipulator is used as a master robot, and 4 DOF planar manipulator is used as a slave robot. Autonomous control is applied to the 1st and 2nd link of slave robot, and bilateral control is applied to 3rd and 4th link of slave robot. In the proposed method, position control and force control are applied to each subsystem, and the influence on force response by the interference of position control and force control may happen. Experiments are conducted to confirm the influence by comparing the force response of conventional master-slave bilateral controller and proposed method. Furthermore, experiment which is introducing impedance control in place of position control is conducted.

## 1. INTRODUCTION

Recently, robots are used in various fields. There are cleaning robots, nursing care robots, rescue robots and so on. Among them, the most important and essential robots are industrial robots. Installation of industrial robots improved productivity tremendously and contributed to social development. These days most of the production tasks are conducted by robots. However, there are still some tasks which are difficult for robots to conduct. These are the tasks which require experienced skill of experts. In order to take the place of such experts, numerous sensors and complex programs are required.

Human-robot cooperation system is gaining attention to get the best of both worlds. One of the human assistive technologies is bilateral control with master and slave robots. Bilateral control is a technique to achieve haptic communication by transmitting position and force information between master and slave robots. This technology can be used for various situations such as disaster relief, surgery and nuclear reactors work.

Many researches about bilateral control have been conducted until today. Hannaford constructed an ideal relationship between master system and slave system based on hybrid matrix [1], and this relationship is formulated as "Transparency" [2]. Then, acceleration control on bilateral teleoperation is achieved by "Disturbance Ob-

server (DOB)" [3][4][5]. This enables to improve transparency of bilateral teleoperation. In addition, utilizing "Reaction Torque Observer (RTOB)", force-sensorless control is realized [6]. By using RTOB, bilateral control can be easily constructed without force sensor.

However, conventional bilateral controller has two serious problems. In practical situations, the operator operates the master robot according to the camera image from a remote place. However, there exist delays in transmission of visual and tactile information due to communication constraints. Thus, it is difficult to operate instantly in dynamic environment. Furthermore, in order to achieve complicated task, slave robot which has multi degree of freedom is needed. However, since the robot is redundant, it is difficult for humans to operate by using only master operation.

Thus, in order to reduce the workload of an operator who cannot obtain accurate information, the slave robot should be decomposed and perform some tasks autonomously rather than being totally controlled by the master robot. For this purpose, the slave robot must accurately detect such data on the manipulated object as its position and posture.

Cameras provide contactless measurement of the external world, which is helpful for operation in unknown environments, or in dynamically changing environments. In particular, with recent progress in cameras and computers, the cycles of both image capture and processing have become faster, and there have been attempts to use cameras as visual sensors for the autonomy of robots[8][9][10].

In this research, 2DOF planar manipulator is used as a master robot, and 4 DOF planar manipulator is used as a slave robot. A unified control of autonomous control and bilateral control in redundant master-slave system is proposed. Autonomous control is applied to the 1st and 2nd link of slave robot, and bilateral control is applied to 3rd and 4th link of slave robot.

However, in the proposed method, position control and force control are applied to each subsystem, and the influence on force response by the interference of position control and force control may happen. Impedance control is introduced in order to simplify the decentralized control system in redundant manipulator[12][13]. In the experiment, position control and impedance control are introduced into a subsystem, and compared each force response.

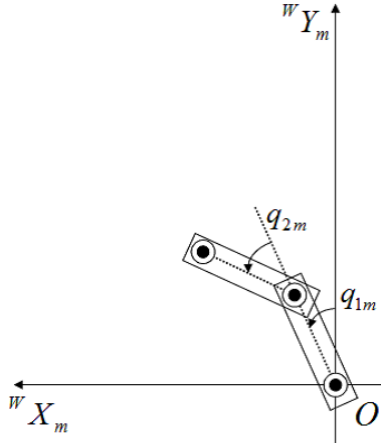


Fig. 1 Model of master robot

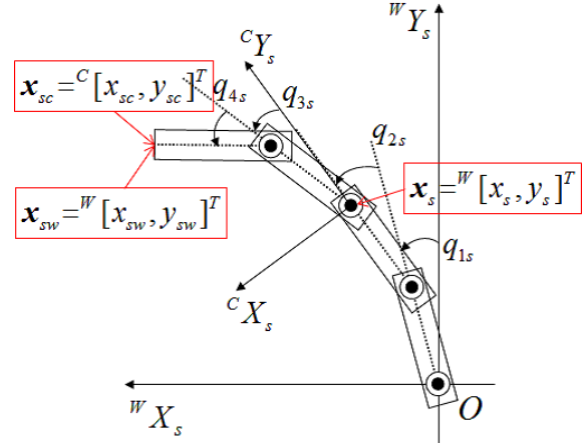


Fig. 2 Model of slave robot

This paper is organized as follows. In section 2, the modeling of master robot is introduced. In section 3, the modeling of slave robot is introduced. In section 4, the control system is designed. In section 5, the experiment is conducted to clarify the influence on interference of introducing proposed method. Finally, this paper is concluded and the future works are described in section 6.

## 2. MODELING OF MASTER ROBOT

In this section, the model of 2 DOF planar manipulator used as a master robot is described. The robot can move in two dimensions according to human operation. The architecture is shown in Fig.1.

### 2.1 Kinematics Modeling

In this subsection, kinematics of the master robot is described. The joint space coordinates can be written as  $\mathbf{q}_m = [q_{1m} \ q_{2m}]^T$ . The position of the master robot in work space is represented as 2-dimensional vector  $\mathbf{x}_m = [x_m \ y_m]^T$ . Forward and inverse kinematics can be derived as follows.

$$\dot{\mathbf{x}}_m = \mathbf{J}_m \dot{\mathbf{q}}_m \quad (1)$$

$$\dot{\mathbf{q}}_m = \mathbf{J}_m^{-1} \dot{\mathbf{x}}_m \quad (2)$$

where  $\mathbf{J}_m$  denotes the Jacobian matrix of the master robot. The Jacobian matrix of the master robot is used to perform mapping from work space to joint space, and it can be written as following equation.

$$\mathbf{J}_m = \begin{bmatrix} J_{m11} & J_{m12} \\ J_{m21} & J_{m22} \end{bmatrix} \quad (3)$$

$$J_{m11} = l_{1m} C_{1m} + l_{2m} C_{1m2m}$$

$$J_{m12} = l_{2m} C_{1m2m}$$

$$J_{m21} = -l_{1m} S_{1m} - l_{2m} S_{1m2m}$$

$$J_{m22} = -l_{2m} S_{1m2m}$$

where  $l_{1m}$  and  $l_{2m}$  represent length of each link.  $C_{im}$  and  $S_{im}$  represent  $\cos q_{im}$  and  $\sin q_{im}$ , respectively.

## 2.2 Dynamics Modeling

Dynamics equation of the master robot is derived from the Euler-Lagrange formulation and can be expressed in the joint space as equation (4).

$$\mathbf{T}_m = \mathbf{M}_m \ddot{\mathbf{q}}_m + \mathbf{h}_m \quad (4)$$

where  $\mathbf{M}_m$  is the inertia matrix, and  $\mathbf{h}_m$  represents the Coriolis and centrifugal force.  $\mathbf{T}_m$  is the 2-dimensional vector of control torques.

## 3. MODELING OF SLAVE ROBOT

In this section, the model of 4 DOF planar manipulator used as a slave robot is described. The architecture is shown in Fig.2.

### 3.1 Kinematics Modeling

In this subsection, kinematics of the slave robot is described. First, kinematics of 1st and 2nd link of the slave robot is described. The joint space coordinates can be written as  $\mathbf{q}_s = [q_{1s} \ q_{2s}]^T$ . The tip position of 2nd link in work space is represented as 2-dimensional vector  $\mathbf{x}_s = [x_s \ y_s]^T$ . Forward and inverse kinematics can be derived as follows.

$$\dot{\mathbf{x}}_s = \mathbf{J}_s \dot{\mathbf{q}}_s \quad (5)$$

$$\dot{\mathbf{q}}_s = \mathbf{J}_s^{-1} \dot{\mathbf{x}}_s \quad (6)$$

where  $\mathbf{J}_s$  denotes the Jacobian matrix of the slave robot. The Jacobian matrix of the slave robot is used to perform mapping from work space to joint space and it can be written as following equation.

$$\mathbf{J}_s = \begin{bmatrix} J_{s11} & J_{s12} \\ J_{s21} & J_{s22} \end{bmatrix} \quad (7)$$

$$J_{s11} = l_{1s} C_{1s} + l_{2s} C_{1s2s}$$

$$J_{s12} = l_{2s} C_{1s2s}$$

$$J_{s21} = -l_{1s} S_{1s} - l_{2s} S_{1s2s}$$

$$J_{s22} = -l_{2s} S_{1s2s}$$

where  $l_{1s}$ ,  $l_{2s}$  represent length of each link.  $C_{is}$  and  $S_{is}$  represent  $\cos q_{is}$  and  $\sin q_{is}$ , respectively.

Then, kinematics of 3rd and 4th link of the slave robot is described. The joint space coordinates can be written as  $\mathbf{q}_{sc} = [q_{3s} \ q_{4s}]^T$ . The position of end-effector in work space which origin is the tip position of 2nd link is represented as 2-dimensional vector  $\mathbf{x}_{sc} = [x_{sc} \ y_{sc}]^T$ . Forward and inverse kinematics can be derived as follows.

$$\dot{\mathbf{x}}_{sc} = \mathbf{J}_{sc} \dot{\mathbf{q}}_{sc} \quad (8)$$

$$\dot{\mathbf{q}}_{sc} = \mathbf{J}_{sc}^{-1} \dot{\mathbf{x}}_{sc} \quad (9)$$

where  $\mathbf{J}_{sc}$  denotes the Jacobian matrix of the slave robot. The Jacobian matrix of the slave robot is used to perform mapping from work space to joint space and it can be written as following equation.

$$\mathbf{J}_{sc} = \begin{bmatrix} J_{sc11} & J_{sc12} \\ J_{sc21} & J_{sc22} \end{bmatrix} \quad (10)$$

$$J_{sc11} = l_{3s}C_{3s} + l_{4s}C_{3s4s}$$

$$J_{sc12} = l_{3s}C_{3s4s}$$

$$J_{sc21} = -l_{3s}S_{3s} - l_{4s}S_{3s4s}$$

$$J_{sc22} = -l_{4s}S_{3s4s}$$

The position of end-effector in work space is represented as 2-dimensional vector  $\mathbf{x}_{sw} = [x_{sw} \ y_{sw}]^T$ .

$$\mathbf{x}_{sw} = \begin{bmatrix} l_{1s}C_{1s} + l_{2s}C_{1s2s} + l_{3s}C_{1s2s3s} + l_{4s}C_{1s2s3s4s} \\ l_{1s}S_{1s} + l_{2s}S_{1s2s} + l_{3s}S_{1s2s3s} + l_{4s}S_{1s2s3s4s} \end{bmatrix} \quad (11)$$

### 3.2 Dynamics Modeling

Dynamics equation of the slave robot is derived from the Euler-Lagrange formulation and can be expressed in the joint space as equation (12).

$$\mathbf{T}_s = M_s \ddot{\mathbf{q}}_s + \mathbf{h}_s \quad (12)$$

where  $M_s$  is the inertia matrix, and  $\mathbf{h}_s$  represents the Coriolis and centrifugal force.  $\mathbf{T}_s$  is the 3-dimensional vector of control torques.

## 4. CONTROL SYSTEM

In this section, the 1st and 2nd link of slave robot are operated autonomously, and the 3rd and 4th link of slave robot are operated by human operation using master-slave system. PD controller and impedance controller are used for autonomous control. 4 channel bilateral controller is used for bilateral control.

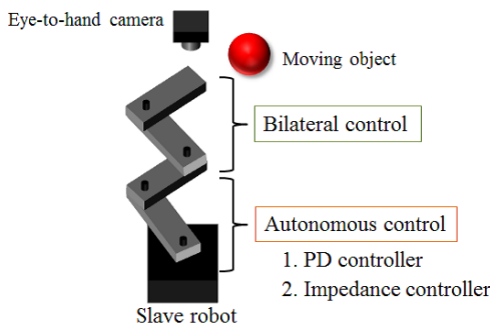


Fig. 3 a unified control of autonomous control and bilateral control

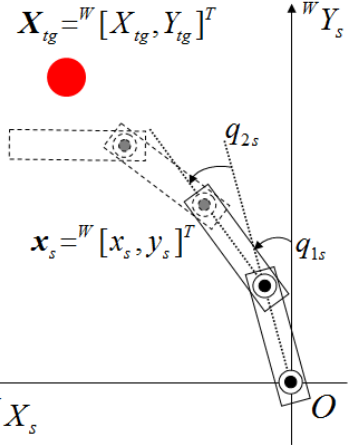


Fig. 4 Work space coordinate

### 4.1 Autonomous control (PD controller)

In this subsection, the 1st and 2nd link of slave robot are controlled autonomously. Autonomous control based on the camera information is designed in the following procedure.

1. As shown Fig.4, measure the position of moving object by using Eye-to-hand camera.
2. Convert to work space coordinate.
3. Design PD controller about the tip position of 2nd link.

$$\mathbf{X}_{tg}^{dev} = \mathbf{X}_{tg}^{res} - \mathbf{X}_{tg}^{init} \quad (13)$$

$$\mathbf{x}_{res}^{dev} = \mathbf{x}_s^{res} - \mathbf{x}_s^{init} \quad (14)$$

$$\ddot{\mathbf{x}}_s^{ref} = K_p(\mathbf{X}_{tg}^{dev} - \mathbf{x}_s^{dev}) + K_v(\dot{\mathbf{X}}_{tg}^{dev} - \dot{\mathbf{x}}_s^{dev}) \quad (15)$$

### 4.2 Autonomous control (Impedance controller)

In this subsection, impedance control is applied to the 1st and 2nd link of slave robot. In the previous subsection, the tip position of 2nd link is controlled by PD controller, and it has stiffness. However the stiffness causes the interference with force control of 3rd and 4th link of slave robot, and deteriorates force response. Then, by using impedance controller, the tip of 2nd link realizes compliant motion and accurate force response.

Acceleration reference given by impedance controller is expressed below.

$$\begin{aligned} \ddot{\mathbf{x}}_s^{ref} &= K_p(\mathbf{X}_{tg}^{dev} - \mathbf{x}_s^{dev}) \\ &+ K_v(\dot{\mathbf{X}}_{tg}^{dev} - \dot{\mathbf{x}}_s^{dev}) - C_f \mathbf{f}_{ext} \end{aligned} \quad (16)$$

### 4.3 Bilateral control (4ch bilateral controller)

In this subsection, the 3rd and 4th link of slave robot are controlled masater-slave system. An ideal response of bilateral control of master-slave system is defined below.

$$\mathbf{f}_{hum}^{ext} + \mathbf{f}_s^{ext} = 0 \quad (17)$$

$$\mathbf{x}_m^{res} - \mathbf{x}_s^{res} = 0 \quad (18)$$

where the subscripts of *hum*, *mst* and *slv* denote human, master and slave respectively. In general, 4 channel bilateral controller[11] which is adapted in this paper shows the best efficiency if the system doesn't have communication delay.

A position control and acceleration control are realized on the same axis simultaneously by using mode transformation based on ideal response of bilateral control which is shown in (17) and (18). The block diagram of 4 channel bilateral controller using mode transformation is shown in Fig.5. 4 channel bilateral control is designed in the following procedure.

1. Calculate a position response of slave in work space from position of end-effector and the tip position of 2nd link.

$$\mathbf{x}_{sc}^{res} = (\mathbf{x}_{sw} - \mathbf{x}_s) \begin{bmatrix} \cos(-\theta) & -\sin(-\theta) \\ \sin(-\theta) & \cos(-\theta) \end{bmatrix} \quad (19)$$

where  $\theta$  denotes  $q_{1s} + q_{2s}$ .

2. Design 4 channel bilateral controller.

$$\ddot{\mathbf{x}}_m^{ref} = C_p (\mathbf{x}_{sc}^{res} - \mathbf{x}_m^{res}) + C_f (\hat{\mathbf{f}}_m + \hat{\mathbf{f}}_s) \quad (20)$$

$$\ddot{\mathbf{x}}_s^{ref} = C_p (\mathbf{x}_m^{res} - \mathbf{x}_{sc}^{res}) + C_f (\hat{\mathbf{f}}_s + \hat{\mathbf{f}}_m) \quad (21)$$

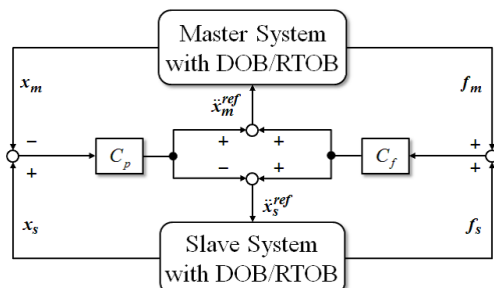


Fig. 5 Block diagram of 4ch controller

## 5. EXPERIMENT

In this section, experiment procedures and results are explained. In the experiment, contact-motion was conducted with the proposed controller and conventional bilateral controller. The parameters of the experiments are shown in table.1. The master-slave robots used in the experiment is shown in Fig.6.

Table 1 Experiment parameters.

Name	Value
Position gain(PD) $K_p$	100
Velocity gain(PD) $K_v$	20
Force gain(Impedance) $C_f$	0.2
Position gain(4ch) $K_p$	100
Velocity gain(4ch) $K_v$	20
Force gain(4ch) $C_f$	0.2
Cut off frequency of DOB $g_{dob}$	100
Cut off frequency of RTOB $g_{rtof}$	100
Cut off frequency of pseudo derivation $g_{pd}$	50
Sampling time $dt$ [ms]	1



Fig. 6 Master-slave robots.

### 5.1 Experiment procedures

In this experiment, the 1st and 2nd link of slave robot are controlled autonomously, and the 3rd and 4th link of slave robot are controlled master-slave system. Experiments are conducted in order to confirm the influence of interference by comparing the force response of next three patterns.

1. Conventional bilateral controller
2. Bilateral controller + PD controller
3. Bilateral controller + Impedance controller

### 5.2 Experiment results

Results of experiment are shown in Fig.7–Fig.9. Fig.7 show a force response of conventional bilateral controller. Fig.8 show a force response of a unified control of bilateral control and PD control. Fig.9 show a force response of a unified control of bilateral control and impedance control. The effect of the interference can be observed through comparing Fig.7 and Fig.8. It can be said that force response become worse because of interference of position control and force control. The effectiveness of using impedance controller can be observed through comparing Fig.8 and Fig.9. It can be said that impedance controller realize more accurate force response in the master robot than PD controller.

## 6. CONCLUSION AND FUTURE WORKS

In this paper, the teleoperation system consisted of 2 DOF master robot and 4 DOF slave robot was proposed. Since two robots were nonidentical, and the slave robot has redundancy, it was difficult to operate. Moreover, conventional bilateral system has time delay between master and slave robot. Thus, it was difficult to operate in dynamic environment. In this paper, a unified control of autonomous control and bilateral control was realized. However, in the proposed method, position control and force control are applied to each subsystem, and the influence on force response by the interference of position control and force control may happen. Experiments were conducted in order to confirm the influence on force response by the interference of position control and force

control, and confirm the effectiveness of a unified control of bilateral control and impedance control.

As a future work, the advanced research related to a unified control of autonomous control and bilateral control must be considered. First, the interference of decentralized system should be analyzed using equivalent mass matrix. Second, the control system which is not affected by the interference should be designed. Finally, the effectiveness of proposed method should be verified by experiment.

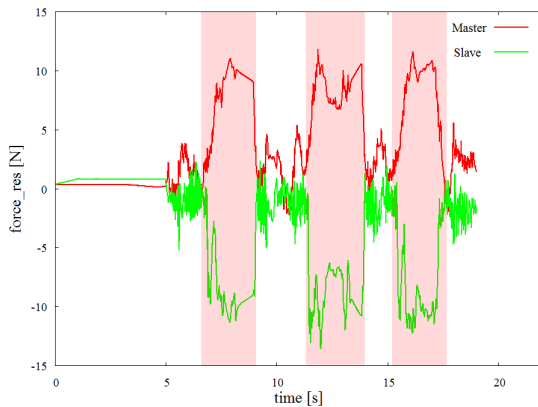


Fig. 7 Force response of conventional bilateral controller

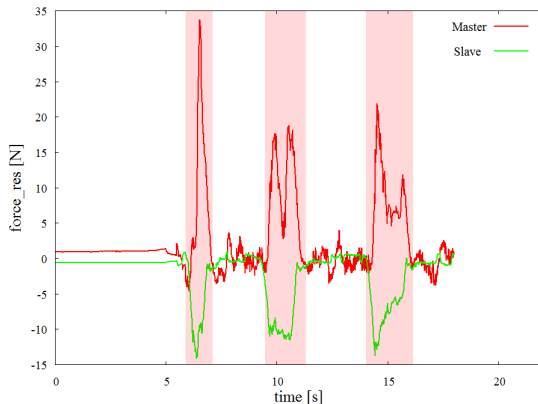


Fig. 8 Force response of bilateral+PD controller

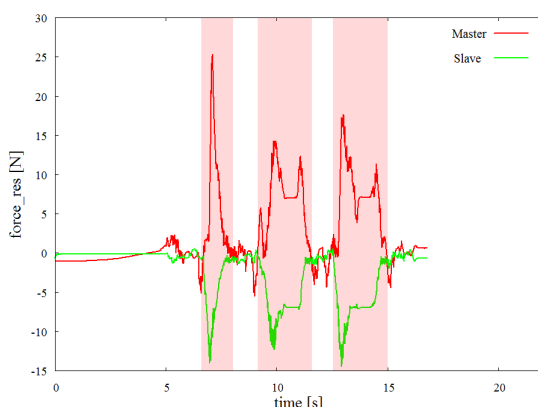


Fig. 9 Force response of bilateral+impedance controller

## REFERENCES

- [1] B.Hannaford: "A Design Framework for Teleoperators with Kinesthetic Feedback", *IEEE Trans. on Robotics and Automation*, Vol. 5, No. 4 , pp.426-434, 1989
- [2] Dale A. Lawrence: "Stability and Transparency in Bilateral Teleoperation", *IEEE Trans. on Robotics and Automation*, Vol. 9, No. 5, pp.624-637, October/June 1993
- [3] K. Ohnishi, M. Shibata, and T. Murakami: "Motion Control for Advanced Mechatronics", *IEEE/ASME Trans. Mechatronics*, Vol. 1, Issue 1, pp. 56-67, Mar. 1996
- [4] K. Ohnishi: "Robust Motion Control by Disturbance Observer", *Journal of the Robotic Society of Japan*, Vol. 11, No. 4, pp. 486-493, 1993 (in Japanese)
- [5] Yuichi Matsumoto, Seiichiro Katsura and Kouhei Ohnishi: "An Analysis and Design of Bilateral Control Based on Disturbance Observer", *Proc. of the 10th IEEE Int. Conf. on Industrial Technology*, pp.802-807, 2003
- [6] T. Murakami, F. Yu, and K. Ohnishi: "Torque Sensorless Control in Multidegree-of-Freedom Manipulator", *IEEE Trans. on Industrial Electronics*, Vol. 40, No. 2, pp. 259-265, Apr. 1993
- [7] N. Fujii, R. Kubo, T. Shimono and K. Ohnishi: "An Approach to Performance Improvement for Bilateral Control based on 4ch-Controller with Acceleration Feedback", *Proceedings of International Conference on Mechatronics*, Kumamoto Japan, 8-10 May 2007
- [8] Y.Nakajima, T.Nozaki, Y.Oyamada, and K.Ohnishi: "An object-coordinate-based bilateral control system using visual information", *Electronics and Communications in Japan*, Vol. 96, No. 8, pp. 41-49, 2013
- [9] T. Ohta and T. Murakami: "A Realization of Posture Control of Redundant Manipulator in Bilateral System", *Master's Course Paper 2007*, No. 2007-13-02, 2007
- [10] K. Okiyama and T. Murakami: "Realization of Human-Robot Interaction System Using Bilateral Control", *Master's Course Paper 2013*, No. 2013-13-02, 2013
- [11] D.A.Lawrence: "Stability and Transparency in Bilateral Teleoperation", *IEEE Trans. on Robotics and Automation*, Vol. 9, No. 5, pp. 624-637, 1993
- [12] H. Ohta, N. Oda, Y. Yan, T. Murakami, and K. Ohnishi: "A Decentralized Control Strategy for Redundant Manipulator Based on Hierarchical Impedance", *IEEE/ASME International Conference on*, Vol. 10, Tokyo Japan, 20 June 1997
- [13] H. Hattori, and K. Ohnishi: "A Decentralized Control in Consideration of Compliant Motion in Redundant Manipulator", *The Japan Society of Mechanical Engineers*, Vol. 7, pp. 336-339, 2001



# Posture Stabilization Control of Two-Wheel Drive Electric Motorcycle with Assistant Pendulum for Rider Motion

*T. Abumi<sup>1</sup>, T. Murakami<sup>2</sup>*

<sup>1</sup>*Department of System Design Engineering, Keio University, Yokohama, Japan  
(Tel : +81-45-566-1741; E-mail: takamasa@sum.sd.keio.ac.jp)*

<sup>2</sup>*Department of System Design Engineering, Keio University, Yokohama, Japan.  
(Tel : +81-45-566-1741; E-mail: mura@sd.keio.ac.jp)*

**Keywords:** Electric Motorcycle, Two-Wheel Drive, Disturbance Observer, Camber Angle, Rider Motion, Double Inverted Pendulum, Posture Stabilization

## Abstract

Recently, global warming is the serious world problem. To solve this issue, many new vehicles appear today. For example, there is electric motorcycle (EM). In the almost conventional approaches, one inverted pendulum model for camber angle is used. This model does not include the rider motion and it is not good enough to consider stabilization of vehicle in the real world. So, this paper proposes a new EM system with assistant pendulum. Also, the proposed human camber angle disturbance observer (HDOB) considers compensation for stabilization of human camber angle. By these proposed approaches, the improvement of posture stabilization of whole electric motorcycle system considering rider motion is validated by the simulations.

## 1. INTRODUCTION

Recently, global warming is the serious world problem. To solve this problem, many new vehicles appear today. For example, there is personal mobility. Specifically, EM is getting attention among the personal mobility. The EM has many merits. Firstly, EM is compact and familiar personal transportation. Secondly, this has good environmental performance because of zero emission, comparing with internal combustion engine motorcycle. Also because of the in-wheel motor equipped with EM, motor torque control is more easily and more precisely than engine motorcycle. Finally, the cost of EM is cheaper than the automobiles and the maintenance of the EM is more easily than the automobiles. Because of these of merits, the demand of this personal mobility will increase in the world, particularly, in Japan, China and southeast Asia.

Many people researched about two-wheeled vehicles until today. In 1970's Sharp [1] had analyzed the stability of two-wheeled vehicles during straight running, using 4-DOF model. The features of two-wheeled vehicle body and wheel had been investigated by this model. However, there are few researches of the Two-Wheel drive EM because the EM is relatively the new mobility. There are some researches of the two-Wheel drive EM such as [2] and [3]. However, these researches have not completely analyzed the dynamics of the two-Wheel drive EM in the research of the during straight forward direction with the

consideration of front and rear slip ratio yet. Also, in the conventional research, one inverted pendulum model for camber angle is used. there are many problems in the conventional research. First of all, human camber angle is not considered. Human camber angle affects posture stabilization in the real world. Moreover, inappropriate human camber angle induced falling accident. Secondly, to estimate human camber angle is difficult without sensor on human. So, easy estimation law of human camber angle is needed. Then the purpose of this paper are posture stabilization control considering rider motion and assist control for realizing appropriate human camber angle

To realize this purpose, this paper proposes new EM system considering rider motion model. Also, this paper proposes the new camber angle disturbance observer (CADO) [4] which considers human camber angle with assistant pendulum. This proposed human camber angle disturbance observer (HDOB) compensates human camber angle disturbance for stabilization of human camber angle. In the proposed method, double inverted pendulum model is used to consider rider motion. Also, human is moved by assistant pendulum behind the human for achieving appropriate human camber angle with seat belt. So human camber angle is assumed to be the same as assistant pendulum angle easily. By this pendulum, assistance for rider motion to stabilize posture is achieved. Because of these proposed methods, the stabilization of whole EM system considering rider motion will be improved. This paper is organized as follows. In section 2, the proposed two-wheel drive EM system with assistant pendulum is introduced. In section 3, the details of the control methods are described. In section 4, the simulation is conducted to clarify the influence on interference of introducing proposed method. Finally, this paper is concluded and the future works are described in section 5.

## 2. MODELING OF ELECTRIC MOTORCYCLE

This section shows the proposed two-Wheel drive EM model such as wheel, vehicle body and front wheel part.

### 2.1 Proposed wheel and vehicle part of dynamics

The proposed model of the EM is the two-Wheel drive system. In this system, there are two in-wheel motors of front and rear wheel respectively. So, instead of the conventional model, the front wheel can have the driving force and detect the slip ratio. The two-Wheel drive ve-

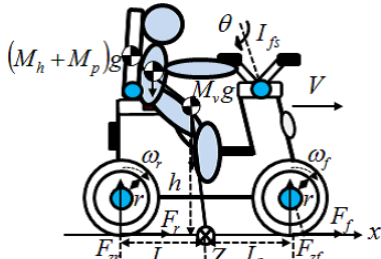


Fig. 1 Side view of EM

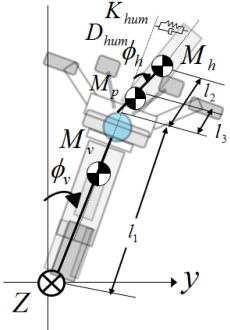


Fig. 2 Back view of EM

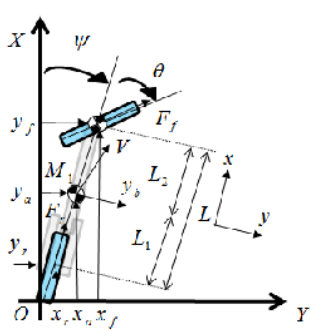


Fig. 3 Top view of EM

hicle model which is appropriate for acceleration on the straight forward direction is described in this paper. In deriving the dynamics equations of the system, the side slip and lateral force are very small in the straight forward direction, so, the lateral motion is not considered in this paper and the rolling resistance and air resistance are also ignored. The dynamics equations for the wheel rotating motion and longitudinal vehicle motion are shown as (1)-(5).

$$J_{trf}\dot{\omega}_{trf} = \tau_{trf} - rF_f \quad (1)$$

$$J_{trr}\dot{\omega}_{trr} = \tau_{trr} - rF_r \quad (2)$$

$$M_{all}\dot{V} = F_f + F_r \quad (3)$$

$$M_{all}\dot{V}_x = F_f \cos \theta + F_r \quad (4)$$

$$M_{all}\dot{V}_y = F_f \sin \theta \quad (5)$$

For simplicity, the front and rear wheel radii are equal and denote both with \$r\$. The tire longitudinal driving force \$F\_f, F\_r\$ are shown as (6) and (7).

$$F_f = \mu_f(\lambda_f)F_{zf} \quad (6)$$

$$F_r = \mu_r(\lambda_r)F_{zr} \quad (7)$$

Dynamic friction coefficient \$\mu\_i(\lambda\_i)\$ is given by Magic Formula Tire Model [5]. Magic formula model shows the relationship between dynamic friction coefficient and slip ratio \$\lambda\_i\$. By using magic formula, the realization of road condition and more real driving model are given. Magic Formula Tire Model is shown as (8).

$$\mu_i(\lambda_i) = d \sin \left( c \tan^{-1} b(1-e)\lambda_i + \frac{e}{b} \tan^{-1} b\lambda_i \right) \quad (8)$$

\$b, c, d, e\$ are the parameters. They are decided in advance. Fig. 4 shows the relationship between friction coefficient \$\mu\_i\$ and slip ratio \$\lambda\_i\$ on the road surface conditions for asphalt, wet asphalt and ice road. If the slip ratio

Table 1 Parameters of figure 1

variables	unit	explanation
\$V\$	m/s	Velocity of vehicle
\$V_x, V_y\$	m/s	Velocity vector about x/y axis
\$M_v\$	kg	Mass of vehicle
\$M_h\$	kg	Mass of human
\$M_p\$	kg	Mass of pendulum
\$M_{all}\$	kg	Mass of all in whole system
\$J_{trf}, J_{trr}\$	kgm <sup>2</sup>	Moment of wheel inertia
\$I_{fs}\$	kgm <sup>2</sup>	Moment of handle inertia
\$I_1\$	kgm <sup>2</sup>	Moment of vehicle body inertia
\$I_2\$	kgm <sup>2</sup>	Moment of human inertia
\$I_3\$	kgm <sup>2</sup>	Moment of pendulum inertia
\$F_f, F_h\$	N	Longitudinal driving force
\$F_{zf}, F_{zr}\$	N	Vertical tire force
\$\tau_{trf}, \tau_{trr}\$	Nm	Driving torque
\$\omega_f, \omega_r\$	m/s	Angular velocity of wheel
\$\theta\$	rad	Steering angle
\$\alpha\$	rad	Caster angle
\$\phi_v\$	rad	Vehicle camber angle
\$\phi_h\$	rad	Human camber angle
\$\psi\$	rad	Direction angle
\$r\$	m	Radius of wheel
\$tr\$	m	Trail
\$L\$	m	Wheelbase
\$L_2\$	m	Front wheelbase
\$L_1\$	m	Rear wheelbase
\$h\$	m	Height of center of vehicle mass
\$l_1\$	m	Length of vehicle
\$l_2\$	m	Height of center of human
\$l_3\$	m	Height of center of pendulum
\$K_{hum}\$	N/m	Spring constant of human
\$D_{hum}\$	Pas	Coefficient of viscosity of human

is controlled to keep the smaller slip ratio than the slip ratio at the maximum value of the friction coefficient, the cohesive zone is kept and stable acceleration is achieved. In this paper, dry road driving is assumed with straight forward direction. To describe the load transfer phenomena between front and rear axles, the vertical force on the front and rear wheels are shown as (9) and (10).

$$F_{zf} = \frac{M_{all}g L_1}{L} \quad (9)$$

$$F_{zr} = \frac{M_{all}g L_2}{L} \quad (10)$$

## 2.2 Front wheel part of dynamics

This subsection shows the dynamic equations of the front wheel part. From Fig. 2, \$\tau\_{fs}\$ denotes the input torque to the front wheel steering motor. The dynamic equation of front wheel part is shown as (11).

$$I_{fs}\ddot{\theta} = \tau_{fs} + \tau_{gyro} - \tau_{trail} + \tau_{fs}^{dis} \quad (11)$$

where \$\tau\_{gyro}, \tau\_{trail}\$ denote the torque of gyro effect and trail effect respectively. \$\tau\_{fs}^{dis}\$ denotes the disturbance

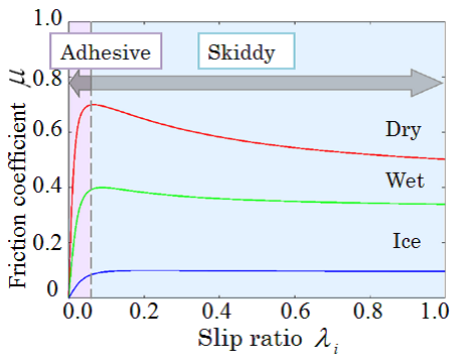


Fig. 4 Relationship between slip ratio and friction coefficient

torque. Although  $\tau_{gyro}$  exercises good effect on the stability of the EM, this research regards it as disturbance. Then, (11) is transformed as (12).

$$I_{fs}\ddot{\theta} = \tau_{fs} - \tau'^{dis}_{fs} \quad (12)$$

### 2.3 Vehicle body part of dynamics

From Fig. 2, the vehicle body can be regarded as the double inverted pendulum. So, the dynamics of vehicle camber angle and human camber angle can be derived by solving the Lagrange equation as (13) [6].

$$\begin{bmatrix} M_{00} & M_{01} \\ M_{10} & M_{11} \end{bmatrix} \begin{bmatrix} \ddot{\phi}_v \\ \ddot{\phi}_h \end{bmatrix} + \begin{bmatrix} C_1 \\ C_2 \end{bmatrix} \dot{\theta} + \begin{bmatrix} D_1 \\ D_2 \end{bmatrix} - \begin{bmatrix} G_1 \\ G_2 \end{bmatrix} - \begin{bmatrix} H_1 \\ H_2 \end{bmatrix} - \begin{bmatrix} F_1 \\ F_2 \end{bmatrix} = \begin{bmatrix} \tau_v \\ \tau_h \end{bmatrix} + \begin{bmatrix} T_v^{dis} \\ T_h^{dis} \end{bmatrix} \quad (13)$$

In (13)  $M$  is inertia term.  $C$  and  $D$  are the term depends on velocity of the motorcycle.  $G$  is the gravity term.  $H$  is the Coriolis force.  $\tau_v$  denotes the corresponding torque by the change of the mass center position of vehicle body system.  $\tau_h$  denotes the input torque by the assistant pendulum motor.  $T_v^{dis}$  and  $T_h^{dis}$  denote the disturbance torque. The variables are defined as follows.

$$\begin{aligned} M_{00} &= I_1 + I_2 + I_3 + h^2 M_v + l_2^2 M_h + l_3^2 M_3 \\ &+ l_1^2(M_h + M_p) + 2l_1(l_2 M_h + l_3 M_3) \cos \phi_h \\ M_{01} &= I_2 + I_3 + l_2^2 M_h + l_3^2 M_3 \\ &+ l_1(l_2 M_h + l_3 M_3) \cos \phi_h \\ M_{10} &= I_2 + I_3 + l_2^2 M_h + l_3^2 M_3 \\ &+ l_1(l_2 M_h + l_3 M_3) \cos \phi_h \\ M_{11} &= I_2 + I_3 + l_2^2 M_h + l_3^2 M_3 \\ C_1 &= \frac{L_1 \cos \theta V}{L} ((h M_v + l_1(M_h + M_p)) \cos \phi_v \\ &+ (l_2 M_h + l_3 M_p) \cos(\phi_v + \phi_h)) + J_{trf} \omega_f \\ C_2 &= \frac{L_1}{L} V \cos \theta (l_2 M_h + l_3 M_3) \cos(\phi_v + \phi_h) \\ D_1 &= \left\{ \frac{L_2}{L} \dot{V} \sin \theta + \frac{V^2}{L^2} (L_2 \cos \theta + L_1) \sin \theta \right\} \\ &\times ((h M_v + l_1(M_h + M_p)) \cos \phi_v \\ &+ (l_2 M_h + l_3 M_p) \cos(\phi_v + \phi_h)) \end{aligned}$$

$$\begin{aligned} &+ \frac{V \sin \theta}{L} (J_{trf} \omega_f + J_{trr} \omega_r) \\ D_2 &= \left\{ \frac{L_2}{L} \dot{V} \sin \theta + \frac{V^2}{L^2} (L_2 \cos \theta + L_1) \sin \theta \right\} \\ &\times (l_2 M_h + l_3 M_p) \cos(\phi_v + \phi_h) \\ G_1 &= g(h M_v + l_1(M_h + M_p)) \sin \phi_v \\ &+ g(l_2 M_h + l_3 M_p) \sin(\phi_v + \phi_h) \\ G_2 &= g(l_2 M_h + l_3 M_p) \sin(\phi_v + \phi_h) \\ H_1 &= l_1(l_2 M_h + l_3 M_p) \sin \phi_h (2\dot{\phi}_v + \dot{\phi}_h) \\ H_2 &= l_1(l_2 M_h + l_3 M_p) \dot{\phi}_v^2 \sin \phi_h \\ F_1 &= K_{hum} (\phi_v + \phi_h) + D_{hum} (\dot{\phi}_v + \dot{\phi}_h) \\ F_2 &= -K_{hum} (\phi_v + \phi_h) - D_{hum} (\dot{\phi}_v + \dot{\phi}_h) \end{aligned}$$

$\tau_v$  is given as (14) by the change of the mass center position due to the steering action [1].

$$\tau_v \simeq \frac{M_v g L_1 t r \sin^2 \alpha}{L} \theta \quad (14)$$

## 3. CONTROL ALGORITHM

In this section, the proposed control system is designed. First, Lyapunov-based control of the human camber angle using HDOB is described. Second, Lyapunov-based control of the vehicle camber angle using camber angle disturbance observer (CADO)[4] is described. Thirdly, the acceleration control of motor is described[4]. Lastly, whole control system is shown.

### 3.1 Control of human camber angle

In this subsection, the control system of human camber angle is described. The command is given by Lyapunov-based theory using DOB. DOB is added to compensate the disturbance such as modeling error and friction. Dynamic equation about human camber angle  $\phi_h$  is given as (13). It is transformed as (15).

$$\left( M_{11} - \frac{M_{10} M_{01}}{M_{00}} \right) \ddot{\phi}_h = \tau_h - T_h^{dis} \quad (15)$$

$T_h^{dis}$  is considered as the disturbance about rider camber angle. (15) is transformed into (16) when inertia matrix of mathematical model is used.

$$\begin{aligned} &\left( M_{n11} - \frac{M_{n10} M_{n01}}{M_{n00}} \right) \ddot{\phi}_h = \tau_h - \left\{ T_h^{dis} \right. \\ &\left. + \left( M_{n11} - \frac{M_{n10} M_{n01}}{M_{n00}} - M_{11} + \frac{M_{10} M_{01}}{M_{00}} \right) \ddot{\phi}_h \right\} \\ &= \tau_h - \tilde{T}_h^{dis} \quad (16) \end{aligned}$$

where subscript  $n$  means mathematical model.  $\tilde{T}_h^{dis}$  is redefined.  $\tilde{T}_h^{dis}$  can be estimated using DOB. Estimated torque that represents disturbance and the modeling error about human camber angle direction is shown in (17).

$$\begin{aligned} \hat{T}_h^{dis} &= \frac{g_d}{s+g_d} \left\{ \left( \frac{M_{n10} M_{n01}}{M_{n00}} - M_{n11} \right) \ddot{\phi}_h + \tau_h \right\} \\ &= \frac{g_d}{s+g_d} \left\{ g_d \left( M_{n11} - \frac{M_{n10} M_{n01}}{M_{n00}} \right) \dot{\phi}_h + \tau_h \right\} \end{aligned}$$

$$- g_d \left( M_{n11} - \frac{M_{n10}M_{n01}}{M_{n00}} \right) \dot{\phi}_h \quad (17)$$

where  $g_d$  is the cutoff frequency of human camber angle disturbance observer. To stabilize the human camber angle as  $\dot{\phi}_h^{res} \rightarrow \dot{\phi}_h^{cmd}$ ,  $\dot{\phi}_h^{res} \rightarrow 0$ , Lyapunov-based control is utilized. The candidate of Lyapunov function  $V_{\phi_h}$  is defined as (18).

$$\begin{aligned} V_{\phi_h} = & \frac{1}{2} \left( M_{n11} - \frac{M_{n10}M_{n01}}{M_{n00}} \right) \dot{\phi}_h^2 \\ & + \frac{1}{2} K_{\phi_h} (\phi_h - \phi_h^{cmd})^2 \end{aligned} \quad (18)$$

where  $K_{\phi_h}$  is a positive gain.  $\dot{V}_{\phi_h}$  is calculated as (19).

$$\begin{aligned} \dot{V}_{\phi_h} = & \left( M_{n11} - \frac{M_{n10}M_{n01}}{M_{n00}} \right) \dot{\phi}_h \ddot{\phi}_h \\ & + K_{\phi_h} (\phi_h - \phi_h^{cmd}) \dot{\phi}_h \\ = & \dot{\phi}_h \left\{ \tau_h - \tilde{T}_h^{dis} + K_{\phi_h} (\phi_h - \phi_h^{cmd}) \right\} \end{aligned} \quad (19)$$

Control input torque  $\tau_h$  is selected as follows to make (19) semi-negative.

$$\tau_h = \hat{T}_h^{dis} - K_{\phi_h} (\phi_h - \phi_h^{cmd}) - K_{\dot{\phi}_h} \dot{\phi}_h \quad (20)$$

where  $K_{\dot{\phi}_h}$  should be a positive gain. As shown in (17),  $\hat{T}_h^{dis}$  is obtained by DOB. If  $\hat{T}_h^{dis}$  equals to  $\tilde{T}_h^{dis}$ , (19) can be transformed into (21) by using (20).

$$\dot{V}_{\phi_h} = -K_{\dot{\phi}_h} \dot{\phi}_h^2 \leq 0 \quad (21)$$

From (21) and Lasalle's theorem,  $\phi_h^{res} \rightarrow \phi_h^{cmd}$ ,  $\dot{\phi}_h^{res} \rightarrow 0$  are guaranteed.  $K_{\phi_h}$  and  $K_{\dot{\phi}_h}$  are determined as (22) and (23) respectively.

$$K_{\phi_h} = \left( M_{n11} - \frac{M_{n10}M_{n01}}{M_{n00}} \right) \omega_{nh}^2 \quad (22)$$

$$K_{\dot{\phi}_h} = 2\zeta\omega_{nh} \left( M_{n11} - \frac{M_{n10}M_{n01}}{M_{n00}} \right) \quad (23)$$

where  $\omega_{nh}$  and  $\zeta_n$  are eigen frequency and damping ratio respectively.

### 3.2 Control of vehicle camber angle

In this subsection, the control system of vehicle camber angle is described. Dynamic equation about vehicle camber angle  $\phi_v$  is given as (13). It is transformed as (24).

$$\begin{aligned} & \left( M_{00} - \frac{M_{01}M_{10}}{M_{11}} \right) \ddot{\phi}_v + \frac{M_{01}}{M_{11}} (\tau_h - T'_h^{dis}) \\ = & - \left( C_1 - \frac{M_{01}C_2}{M_{11}} \right) \dot{\phi}_v - T'_v^{dis} \end{aligned} \quad (24)$$

$T'_v^{dis}$  is considered as the disturbance about vehicle camber angle. (24) is transformed into (25) when inertia matrix of mathematical model is used.

$$\begin{aligned} & \left( M_{n00} - \frac{M_{n01}M_{n10}}{M_{n11}} \right) \ddot{\phi}_v + \frac{M_{n01}}{M_{n11}} (\tau_h - \tilde{T}_v^{dis}) \\ = & - \left( C_{n1} - \frac{M_{n01}C_{n2}}{M_{n11}} \right) \dot{\phi}_v - \tilde{T}_v^{dis} \end{aligned} \quad (25)$$

$\tilde{T}_v^{dis}$  is redefined.  $\tilde{T}_v^{dis}$  can be estimated using CADO. Estimated torque that represents disturbance and the modeling error about vehicle camber angle direction is shown in (26).

$$\begin{aligned} \hat{T}_v^{dis} = & \frac{g_c}{s+g_c} \left\{ g_c \left( M_{n00} - \frac{M_{n01}M_{n10}}{M_{n11}} \right) \dot{\phi}_v \right. \\ & - \frac{M_{n01}}{M_{n11}} (\tau_h - \hat{T}_h^{dis}) \\ & - \left. \left( C_{n1} - \frac{M_{n01}C_{n2}}{M_{n11}} \right) \dot{\theta} \right\} \\ & - g_c \left( M_{n00} - \frac{M_{n01}M_{n10}}{M_{n11}} \right) \dot{\phi}_v \end{aligned} \quad (26)$$

where  $g_c$  is the cutoff frequency of vehicle camber angle disturbance observer. To stabilize the vehicle camber angle as  $\phi_v^{res} \rightarrow \phi_v^{cmd}$ ,  $\dot{\phi}_v^{res} \rightarrow 0$ , Lyapunov-based control is utilized. The candidate of Lyapunov function  $V_{\phi_v}$  is defined as (27).

$$\begin{aligned} V_{\phi_v} = & \frac{1}{2} \left( M_{n00} - \frac{M_{n01}M_{n10}}{M_{n11}} \right) \dot{\phi}_v^2 \\ & + \frac{1}{2} K_{\phi_v} (\phi_v - \phi_v^{cmd})^2 \end{aligned} \quad (27)$$

where  $K_{\phi_v}$  is a positive gain.  $\dot{V}_{\phi_v}$  is calculated as follows.

$$\begin{aligned} \dot{V}_{\phi_v} = & \left( M_{n00} - \frac{M_{n01}M_{n10}}{M_{n11}} \right) \dot{\phi}_v \ddot{\phi}_v + K_{\phi_v} (\phi_v - \phi_v^{cmd}) \dot{\phi}_v \\ = & \dot{\phi}_v \left\{ - \left( C_{n1} - \frac{M_{n01}C_{n2}}{M_{n11}} \right) \dot{\theta} - \tilde{T}_v^{dis} \right. \\ & \left. - \frac{M_{n01}}{M_{n11}} (\tau_h - \tilde{T}_h^{dis}) + K_{\phi_v} (\phi_v - \phi_v^{cmd}) \right\} \end{aligned} \quad (28)$$

Control input  $\dot{\theta}^{cmd}$  is selected as follows to make (28) semi-negative.

$$\begin{aligned} \dot{\theta}^{cmd} = & \frac{M_{n11}}{(M_{n01}C_{n2} - M_{n11}C_{n1})} \left\{ \hat{T}_v^{dis} + \frac{M_{n01}}{M_{n11}} (\tau_h - \hat{T}_h^{dis}) \right. \\ & \left. - K_{\phi_v} (\phi_v - \phi_v^{cmd}) - K_{\dot{\phi}_v} \dot{\phi}_v \right\} \end{aligned} \quad (29)$$

where  $K_{\dot{\phi}_v}$  should be a positive gain. As shown in (26),  $\hat{T}_v^{dis}$  is obtained by CADO. If  $\hat{T}_v^{dis}$  equals to  $\tilde{T}_v^{dis}$ , (28) is transformed into (30) using (29).

$$\dot{V}_{\phi_v} = -K_{\dot{\phi}_v} \dot{\phi}_v^2 \leq 0 \quad (30)$$

From (30) and Lasalle's theorem,  $\phi_v^{res} \rightarrow \phi_v^{cmd}$ ,  $\dot{\phi}_v^{res} \rightarrow 0$  are guaranteed.  $K_{\phi_v}$  and  $K_{\dot{\phi}_v}$  are determined as (31) and (32) respectively.

$$K_{\phi_v} = \left( M_{n00} - \frac{M_{n01}M_{n10}}{M_{n11}} \right) \omega_{nv}^2 \quad (31)$$

$$K_{\dot{\phi}_v} = 2\zeta\omega_{nv} \left( M_{n00} - \frac{M_{n01}M_{n10}}{M_{n11}} \right) \quad (32)$$

where  $\omega_{nv}$  and  $\zeta$  are eigen frequency and damping ratio respectively. The control input to the front wheel steering motor is derived from PD control. The acceleration reference can be calculated as (33).

$$\ddot{\theta}^{ref} = \dot{\theta}^{cmd} + D_\theta (\dot{\theta}^{cmd} - \dot{\theta}^{res}) + K_\theta (\theta^{cmd} - \theta^{res}) \quad (33)$$

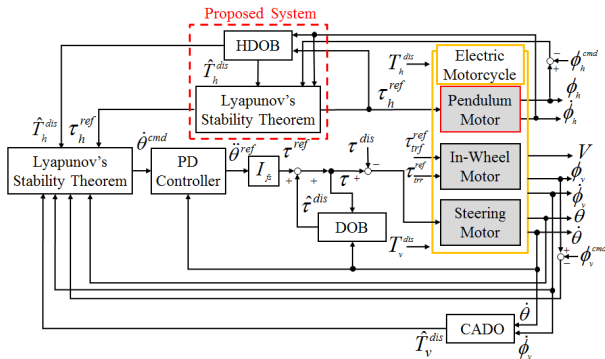


Fig. 5 Block diagram of Two-Wheel drive Electric motorcycle

### 3.3 Acceleration control of motor

The product of reference value of steering angle acceleration  $\dot{\theta}^{ref}$  and moment of inertia about steering wheel axis  $I_h$  reaches the torque reference value  $\tau^{ref}$ .

$$\tau^{ref} = I_f \ddot{\theta}^{ref} \quad (34)$$

It is assumed that an ideal steer angle acceleration response is obtained in each control system. Therefore, Disturbance Observer(DOB) [7] is applied to achieve robust control system. Disturbance torque  $\hat{\tau}^{dis}$  is estimated as (35) [4].

$$\begin{aligned} \hat{\tau}^{dis} &= \frac{g_s}{s + g_s} \tau^{dis} \\ &= \frac{g_s}{s + g_s} (\tau - I_{fs} \ddot{\theta}) \\ &= \frac{g_s}{s + g_s} \tau + \frac{g_s^2 I_{fs}}{s + g_s} \dot{\theta} - g_s I_{fs} \ddot{\theta} \end{aligned} \quad (35)$$

The value that estimated disturbance torque  $\hat{\tau}^{dis}$  is added to the torque reference value  $\tau^{ref}$  is output to the motor.

$$\tau = \tau^{ref} + \hat{\tau}^{dis} \quad (36)$$

The whole block diagram is shown in Fig. 5.

## 4. SIMULATION

In this section, the simulation with proposed method is carried out to confirm the posture stabilization to validate the proposal. In the outline of the simulation, the proposed Two-Wheel drive electric motorcycle is driving dry asphalt road for straight driving direction. Table 2 shows the parameters of simulations. Table 3 shows the gains of simulations.

The following two cases are compared in this simulation.  
 · With assistant pendulum motor and  $\phi_v^{cmd} = \phi_h^{cmd} = 0.0$   
 · Without assistant pendulum motor and  $\phi_v^{cmd} = 0.0$

The simulation setup is as follows,

$$\tau_{trf}^{ref}, \tau_{trr}^{ref} = \begin{cases} 92.0 \text{ Nm} & (0.0 \leq t < 1.5) \\ 0.0 \text{ Nm} & (1.5 \leq t) \end{cases} \quad (37)$$

$$T_v^{dis}, T_h^{dis} = 50.0 \text{ Nm} \quad (2.0 \leq t \leq 3.0) \quad (38)$$

Table 2 Parameters for Simulation

Mass of vehicle system $M_v$	kg	50.0
Mass of human system $M_h$	kg	60.0
Mass of pendulum system $M_p$	kg	2.5
Wheel base $L$	m	1.0
Front and rear wheel base $L_2, L_1$	m	0.5
Trail $tr$	m	0.05
Caster angle $\alpha$	m	1.25
Height of COG of vehicle $h$	m	0.4
Radius of wheel $r$	m	0.25
Inertia of vehicle system $I_1$	$\text{kNm}^2$	12.8
Inertia of human system $I_2$	$\text{kNm}^2$	2.9
Inertia of pendulum system $I_3$	$\text{kNm}^2$	0.9
Length of vehicle system $l_1$	m	0.6
Inertia of human system $I_2$	m	0.6
Inertia of pendulum system $I_3$	m	0.6
Inertia of front wheel steering $I_{fs}$	$\text{kNm}^2$	0.18
Inertia of wheels $J_{trf}, J_{trr}$	$\text{kNm}^2$	2.0
Spring constant of rider $K_{hum}$	N/m	1600.0
Coefficient of viscosity of rider $D_{hum}$	Pas	250.0

Table 3 Gains for Simulation

Cutoff frequency of steering DOB $g_s$	50.0
Cutoff frequency of DOB $g_d$	100.0
Cutoff frequency of CADO $g_c$	100.0
P gain about front steering motor $K_\theta$	900.0
D gain about front steering motor $D_\theta$	60.0
Eigen frequency for steering Lyapunov $\omega_{nv}$	10.0
Eigen frequency for pendulum Lyapunov $\omega_{nh}$	6.0
Damping ratio for steering Lyapunov $\zeta_n$	0.7

where  $V = 6.26[\text{V/m}] (1.54 \leq t)$  which is the velocity of motorcycle is set in the simulation.  $T_v^{dis}, T_h^{dis}$  are external torques to vehicle camber angle and human camber angle. The simulation results are described. Fig. 6 shows the steering angle comparison between with proposed control and without control. From Fig. 6, in with control, steering angle has smaller value under the disturbance than without the control. Also, with control, the convergence time of steering angle is shorter than without control. So, Fig. 6 means the operability of steering in with control is better than without control. Fig. 7 and Fig. 8 which show the vehicle camber angle and human camber angle comparisons between with proposed control and without control mean the improvement of the posture stabilization by proposed control. In Fig. 7, vehicle camber angle with the control is smaller than without control. Also, in Fig. 8, human camber angle with the control is much smaller than without control. By these two figures, the whole electric motorcycle system considering rider motion is stabilized by the proposed control system with assistant pendulum. So, these three figures show that the stability of straight forward direction driving is improved by proposed methods. Therefore the

validity of the proposal is verified.

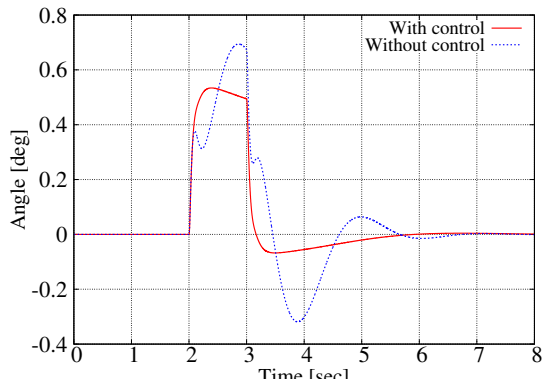


Fig. 6 Steering angle

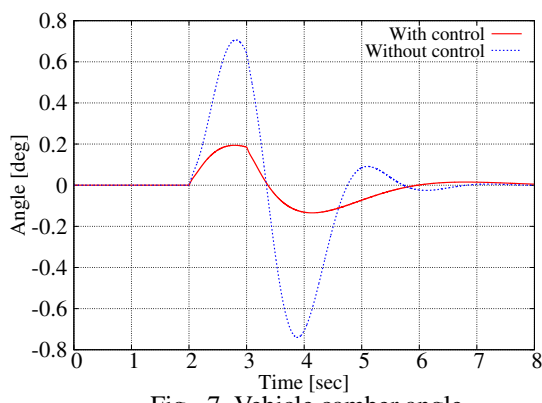


Fig. 7 Vehicle camber angle

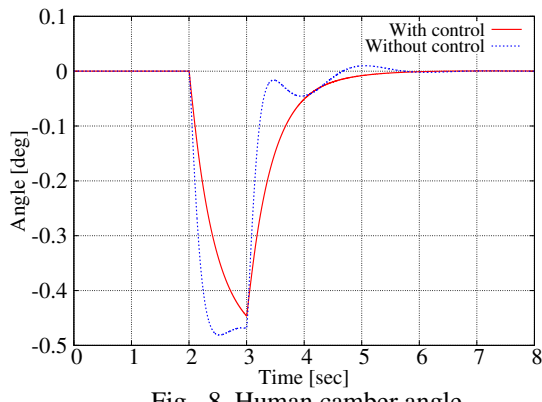


Fig. 8 Human camber angle

## 5. CONCLUSION AND FUTURE WORKS

In the traditional EM model rear-wheel drive system is researched. However, most conventional EM models does not consider the rider motion for camber angle. Therefore, this paper proposes a new two-wheel

drive EM system. In this system, the assistant pendulum control for rider motion is proposed. By this assistant pendulum, human camber angle is estimated easily and appropriate rider motion for camber angle which is calculated through CADO by double inverted pendulum model. Also, the new HDOB system which considers compensation for stabilization of human camber angle to stabilize the vehicle posture by CADO considering estimated human camber angle disturbance is proposed. By these proposed approaches, the improvement of posture stabilization of whole electric motorcycle system considering rider motion is validated by the simulations because of the smaller human and vehicle camber angles for disturbances. As the future works, validity of proposed method will be verified by the experiments. Also, the two-steering structure for two wheel drive electric motorcycle will be developed for stabilization. Moreover, the proposed EM system will be made.

## REFERENCES

- [1] R. S. Sharp: "The Stability and Control of Motorcycle", *Journal Mechanical Engineering Science*, vol.13, No.5, pp.316-329,1971
- [2] Bo-Chiuan Chen, Chia-Hsing Chu and Shiu-Jer Huang: "Fuzzy sliding mode control of traction control system for electric scooter", *Fuzzy Systems and Knowledge Discovery (FSKD)*, 2010 Seventh International Conference, May 9-13, 2011, Shanghai, China
- [3] Chun-Liang Lin and Weng-Ching Lin: "ABS control design for two-wheel drive electric vehicles", *Mechanic Automation and Control Engineering (MACE)*, 2011 Second International Conference, 1011 - 1014 (2011)
- [4] T. Kawamura, T. Murakami: "Robust Stabilization Control for an Electric Bicycle", *The 8th edition of France-Japan and 6th Europe-Asia Congress on Mechatronics*, Yokohama(Japan), 22-24th Nov, 2010.
- [5] H.B.Pacejka, and E.Bakker: "The Magic Formula Tyre Model", *Proc. 1st International Colloquium on Tyre Models for Vehicle Dynamics Analysis*, Delft, The Netherlands, Oct 21-22 (1991)
- [6] Yamaguchi, T.;Shibata, T.;Murakami, T: "Self-Sustaining Approach of Electric Bicycle by Acceleration Control Based Backstepping", *The 33rd Annual Conference of the IEEE Industrial Electronics Society (IECON)*, Nov.5-8,2007,Taipei,Taiwan
- [7] K. Ohnishi: "Robust Motion Control by Disturbance Observer", *Journal of the Robotic Society of Japan*, Vol. 11, No. 4, pp. 486-493, 1993 (in Japanese)
- [8] Tanaka, Y. ; Murakami, T. "A Study on Straight-Line Tracking and Posture Control in Electric Bicycle", *Industrial Electronics, IEEE Transactions on*, Volume:56, Issue:1, pp.159-168 Jan.2009.

# Driving Assist Control of Electric Vehicle by Steer-by-Wire System Considering Collision Avoidance of Traveling Bicycle

Sotaro MAEJIMA

Department of System Design Engineering,  
Keio University,  
Yokohama, Japan.  
Email: maejima@sum.sd.keio.ac.jp

Toshiyuki MURAKAMI

Department of System Design Engineering,  
Keio University,  
Yokohama, Japan.  
E-mail: mura@sd.keio.ac.jp

**Abstract**— Various driving support systems to avoid traffic accident have developed and have been put in the real world. On the other hand, only a few collision avoidance systems with the steering wheel have been put in the real world. In addition, most of these systems target avoiding other vehicle. But the number of traffic accidents concerned with a bicycle is next to it of a vehicle. So driving support system for collision avoidance of the bicycle is necessary.

In this paper, steer-by-wire is introduced into the steering wheel of the vehicle and the driving support system which realizes the most suitable steerage to avoid collision with the bicycle by considering position, velocity, and inclination of running bicycle is proposed. First, the modeling of the driving support system is introduced. Second, the control system is designed which is composed of impedance control and model predictive control. Third, the driving simulation is conducted to verify the effect of the proposed method. Finally, conclusion and the future works are described.

**Index Terms**—Electric Vehicle, Stereo Camera, Steer-by-Wire, Model Predictive Control, Impedance Control

## I. INTRODUCTION

In recent years, vehicle have been indispensable for life of men of today because of its convenience. The number of vehicles possessed increases worldwide and also increases in Japan. Simultaneously, the number of people who possess driver's license increases in Japan, too. So it can be said that the number of driver increases and driver becomes diversified. However, it makes the traffic accident social problem. To prepare for it, the demand for the driving assist systems that enable everyone to drive a vehicle always safely increases.

For example of such a system, parking assist system which supports steering wheel operation in the case of a column parking and garaging[1], lane keeping assist system which supports steering wheel operation of keeping driving lane[2], Adaptive Cruise Control (ACC) system which keeps distance between the vehicle and other vehicle running at the front and warns to the driver as needed[3], and a force sensory pedal system which transmits some information as the sense of touch[4][5]. A part of these systems has been already put to practical use. In addition, the study for the purpose of the driving support depending on road-surface condition system

has been conducted. Igari realized stabilization of vehicle and recognition of danger on a slippery road surface to a driver by estimating a slip rate without sensor and giving reaction force feedback depending on the road-surface condition to pedal and steering[6].

There are systems to avoid collision other than above mentioned. The one of these is pre-crush safety system. If the driver is in danger of colliding to a forward obstacle by delay of braking or insufficient slowdown, this system will have brake the car automatically and the vehicle will avoid collision or cut damage of it. In addition, automatic steering collision avoidance system is suggested which will operate steering automatically if the vehicle can't avoid collision. However the possibility that this system causes second accident in practical traffic situation is pointed out so that it can't reach the stage of practical realization. So most steering support system to avoid collision help active operation of the driver[7].

However, in recently, there are few steering supports system to avoid collision and most of these target avoiding other vehicle. Police white paper reported that 19.2% of the number of all traffic accident in 2013 have to do with bicycle, and 80% of the number of it consist of collision with vehicle. So it can be said that not only the anti-vehicle steering support system but also anti-bicycle one is necessary. Also most of steering support system support promoting collision avoidance based on distance toward the obstacle which a sensor detect, but there are few systems which consider behavior of the obstacle. So realization of the system which promotes safer and more effective steering collision avoidance than it of conventional system can be expected by considering dynamics of bicycle.

In this paper, anti-bicycle steering support system is proposed which changes handling quality with impedance control and generates support torque with model predictive control. To achieve it, we use steer-by-wire system and stereo-camera to obtain condition of running bicycle. This system realizes steering and recognition support for vehicle driver by changing reaction force of steering depending on condition of running bicycle. To validate the proposed system, driving simulator with OpenGL and steering with motor which acts same as



Fig. 1. Experimental system

steer-by-wire system are used. Experimental system is shown in Fig. 1. This paper is organized as follows. In section II, the modeling of the driving support system is introduced. In section III, the control system is designed. In section IV, the simulation is conducted to evaluate the proposed method. Finally, this paper is concluded and the future works are described in section V.

## II. MODELING

In this section, the model of steer-by-wire system, stereo camera, and conversion from the lateral distance between a vehicle and the bicycle to inclination of the bicycle are described.

### A. Steer-by-wire system

In this research, steer-by-wire system is used which removes mechanical and connected with electric wire. The architecture is shown in Fig. 2. Motion equation of upper and lower motor are described as follows.

$$\begin{aligned} J_u \ddot{\theta}_u &= \tau_u^{hum} + \tau_u^{mot} + \tau_u^{dis} \\ J_l \ddot{\theta}_l &= \tau_l^{mot} + \tau_l^{dis} \end{aligned} \quad (1)$$

where  $J$  is inertia of motor,  $\theta$  is angle of steering,  $\tau^{hum}$  is steering torque of driver, and  $\tau^{mot}$  represent torque of motor.

### B. Stereo camera

In this research, stereo camera is fixed on the front of the vehicle. Stereo camera model is shown in Fig. 3. Here, we consider the camera as a pinhole camera, which is an ideal model. The position of the target object can be written as  $\mathbf{P} = [P_x, P_y, P_z]$  in a camera coordinates. The target object is projected to image plane as  $\mathbf{p} = [u, v]$ .  $\mathbf{p}$  is written in pixel. Relation between the camera coordinate and the image coordinate can be written as follows.

$$u = k_u p_y = k_u \lambda \frac{P_y}{P_x} \quad (3)$$

$$v = k_v p_z = k_v \lambda \frac{P_z}{P_x} \quad (4)$$

where  $k_u, k_v$  indicate the inverse size of 1 pixel, horizontal and longitudinal respectively. Using equation (3), (4), transformation between the camera coordinate and the image coordinate can be obtained as follows.

$$P_x = \frac{b\lambda}{u_r - u_l} \quad (5)$$

$$P_y = \frac{b(u_r + u_l)}{2(u_r - u_l)} \quad (6)$$

$$P_z = \frac{bv_{l,r}}{u_r - u_l} \quad (7)$$

where  $b$  is baseline length and  $\lambda$  denotes the focal length. In addition,  $v_{l,r} = v_l = v_r$

### C. Lateral distance

In this research, situation in which the vehicle and the bicycle run side by side is considered as shown in Fig. 4. Lateral distance is modeled to control it to make distance. Here, we consider that lateral distance must be chosen when it becomes minimum value to calculate lateral distance, precisely. So  $y$ -coordinate of the bicycle for calculation of lateral distance is classified as follows.

$$y_b(t) = \begin{cases} y_{gb}(t) + L_{2b} \sin \psi_b(t) & (\psi_b(t) \leq 0.0) \\ y_{gb}(t) - L_{1b} \sin \psi_b(t) & (\psi_b(t) \geq 0.0) \end{cases} \quad (8)$$

where  $y_{gb}$  represent the barycentric  $y$ -coordinate of the bicycle,  $L_{1b}$  and  $L_{2b}$  represent the distance between the center of gravity and rear tire and front tire of it respectively. Also,  $y$ -coordinates of the vehicle is classified as follows.

$$y_h(t) = \begin{cases} y_{gh}(t) + p_{1r} \sin p_{2r} & (\theta_{yaw}(t) \leq 0.0) \\ y_{gh}(t) + p_{1f} \sin p_{2f} & (\theta_{yaw}(t) \geq 0.0) \end{cases} \quad (9)$$

where  $y_{gh}$  represent the barycentric  $y$ -coordinate of the vehicle. In addition,  $p_{1r}, p_{1f}, p_{2r}$  and  $p_{2f}$  are described as follows.

$$p_{1r} = \sqrt{(L_b/2)^2 + l_r^2} \quad (10)$$

$$p_{1f} = \sqrt{(L_b/2)^2 + l_f^2} \quad (11)$$

$$p_{2r} = \tan^{-1} \left( \frac{L_b}{2l_r} + \theta_{yaw}(t) \right) \quad (12)$$

$$p_{2f} = \tan^{-1} \left( \frac{L_b}{2l_f} - \theta_{yaw}(t) \right) \quad (13)$$

where  $L_b$  denotes sum of  $L_{1b}$  and  $L_{2b}$ . Eq.(8), (9) enables us to calculate lateral distance precisely.

### D. Feature points of the bicycle

In this research, we assume that two feature points can be detected from the bicycle as shown in Fig. 5 by stereo camera. Coordinates of these feature points give us azimuth angle  $\psi_b$  of the bicycle as eq.(14).

$$\psi_b = \tan^{-1} \left( \frac{P_{y2} - P_{y1}}{P_{x2} - P_{x1}} \right) - \theta_{yaw} \quad (14)$$

where  $\mathbf{P}_1 = [P_{x1}, P_{y1}, P_{z1}]$  and  $\mathbf{P}_2 = [P_{x2}, P_{y2}, P_{z2}]$  are position coordinate of feature point detected from rear tire and frame of the bicycle respectively. Using value of  $\psi_b$ , camber

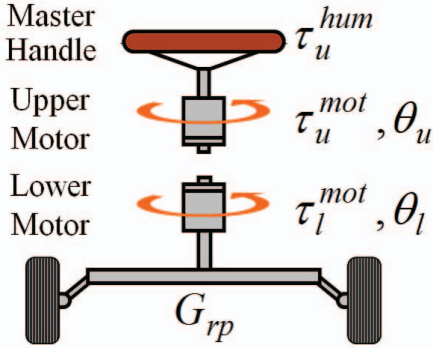


Fig. 2. Steer-by-wire system

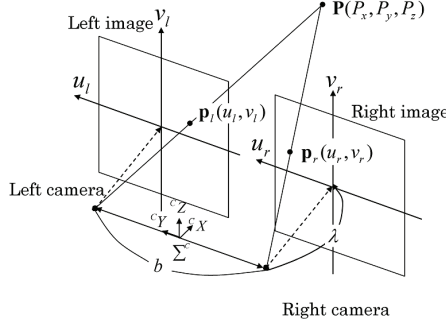


Fig. 3. Stereo camera

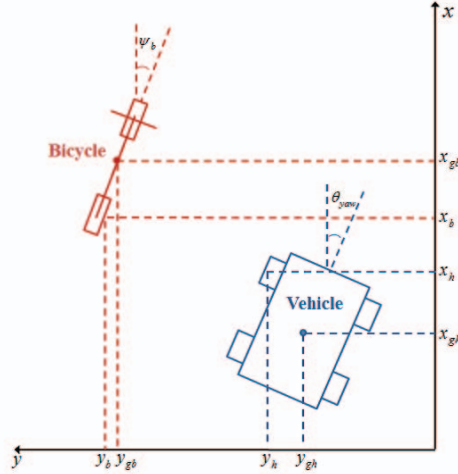


Fig. 4. Lateral distance

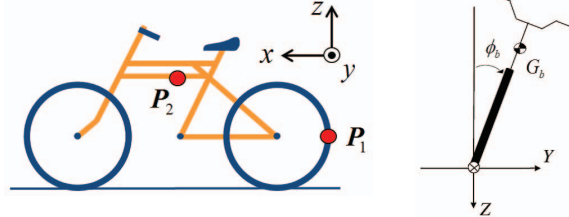


Fig. 5. Feature points of the bicycle

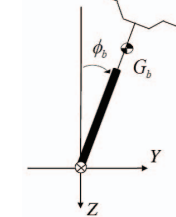


Fig. 6. Back of the bicycle

angle  $\phi_b$  of the bicycle shown in Fig. 6 can be described as eq.(15).

$$\phi_b = \tan^{-1} \left( \frac{dP_2 - dP_1}{P_{z2} - P_{z1}} \right) - \psi_b \quad (15)$$

where  $dP_1$ ,  $dP_2$  are described as follows.

$$dP_1 = P_{y2} \cos \psi_b - P_{x2} \sin \psi_b \quad (16)$$

$$dP_2 = P_{y1} \cos \psi_b - P_{x1} \sin \psi_b \quad (17)$$

### III. CONTROL SYSTEM

In this research, support torque is generated and reaction force of steering is changed by model predictive control and virtual impedance control which consider condition of the running bicycle to assist steering avoidance.

#### A. Model predictive control

In this subsection, evaluation functions which are used for model predictive control are described. These functions realize steering support control prevents such danger as the bicycle changing running course or the oncoming vehicle.

$$L_1(t) = \frac{\dot{y}_h(t)}{y_r(t)} + \frac{1}{1 + e^{-\lambda \dot{y}_r(t)}} \frac{\dot{y}_r(t)}{y_r(t)} \quad (18)$$

$$L_2(t) = \frac{1}{2} (\dot{y}_h(t) - \dot{y}_b(t))^2 \quad (19)$$

$$L_3(t) = \frac{1}{2} (\gamma(t) - \dot{\psi}_b(t))^2 \quad (20)$$

$$L_4(t) = \frac{1}{2} \ddot{y}_h(t)^2 \quad (21)$$

where  $y_r$  denotes lateral distance,  $\lambda$  denotes weighting factor.

#### B. Generating command angle of steering

To complement when the vehicle don't follow command of model predictive control, PD controller shown as follows is designed.

$$\dot{y}^{fbc} = -k_{p1} (y_r^* - y_r^{res}) - k_{d1} (\dot{y}_r^* - \dot{y}_r^{res}) \quad (22)$$

$$\dot{y}^{fbc} = -k_{p2} (y_r^* - y_r^{res}) - k_{d2} (\dot{y}_r^* - \dot{y}_r^{res}) \quad (23)$$

$$\gamma^{fbc} = -k_{p3} (\theta_{yaw}^* - \theta_{yaw}^{res}) - k_{d3} (\gamma^* - \gamma^{res}) \quad (24)$$

where  $\gamma$  the denotes yaw-rate,  $*$  denotes a desired value,  $k \odot$  denotes a gain. Adding those reference value and model predictive control reference value, final reference value  $\mathbf{u}^{MPC} = [\dot{y}^{MPC}, \ddot{y}^{MPC}, \gamma^{MPC}]$  can be obtained. Equation from kinematics of the vehicle dynamics, command angle of the steering  $\theta_u^{cmd}$  is described as shown follow.

$$\theta_u^{cmd} = \frac{M (\ddot{y}^{MPC} - A_1 \gamma^{MPC} - A_2 \theta_{yaw} - A_3 \dot{y}^{MPC})}{2C_{fl}} \quad (25)$$

where  $A_1$ ,  $A_2$  and  $A_3$  are described as shown follows.

$$A_1 = \frac{-2(l_f C_{fl} + l_r C_{fr})}{MV} \quad (26)$$

$$A_2 = \frac{2(C_{fl} + C_{fr})}{M} \quad (27)$$

$$A_3 = \frac{-2(C_{fl} + C_{fr})}{MV} \quad (28)$$

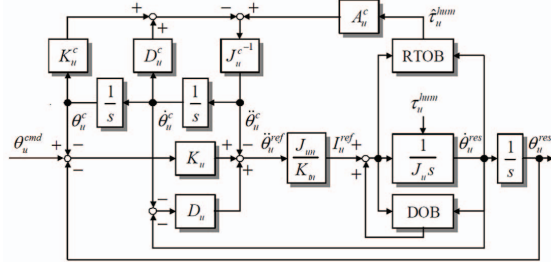


Fig. 7. Block diagram of upper motor

where  $l_f$  and  $l_r$  denote distance between the vehicle center of gravity and axle of front and rear respectively,  $C_\bigcirc$  denotes cornering stiffness of the tire.

### C. Virtual impedance control

In this section, virtual impedance control which changes reaction force of steering based on information of the running bicycle obtained by camera is described. To introduce virtual impedance control, Disturbance observer(DOB)[8] which gives robustness to the steering and Reaction torque observer(RTOB)[9] estimate human input torque to the steering without sensors are used. By applying RTOB, driver's input torque is acceptable to the handle. Using second order filter which consists of characteristic of impedance  $J_u^c$ ,  $D_u^c$ ,  $K_u^c$  and feedback gain  $A_u^c$ , estimated reaction force  $\hat{\tau}_u^{hum}$  are converted to command input of angle  $(\theta_u^c, \dot{\theta}_u^c, \ddot{\theta}_u^c)$ . Model of virtual impedance control is shown as following equation.

$$J_u^c \ddot{\theta}_u^c + D_u^c \dot{\theta}_u^c + K_u^c \theta_u^c = A_u^c \hat{\tau}_u^{hum} \quad (29)$$

Using command input of angle  $(\theta_u^c, \dot{\theta}_u^c, \ddot{\theta}_u^c)$ , acceleration reference value can be written as shown following equation.

$$\ddot{\theta}_u^{ref} = K_u(\theta_u^{cmd} - \theta_u^{res} - \theta_u^c) + D_u(-\dot{\theta}_u^{res} - \dot{\theta}_u^c) - \ddot{\theta}_u^c \quad (30)$$

where  $c$  denote command value of compliance control,  $K_u$  and  $D_u$  denotes gain of position and velocity respectively. Fig. 7 shows control block diagram of upper motor of steer-by-wire system applied virtual impedance control.

1) *Design of impedance gain:* Way of determining impedance gain by use of information of running bicycle obtained by camera is described. In this research, impedance gains are designed as shown follow equations.

$$Q_1 = w_{11}(y_r - y_{r2}^*) \dot{y}_r + w_{12}(1.0 + w_{13}\psi_b + w_{14}\phi_b) \dot{y}_r \quad (31)$$

$$Q_2 = w_{21}(y_r - y_{r2}^*) \dot{y}_r + w_{22}(1.0 + w_{23}\psi_b + w_{24}\phi_b) \dot{y}_r \quad (32)$$

When the bicycle is near to the vehicle,  $Q$  will become very small, but when the bicycle is far from,  $Q$  will become big relatively.  $Q_1$  and  $Q_2$  change if necessary. In turn, crosscut of handle is necessary after keeping a distance from the running bicycle so that better handling quality can be obtained by switching  $Q_1$  and  $Q_2$  with including impedance gain  $D_u^c$  and  $K_u^c$ . In addition, effect of support of recognition is enhanced by use of feedback gain  $A_u^c$ . Due to those factors, virtual

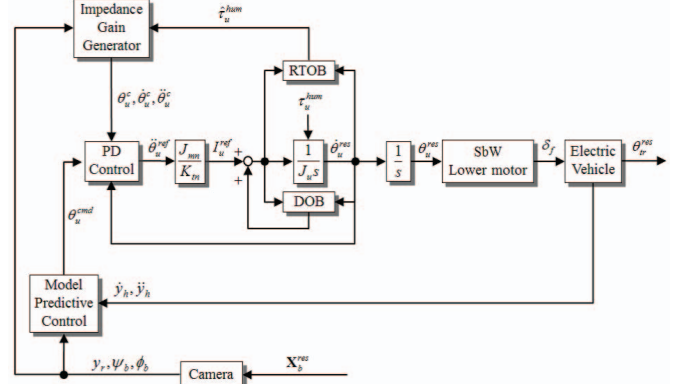


Fig. 8. Block diagram of entire control system

impedance gain can be changed appropriately in response to the danger of collision as shown eq.(33).

$$J_u^c \ddot{\theta}_u^c + D_u^c \dot{\theta}_u^c + (K_u^c + P_u^K Q) \theta_u^c = (A_u^c P_u^A Q) \hat{\tau}_u^{hum} \quad (33)$$

where  $P_u^K$  and  $P_u^A$  denote a gain.

## IV. DRIVING SIMULATION

In this section, the validity of proposed method was evaluated. The detail of the driving simulator is explained at first. Then, the experimental setup and results are shown.

### A. Simulation setup

The situation was supposed that the bicycle whose speed is 18km/h runs in front of the vehicle whose speed is 40km/h. The vehicle driver doesn't recognize it because of his carelessness. When the space distance between the vehicle and the bicycle in front become 11m and lateral distance become 2m, the bicycle leans to the vehicle for changing course suddenly. In this time, the driver recognizes it and turn off steering for collision avoidance. These distances are theoretical limit that vehicle can avoid front obstacle by steering in this speed[7]. So it is dangerous for the driver to avoid the running bicycle without driving assist control. Model predictive control was begun when lateral distance falls below 2m, and virtual impedance control was begun when distance in front falls below 15m. Gain parameter used were shown in Table. I. These parameters are designed by try and error.

TABLE I  
GAIN PARAMETER

Position gain $K_u$	4.0
Velocity gain $D_u$	1.2
$g_{dob}$	10.0
$g_{rto}$	10.0

### B. Simulation results

Angle of the handle is shown in Fig. 9, lateral distance is shown in Fig. 10, command angle of the handle is shown in Fig. 11, impedance gains are shown in Fig. 12 and running path of the vehicle is shown in Fig. 13 respectively.

Fig. 9, Fig. 10 and Fig. 13 shows that safety improved

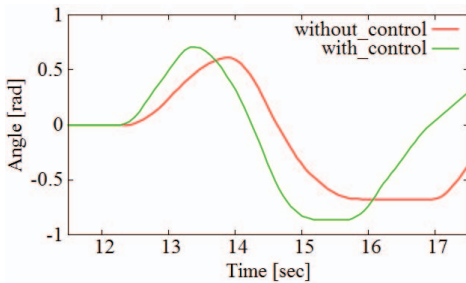


Fig. 9. Degree of the handle

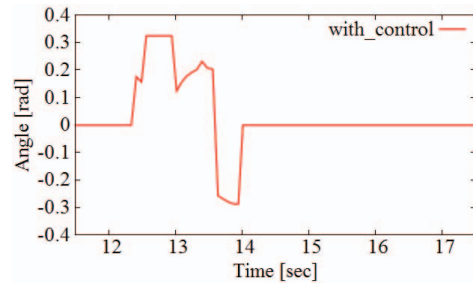


Fig. 11. Command angle of the steering

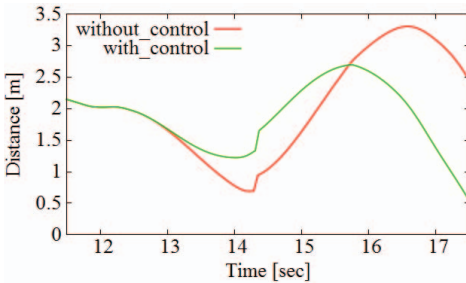


Fig. 10. lateral distance

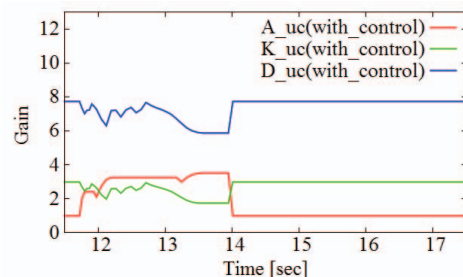


Fig. 12. Impedance gain

by steering more quickly and it provided more lateral distance in case of applying proposed control method. After collision avoidance, the vehicle came back to the original traffic lane immediately so it can be said that a risk of the danger of the collision with the leaning bicycle decreases.

## V. CONCLUSION AND FUTURE WORKS

In this paper, the system which changes handling quality by using condition of running bicycle as the driving support system to avoid collision was proposed. To realize this system, driving simulator with OpenGL and steering with motor which acts same as steer-by-wire system were used. The simulation results showed the validity of the proposed system.

As a future works, we will apply steer-by-wire system to a real vheicle and perform experiment with proposed system and experiment using some subjects is necessary to validate objective efficacy of it. In addition, for dealing other traffic situation, we will propose driving assist system which controls steering and pedal simultaneously.

## ACKNOWLEDGEMENT

This report was subsidized in part by JKA(27-130) through its promotion funds from KEIRIN RACE.

## REFERENCES

- [1] Massaki Wada, Kangsup Yoon, Hideki Hashimoto, Shinichi Matsuda, "Parking Assistance System Based on High Accuracy Position Sensing", *Intelligent Transport Systems*, Vol. 9, Issue. 3, 1999, pp. 323-332.
- [2] Liang-kuang Chen and Chuan-hui Yang, "Control Authority Determination of a Vehicle Lane Keeping Assist Controller", *IEEE Intelligent Vehicles Symposium*, June, 2009, pp. 1383-1388.
- [3] M. Brackstone and M. McDonald, "Car-following: A historical review", *Pergamon, Transportation Research F 2*, 2000, pp. 181-196.
- [4] El Saddik: "The Potential of Haptics Technologies", *IEEE Instrumentation & Measurement Magazine*, Vol. 10, pp. 10-17, Feb. 2007
- [5] T. Shimono, S. Katsura and K. Ohnishi: "Abstraction and Reproduction of Force Sensation From Real Environment by Bilateral Control", *IEEE Trans. on Industrial Electronics*, Vol. 54, Issue 2, pp. 907-918, Apr. 2007
- [6] Y. Igari and T. Murakami: "Drive Assist System of Electric Vehicle for Road Condition Cognition by Torque Feedback based on Road Frictional Force", *Master's Course Paper 2010*, No. 2010-15-02, 2010
- [7] Y. Fuma and H. Nishimura: "Design of Vehicle Collision Avoidance System Using Interruption Decision Based on Risk Analysis", *JSME annual meeting 2009(7)*, pp. 387-388, 2009-09-12
- [8] K. Ohnishi, M. Shibata and T. Murakami : "Motion control for Advanced Mechatronics", *IEEE/ASME Transactions on Mechatronics*, Vol.1, No.1, pp.56-57, March, 1996.
- [9] K. Ohnishi, M. Shibata and T. Murakami : "Torque Sensorless Control in Multidegree-of-Freedom Manipulator", *IEEE Transactions on Industrial Electronics*, Vol.40, No.2, April, 1993.

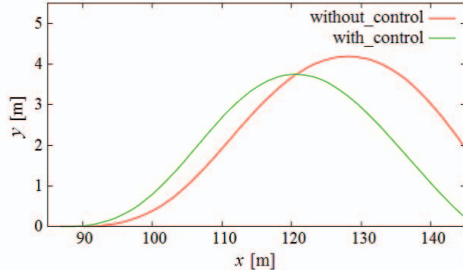


Fig. 13. Running path of the vehicle



事業内容についての問い合わせ先  
慶應義塾大学 理工学部 システムデザイン工学科 村上俊之研究室  
〒223-8522  
横浜市港北区日吉3-14-1  
教授 村上俊之  
E-mail: mura@sd.keio.ac.jp  
URL: www.fha.sd.keio.ac.jp